Radial perfectly matched layers and infinite elements for the anisotropic wave equation

Martin Halla, Maryna Kachanovska, Markus Wess

Radial perfectly matched layers and infinite elements for the anisotropic wave equation

Martin Halla[a], Maryna Kachanovska[b], Markus Wess[c]

[a] *Institut für Numerische und Angewandte Mathematik, Georg-August-Universität Göttingen, Lotzestr. 16-18, Göttingen, 37083, Niedersachsen, Germany*
[b] *POEMS, ENSTA Paris, CNRS, Inria, Institut Polytechnique de Paris, 828 Boulevard des Maréchaux, Palaiseau, 91120, France*
[c] *Institute of Analysis and Scientific Computing, TU Wien, Wiedner Hauptstraße 8-10, 1040, Vienna, Austria*

Abstract

We consider the scalar anisotropic wave equation. Recently a convergence analysis for radial perfectly matched layers (PML) in the frequency domain was reported and in the present article we continue this approach into the time domain. First we explain why there is a good hope that radial complex scalings can overcome the instabilities of PML methods caused by anisotropic materials. Next we discuss some sensitive details, which seem like a paradox at the first glance: if the absorbing layer and the inhomogeneities are sufficiently separated, then the solution is indeed stable. However, for more general data the problem becomes unstable. In numerical computations we observe instabilities regardless of the position of the inhomogeneities, although the instabilities arise only for fine enough discretizations. As a remedy we propose a complex frequency shifted scaling and discretizations by Hardy space infinite elements or truncation-free PMLs. We show numerical experiments which confirm the stability and convergence of these methods.

Keywords: perfectly matched layers, Hardy spaces, infinite elements, anisotropic wave equation

1. Introduction

In the 1990s Bérenger [14] introduced the perfectly matched layer method as an approximate transparent boundary condition for transient electromagnetic wave equations. Soon it was recognized [20] that the PML equations can be derived by means of a complex scaling technique, which was already extensively used under the names complex scaling/analytic dilation/spectral deformation since the 1970s in mathematical physics for analysis and resonance computations, see [3, 4, 57], and a detailed review in [37]. We refer to the introduction of [30] for an extensive literature review on PML. No doubt, the reason for the popularity of the PML method stems from the fact that it is very easy to implement: for transient equations one only needs to introduce some additional auxiliary unknowns (without any knowledge of a fundamental solution or Dirichlet-to-Neumann operator). For this reason it is easily possible to apply the PML method to all kinds of equations. However, as soon as one deviates from classical applications it is a delicate question if the PML method yields physically correct and stable solutions. In particular, backward waves which can occur in dispersive materials [12, 6] and waveguide geometries [18, 27] lead to challenges for the PML. Another important challenge, which is the focus of this article, are anisotropic materials. Indeed also the application/construction of absorbing boundary conditions for anisotropic equations requires a careful analysis and has received quite some attention, see e.g., [11, 54, 55, 51, 45].

Up to our knowledge, the instability of Bérenger's Cartesian perfectly matched layers for anisotropic media was noticed as early as in 1996 by Fang Q. Hu [39] when applying PMLs to Euler equations, and, as a first remedy, the author suggested numerical filtering. The reason for the appearance of such instabilities was

Email addresses: m.halla@math.uni-goettingen.de (Martin Halla), maryna.kachanovska@inria.fr (Maryna Kachanovska), markus.wess@tuwien.ac.at (Markus Wess)

investigated in particular in [36, 1], and at first was attributed to the possible loss of the strong well-posedness of the PML problem. In [40] it was shown that a strongly well-posed PML system can be constructed, but it is still unstable: the PML instability is induced by so-called backward propagating waves in the direction of the PML absorption. While the explanation in [40] was given using somewhat semi-heuristic arguments, it found its mathematical justification in the seminal work by Bécache, Fauqueux and Joly [9]. There, it was proven that the classical Cartesian Bérenger's PMLs in one direction with constant absorption can be unstable when applied to anisotropic media. The analysis in [9] is based on a plane-wave analysis of the Cauchy problem for the constant-coefficient PML media filling the free space. It is proven that some (but not all) of the instabilities of the PMLs are high-frequency instabilities, caused by so-called backward propagating waves in the direction of the PMLs, occurring in particular in many anisotropic materials.

At the numerical level, the fact that instabilities appear for high frequencies implies that coarse discretizations are not likely to exhibit them, see [43]. Since the usual goal is to construct numerical methods for which the error can be made arbitrarily small, this is not a very satisfactory solution (though it indeed can be used in practice). While there exist several works discussing and predicting the behaviour of Cartesian Bérenger's PMLs in anisotropic media (whereas the treatment against the instabilities is typically problem-dependent), there exists only little knowledge about the behaviour of the other types of PMLs, in particular radial PMLs, introduced in [21]. The analysis of [9] does not apply to this case, and the numerical experiments are not always conclusive. The principal goal of this work is to address this question in detail. More precisely, we would like to answer the following questions:

Q1. Are radial PMLs stable when applied to anisotropic problems?

Q2. If not, what is the reason for the instability?

Q3. If the answer to Question 1 is negative, can we find a workaround, **which would not be specific to the anisotropic *scalar* problem in question**?

To answer these questions we concentrate on the simplest model problem, namely the anisotropic wave equation, for which many computations can be done explicitly. This model already contains some of the difficulties which occur when applying PMLs to more challenging problems (e.g., anisotropic elasticity).

Answers to Questions 1 and 2. Our answers to Questions 1 and 2 are given in Section 3. For theoretical purposes, we work with radial perfectly matched layers of *infinite length* (which we will refer to as *truncation-free* PMLs), which already exhibit many interesting phenomena observed in truncated PMLs. If the spatial support of the source term (compactly supported in space and time) is located far enough from the damping layer, then the solutions to the PML problem are stable, i.e. exhibit at most time-polynomial growth. On the other hand, the PML system itself allows for unstable solutions. We believe that this is due to the presence of an essential spectrum of the underlying operator in the right-half of the complex plane. We prove the existence of such a spectrum. Our numerical experiments (Section 2.3.1) indicate that the instabilities occur at the discrete level, when the discretizations are chosen fine enough, independently of the support of the data. Our findings for the radial PMLs complement those by K. Duru and G. Kreiss [26, 43] who observed similar phenomena for Cartesian PMLs applied to anisotropic elasticity and wave equations.

One answer to Question 3. Indeed, stable Cartesian PMLs for the anisotropic wave equation were constructed by a clever change of variables in [23]. Nonetheless, because our goal is to propose a method that **is possibly** suitable for other anisotropic problems apart from the scalar anisotropic wave equation, we choose a different path. Our starting point is the PML time-harmonic work by one of the authors of the present article [31], where it is suggested to use complex frequency shifted PMLs. However, we show that, like in the time-harmonic case, in the time domain the complex frequency shift has to be chosen proportionally to the damping parameter of the layer, with the proportionality coefficient limited by the anisotropy. In this setting increasing the damping parameter does not allow to decrease the PML error, and the convergence can be ensured by increasing the width of the layer only. See Section 4 for details. We propose two solutions to this problem in Section 5, and test their performance numerically. They are outlined below.

S1. We do not truncate the perfectly matched layer, but rather use the complex-shifted change of variables combined with the discretization by infinite element methods. To do so we use the Hardy space infinite

elements (HSIE), see [38, 29] for their introduction, analysis and numerical experiments in the time-harmonic case, and [53], [58, Chapter 10.2.4], [49] for the time-domain formulation and experiments. In particular, we use a time-domain equivalent of the two-scale method presented in [32].

S2. We exploit so-called exact PML methods, where the exactness is ensured either by choosing a non-integrable damping parameter [16], or a coordinate transformation mapping an infinite domain to a finite one [41, 59] and [30, Chapter 4.5.1]. We concentrate on this latter choice.

The complex frequency shift appeared already in the literature to prevent long-time instabilities of Cartesian PMLs [10], or as a practical approach to stabilize perfectly matched layers in anisotropic elasticity, cf. [26]. Studies combining classical, Cartesian PMLs, and infinite finite elements, can be found in [50].

This article is organized as follows. In Section 2 we state the problem under consideration and the associated PML equations derived by the radial complex scaling. We provide some heuristic arguments why radial PMLs might be stable when applied to anisotropic media. Next, we present different computational radial PML examples, some with stable and some with unstable behaviour. In Section 3 we investigate the cause of the instabilities: the equations are well-posed and for convenient configurations the solutions are stable. Nevertheless for small spectral parameters s, $\operatorname{Re} s > 0$, there exists an essential spectrum, which indicates the unstable character of the PML equations. As a remedy we introduce in Section 4 a complex frequency shifted Hardy space infinite element method, as well as a corresponding truncation-free PML. We report computational results, which confirm stability and convergence of these methods, in Section 5.

2. Problem setting and motivation

2.1. Problem setting

2.1.1. The model

We consider wave propagation in anisotropic media, described by a scalar anisotropic wave equation. Namely, we look for $u\colon \mathbb{R}_0^+ \times \mathbb{R}^2 \to \mathbb{R}$ and $\mathbf{p}\colon \mathbb{R}_0^+ \times \mathbb{R}^2 \to \mathbb{R}^2$, where $\mathbb{R}_0^+ := \{t \in \mathbb{R} : t \geq 0\}$, s.t.

$$\partial_t u = \operatorname{div} \mathbf{p} + f \quad \text{in } \mathbb{R}_0^+ \times \mathbb{R}^2, \qquad \mathbf{A}^{-1}\partial_t \mathbf{p} = \nabla u \quad \text{in } \mathbb{R}_0^+ \times \mathbb{R}^2, \tag{1}$$

$$u(0,\mathbf{x}) = 0, \quad \mathbf{p}(0,\mathbf{x}) = 0 \text{ in } \mathbb{R}^2, \tag{2}$$

where the source f is sufficiently regular, $f(0,\cdot) = 0$, and $f(t,\cdot)$ is compactly supported inside a bounded domain Ω_f for all $t > 0$. The matrix $\mathbf{A} \in \mathbb{R}^{2\times 2}$ is symmetric strictly positive definite. By eliminating $\mathbf{p}$ we write this system as a second order equation, and equip it with homogeneous initial conditions:

$$\partial_t^2 u - \operatorname{div}(\mathbf{A}\nabla u) = \partial_t f \quad \text{in } \mathbb{R}_0^+ \times \mathbb{R}^2, \qquad u(0,\mathbf{x}) = 0, \quad \partial_t u(0,\mathbf{x}) = 0 \quad \text{in } \mathbb{R}^2. \tag{3}$$

We are interested in the solution to the above problem inside a bounded convex domain Ω_{int}, s.t. $\Omega_f \subset \Omega_{\text{int}}$. To bound the computational domain we surround Ω_{int} by an absorbing perfectly matched media $\Omega_{\text{pml}}^{\infty} := \mathbb{R}^2 \setminus \overline{\Omega_{\text{int}}}$, which is usually then truncated to a bounded layer Ω_{pml}. Inside this layer, the original PDE is modified in such a way that, on one hand, the Laplace transform of its solution decays exponentially fast in space, and, on the other hand, the waves propagating from Ω_{int} into Ω_{pml} do not get reflected at the interface Σ between Ω_{int} and Ω_{pml}. The absorbing system is constructed via a certain frequency-dependent change of variables applied in the direction normal to Σ (this will be discussed in detail later). In the literature there are several common choices of the geometry of Ω_{int} and the construction of the corresponding PMLs:

1. Cartesian PMLs [14, 15] where Ω_{int} is a box $(-a,a)^2$, and $\Omega_{\text{pml}} = (-a-L, a+L)^2 \setminus \overline{\Omega_{\text{int}}}$;
2. radial PMLs [21], where Ω_{int} is a circle $B_{R_{\text{pml}}} := \{\mathbf{x} \in \mathbb{R}^2 : \|\mathbf{x}\| < R_{\text{pml}}\}$, and $\Omega_{\text{pml}} = B_{R_{\text{pml}}+L} \setminus \overline{\Omega_{\text{int}}}$;
3. general convex PMLs (see e.g., [44] or [21]), where Ω_{int} is a general convex domain.

For anisotropic wave propagation problems (generalizing (3)), in [9] it has been shown that the Cartesian PMLs may exhibit time-domain instabilities, i.e., exponentially growing in time solutions. The arguments of [9] are based on a plane-wave analysis, which cannot be applied to radial PMLs. As discussed before, the goal of this article is to examine the question of stability of radial PMLs for anisotropic problems. Because in its full generality this problem is challenging, we concentrate on the simplest model (3). We first introduce the radial PMLs and next explain why their use may seem to be promising in the anisotropic media setting.

2.1.2. Radial perfectly matched layers

To apply radial PMLs to (3), we start by rewriting it in the Laplace domain. For $v \in L^1(\mathbb{R})$ s.t. $v(t) = 0$ for $t < 0$ (i.e., v is a causal function) the Laplace transform is defined by

$$\hat{v}(s) := (\mathcal{L}v)(s) := \int_0^{+\infty} \mathrm{e}^{-st} v(t) dt, \quad s \in \mathbb{C}^+ := \{s \in \mathbb{C} \colon \operatorname{Re} s > 0\}.$$

Next we rewrite the problem in the polarcoordinates $(r, \phi) \in \mathbb{R}_0^+ \times [0, 2\pi)$. Denoting by $\nabla_{r,\phi} v = (\partial_r, r^{-1}\partial_\phi)^\top v$, $\operatorname{div}_{r,\phi} \boldsymbol{v} = r^{-1}(\partial_r(r v_r) + \partial_\phi v_\phi)$, we obtain the following Laplace-domain counterpart of (3):

$$s^2 \hat{u} - \operatorname{div}_{r,\phi}(\mathbf{A}^\phi \nabla_{r,\phi} \hat{u}) = s\hat{f} \quad \text{in } \mathbb{R}^2,$$

with $\mathbf{A}^\phi := \mathbf{R}_\phi^\top \mathbf{A} \mathbf{R}_\phi$ and the rotation matrix $\mathbf{R}_\phi := \begin{pmatrix} \cos\phi & -\sin\phi \\ \sin\phi & \cos\phi \end{pmatrix}$. Here we used the same notation $\hat{u}$ for the unknown in the Cartesian and polar coordinates. The radial PMLs are based on a change of variables

$$r_\sigma(s, r) := \begin{cases} r + s^{-1} \int_{R_{\mathrm{pml}}}^r \sigma(r') dr', & r > R_{\mathrm{pml}}, \\ r, & r \le R_{\mathrm{pml}}, \end{cases} \quad \text{where } \sigma \text{ is as in Assumption 2.1.} \tag{4}$$

Assumption 2.1. $\sigma \in L^\infty(\mathbb{R}^+)$ is s.t. $\sigma(r) = 0$ for $r \le R_{\mathrm{pml}}$ and $\sigma(r) > 0$ for $r > R_{\mathrm{pml}}$.

The function σ is called a damping (absorption) parameter. Let us additionally introduce

$$\begin{aligned} &\tilde{d}_\sigma(s, r) := \frac{r_\sigma(s, r)}{r} = 1 + s^{-1}\tilde{\sigma}(r), \qquad \tilde{\sigma}(r) := r^{-1} \int_{R_{\mathrm{pml}}}^r \sigma(r')\, dr', \\ &d_\sigma(s, r) := \frac{dr_\sigma(s, r)}{dr} = 1 + s^{-1}\sigma(r), \quad \mathbf{x}_\sigma(s, \mathbf{x}) := \mathbf{x}\tilde{d}_\sigma(s, \|\mathbf{x}\|). \end{aligned} \tag{5}$$

Where convenient, we will abuse the notation as follows: we will write $d_\sigma(s)$ for $d_\sigma(s, r)$, when d_σ is considered as a function of the Laplace variable s and r is fixed, or, resp., $d_\sigma(r)$. The same applies to $\tilde{d}_\sigma$ and $\mathbf{x}_\sigma$ respectively. In addition, we use the overloaded notation $\tilde{d}_\sigma(s, \mathbf{x}) := \tilde{d}_\sigma(s, \|\mathbf{x}\|)$, $\sigma(\mathbf{x}) := \sigma(\|\mathbf{x}\|)$, etc. With this new change of variables and the above notation, we obtain the following problem for $\hat{u}^\sigma(s, \mathbf{x}) := \hat{u}(s, \mathbf{x}_\sigma)$[1]:

$$s^2 \tilde{d}_\sigma d_\sigma \hat{u}^\sigma - \operatorname{div}_{r,\phi}(\mathbf{A}_\sigma^\phi \nabla_{r,\phi} \hat{u}^\sigma) = s\hat{f} \quad \text{in } \mathbb{R}^2, \qquad \mathbf{A}_\sigma^\phi := \operatorname{diag}(\tilde{d}_\sigma, d_\sigma) \mathbf{A}^\phi \operatorname{diag}(d_\sigma^{-1}, \tilde{d}_\sigma^{-1}). \tag{6}$$

Let us rewrite the above in the time domain, and in a form more suitable for the numerical implementation, based on a reformulation of (6) in Cartesian coordinates. Given $\mathbf{x} \in \mathbb{R}^2 \setminus \{0\}$, we denote by $\Pi_\parallel(\mathbf{x})$ and $\Pi_\perp(\mathbf{x})$ the orthogonal projections onto the spaces $\operatorname{span}\{\mathbf{x}\}$ and $(\operatorname{span}\{\mathbf{x}\})^\perp$ respectively. Then the Jacobian reads

$$\begin{aligned} \mathbf{J}_\sigma := D_{\mathbf{x}} \mathbf{x}_\sigma &= \tilde{d}_\sigma \operatorname{Id} + \frac{\mathbf{x}\mathbf{x}^\top}{\|\mathbf{x}\|} \partial_r \tilde{d}_\sigma = \tilde{d}_\sigma(\Pi_\parallel + \Pi_\perp) + \|\mathbf{x}\| \Pi_\parallel \partial_r \tilde{d}_\sigma \\ &= (\tilde{d}_\sigma + \|\mathbf{x}\| \partial_r \tilde{d}_\sigma)\Pi_\parallel + \tilde{d}_\sigma \Pi_\perp = d_\sigma \Pi_\parallel + \tilde{d}_\sigma \Pi_\perp. \end{aligned} \tag{7}$$

[1]Here, we assume that the holomorphic continuation is well-defined.

Its determinant is $\det \mathbf{J}_\sigma = d_\sigma \tilde{d}_\sigma$. Then (6) rewrites, based on the usual Piola transform [17, pp. 59-60],

$$s^2 \det \mathbf{J}_\sigma \hat{u}^\sigma - \operatorname{div}(\mathbf{A}_\sigma \nabla \hat{u}^\sigma) = s\hat{f}, \quad \mathbf{A}_\sigma(s,\mathbf{x}) := \mathbf{J}_\sigma(s,\mathbf{x})^{-1}\mathbf{A}\mathbf{J}_\sigma(s,\mathbf{x})^{-\top} \det \mathbf{J}_\sigma(s,\mathbf{x}). \tag{8}$$

The above can be written as a first-order system:

$$s \det \mathbf{J}_\sigma \hat{u}^\sigma = \operatorname{div} \hat{\mathbf{p}}^\sigma + \hat{f}, \qquad s\mathbf{A}_\sigma^{-1}\hat{\mathbf{p}}^\sigma = \nabla \hat{u}^\sigma.$$

This rewriting preserves the skew symmetry of the first-order counterpart of our original problem (3). Using

$$\begin{aligned} sd_\sigma(s)\tilde{d}_\sigma(s) = s + \sigma + \tilde{\sigma} + \frac{\sigma\tilde{\sigma}}{s}, \qquad & s\frac{d_\sigma(s)}{\tilde{d}_\sigma(s)} = s + \sigma - \tilde{\sigma} - \frac{(\sigma-\tilde{\sigma})\tilde{\sigma}}{s+\tilde{\sigma}}, \\ & s\frac{\tilde{d}_\sigma(s)}{d_\sigma(s)} = s - (\sigma - \tilde{\sigma}) + \frac{(\sigma-\tilde{\sigma})\sigma}{s+\sigma}, \end{aligned} \tag{9}$$

we obtain that the left-hand-sides of the above can be rewritten as

$$s \det \mathbf{J}_\sigma \hat{u}^\sigma = s\hat{u}^\sigma + \left(\sigma + \tilde{\sigma} + \frac{\sigma\tilde{\sigma}}{s}\right)\hat{u}^\sigma, \tag{10}$$

$$\begin{aligned} s \det \mathbf{J}_\sigma^{-1}\mathbf{J}_\sigma^\top \mathbf{A}^{-1}\mathbf{J}_\sigma \hat{\mathbf{p}}^\sigma = s\mathbf{A}^{-1}\hat{\mathbf{p}}^\sigma &+ \left(\sigma - \tilde{\sigma} - \frac{(\sigma-\tilde{\sigma})\tilde{\sigma}}{s+\tilde{\sigma}}\right)\Pi_\parallel \mathbf{A}^{-1}\Pi_\parallel \hat{\mathbf{p}}^\sigma, \\ &+ \left(-(\sigma-\tilde{\sigma}) + \frac{(\sigma-\tilde{\sigma})\sigma}{s+\sigma}\right)\Pi_\perp \mathbf{A}^{-1}\Pi_\perp \hat{\mathbf{p}}^\sigma. \end{aligned} \tag{11}$$

Thus, introducing the auxiliary unknowns

$$\begin{aligned} & s\hat{v} := \hat{u}^\sigma, \\ & \hat{\mathbf{q}} := \frac{\tilde{\sigma}}{s+\tilde{\sigma}}\Pi_\parallel \hat{\mathbf{p}}^\sigma + \frac{\sigma}{s+\sigma}\Pi_\perp \hat{\mathbf{p}}^\sigma \quad \Longleftrightarrow \quad s\hat{\mathbf{q}} = \tilde{\sigma}\left(1 - \frac{\tilde{\sigma}}{s+\tilde{\sigma}}\right)\Pi_\parallel \hat{\mathbf{p}}^\sigma + \sigma\left(1 - \frac{\sigma}{s+\sigma}\right)\Pi_\perp \hat{\mathbf{p}}^\sigma, \end{aligned}$$

and applying the inverse Laplace transform (where the respective time-domain functions are indicated by omitting the hats) leads to the first order system

$$\begin{aligned} \partial_t u^\sigma &= -(\sigma+\tilde{\sigma})u^\sigma - \sigma\tilde{\sigma}v + \operatorname{div}\mathbf{p}^\sigma + f, \\ \partial_t v &= u^\sigma, \\ \mathbf{A}^{-1}\partial_t \mathbf{p}^\sigma &= (\sigma-\tilde{\sigma})\left(\Pi_\perp \mathbf{A}^{-1}\Pi_\perp \mathbf{p}^\sigma - \Pi_\parallel \mathbf{A}^{-1}\Pi_\parallel \mathbf{p}^\sigma - \Pi_\perp \mathbf{A}^{-1}\Pi_\perp \mathbf{q} + \Pi_\parallel \mathbf{A}^{-1}\Pi_\parallel \mathbf{q}\right) + \nabla u^\sigma, \\ \partial_t \mathbf{q} &= \tilde{\sigma}\left(\Pi_\parallel \mathbf{p}^\sigma - \Pi_\parallel \mathbf{q}\right) + \sigma\left(\Pi_\perp \mathbf{p}^\sigma - \Pi_\perp \mathbf{q}\right). \end{aligned} \tag{12}$$

In practice, the radial PMLs are truncated by imposing homogeneous boundary conditions at $r = R_{\mathrm{pml}} + L$.

2.2. Potential stability of radial PMLs

Studies of radial PMLs for time-harmonic anisotropic wave equations were initiated in [31], wherein the convergence of a radial PML for anisotropic scalar resonance problems was proven rigorously. However, these results do not allow any direct deduction of stability for the time-dependent equation. An argument which may indicate a potential stability of radial PMLs for anisotropic *time-dependent* problems is the following. If we apply the radial PMLs in the free space with $\sigma = \mathrm{const} > 0$ (which is the setting in which Cartesian PMLs are often analyzed), we have that $d = \tilde{d}$, and thus we obtain the following PML problem:

$$\partial_t^2 u^\sigma + 2\sigma\partial_t u^\sigma + \sigma^2 u^\sigma - \operatorname{div}\mathbf{A}\nabla u^\sigma = 0, \quad (t,\mathbf{x}) \in \mathbb{R}^+ \times \mathbb{R}^2.$$

It is straightforward to verify that the associated energy is non-increasing:

$$\frac{d}{dt}E^\sigma(t) = -2\|\sigma^{1/2}\partial_t u^\sigma(t)\|^2_{L^2(\mathbb{R}^2)}, \quad E^\sigma(t) := \frac{1}{2}\left(\|\partial_t u^\sigma(t)\|^2_{L^2(\mathbb{R}^2)} + \|\sigma u^\sigma(t)\|^2_{L^2(\mathbb{R}^2)} + \|\mathbf{A}^{1/2}\nabla u^\sigma(t)\|^2_{L^2(\mathbb{R}^2)}\right).$$

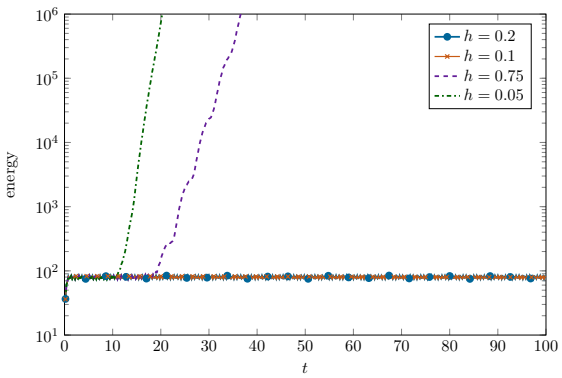

(a) Long-time (in-)stability of PML discretizations for different mesh sizes. The energy curve corresponding to the coarsest mesh size $h = 0.2$ is hardly visible, because it is overlapped by the energy curve for $h = 0.1$.

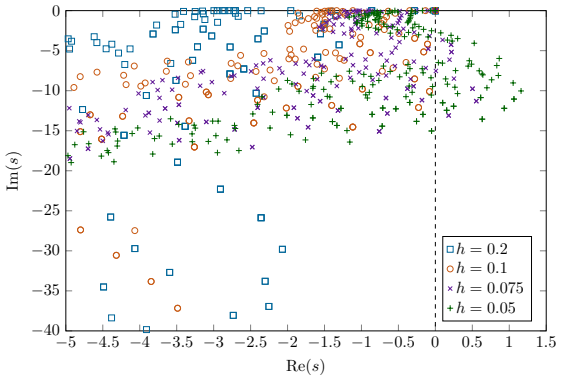

(b) Spectra of the time harmonic problems corresponding to Figure 1a.

Figure 1: (In-)stability of standard PMLs.

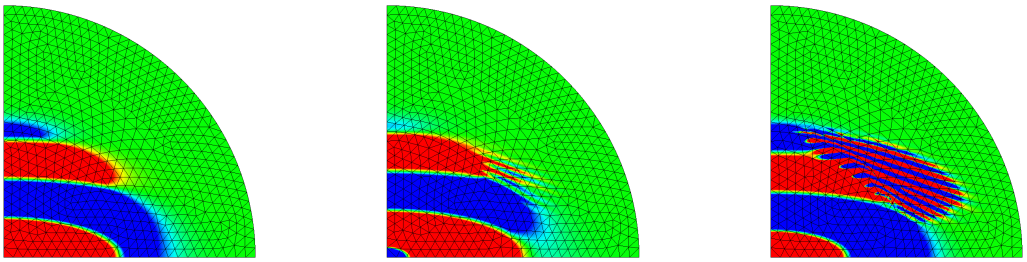

(a) $t = 4$ **(b)** $t = 16$ **(c)** $t = 24$

Figure 2: Unstable PML solution with $h = 0.075$ at different times t (cf. also Figure 1a).

2.3. Numerical experiments and their interpretation

To motivate our following analysis we present the results of some preliminary numerical experiments which already showcase the quite surprising behavior of radial PMLs for anisotropic materials.

2.3.1. Two different types of behaviour

We implement a discretization of the radial PML system (12) using fourth order finite elements (for details see Section 5.1, discretization of the interior domain). We choose $\Omega_{\text{int}} = B_1 := \{\mathbf{x} \in \mathbb{R}^2 : \|\mathbf{x}\| < 1\}$, $\Omega_{\text{pml}} = B_2 \setminus \overline{B_1}$ and an anisotropy with $\mathbf{A} = \text{diag}(1, 9)$. We use a piecewise constant damping with $\sigma_c = 20$ (cf. Assumption 3.3) and a time-harmonic source $f(t, \mathbf{x}) = 1200 \sin(10t) \exp\left(-200\|\mathbf{x}\|^2\right)$. The resulting problem is discretized in time with the help of the implicit Crank-Nicholson time-stepping scheme (with the time step $\tau = 0.02$) to rule out possible instabilities caused by a violated CFL condition. To reduce computational time we exploit the symmetry of the problem and simulate merely one quarter of the domain.

Figure 1a shows the energy $E(t) = \frac{1}{2}(\|\partial_t u^\sigma\|^2_{L^2(\mathbb{R}^2)} + \|\nabla u^\sigma\|^2_{L^2(\mathbb{R}^2)})$ of the time-domain solutions in Ω_{int} for different mesh sizes h. We observe that for the coarser meshes ($h = 0.2, 0.1$) the solution appears to be stable even for large computation times. For finer meshes ($h = 0.075, 0.05$) we observe an exponential growth of the energy (i.e., unstable solutions, see also Figure 2 for snapshots of the unstable time domain solution for $h = 0.075$). However, these instabilities occur at different times and with different exponential rates. These observations are confirmed by studying the eigenvalues of the eigenvalue problem corresponding to the Laplace transform of the system (12) where the Laplace parameter s is the unknown spectral parameter.

Figure 1b shows parts of the spectra of the eigenvalue problems corresponding to the time domain problems from Figure 1a. We observe that for the coarser meshes ($h = 0.2, 0.1$) all of the approximated eigenvalues have negative real part, which indicates stable time-domain solutions. The spectra computed using finer meshes contain eigenvalues with positive real parts which correspond to exponentially growing time-domain solutions. Note that the finer the discretization, the larger the maximal real part of the eigenvalues. This explains the different exponential growth rates in the time-domain experiments.

2.3.2. Discussion of the results

The numerical results above clearly show that PMLs are not unconditionally stable for anisotropic media. Ad hoc there seem to be two possible causes for the instability:

a) the untruncated, continuous system (12) is already unstable,

b) the instabilities are caused by the truncation and the discretization (in space and time).

As the instability worsens for finer discretizations, there seems to be little hope for stability for sufficiently fine discretizations. Next, we will argue that there exist some configurations where the solution to the untruncated, continuous system is stable, and some where instabilities already occur on the continuous level. Nonetheless, even in the configurations with stable continuous solutions, we will show the existence of an essential spectrum in $\mathbb{C}^+$ that causes discrete instabilities.

A similar behavior was already observed in [43] for Cartesian PMLs and anisotropies which are not aligned with the coordinate axes. Therein the authors exploit that for coarse meshes the discrete solutions are stable. Moreover they provide stability conditions on the mesh size. In the article at hand our goal is to construct a stable numerical method for arbitrarily fine discretizations.

3. Well-posedness and stability analysis of radial PMLs

In this section we argue that the instabilities observed in the previous section are not entirely numerical (the meaning of 'entirely' will become clear later). We call the problem (12), equipped with the right-hand side $\boldsymbol{f} := (f, f_v, \boldsymbol{f}_p, \boldsymbol{f}_q)$ and vanishing initial conditions,

- well-posed, if there exist m_t, m_s, C, a, $p \geq 0$, s.t. for each $\boldsymbol{f} \in H^{m_t}(\mathbb{R}^+; (H^{m_s}(\mathbb{R}^2))^6)$, with $\boldsymbol{f}(0) = \ldots = \partial_t^{m_t - 1}\boldsymbol{f}(0) = 0$, and for each $T > 0$, there exists a unique solution $u^\sigma \in L^\infty(0, T; L^2(\mathbb{R}^2))$, s.t.

$$\|u^\sigma\|_{L^\infty(0,T;L^2(\mathbb{R}^2))} \leq C\mathrm{e}^{aT}(1+T)^p \|\boldsymbol{f}\|_{H^{m_t}(0,T;H^{m_s}(\mathbb{R}^2))}. \tag{13}$$

- stable, if the above holds with $a = 0$.

We formulate the well-posedness and stability definitions for u^σ only, since the remaining unknowns can be expressed via u^σ in a unique way.

Remark 3.1. The vanishing initial conditions for $\boldsymbol{f}$ ensure that $\boldsymbol{f}$ can be continued to a causal function in $H^{m_t}(\mathbb{R}; (H^{m_s}(\mathbb{R}^2))^6)$.

Remark 3.2. In the above definition, we allow the support of the sources to lie inside the PMLs, even though in practical applications the starting radius of the PML should always be chosen to avoid this setting.

Since we are in the setting of radial PMLs, from now on we assume without loss of generality that

$$\mathbf{B} := \mathbf{A}^{-1} = \mathrm{diag}(\lambda_{\max}, \lambda_{\min}), \tag{14}$$

with $\lambda_{\max} \geq \lambda_{\min} > 0$. For simplicity, we will work with a piecewise constant absorption parameter σ.

Assumption 3.3. The absorption parameter σ satisfies $\sigma(r) = 0$ for $r < R_{\mathrm{pml}}$ and $\sigma(r) = \sigma_c > 0$ otherwise.

Some results will be valid for more general classes of σ, which will be made precise in their statements.

Theorem 3.4. *Let σ satisfy Assumption 3.3. Then:*

1. *The problem* (12) *is well-posed.*
2. *If for all $t > 0$, $\operatorname{supp} \boldsymbol{f}(t,.) \subset B_{r_*}$, where $r_* < R_{\mathrm{pml}}/\mu_*$, with*

$$\mu_* := \frac{\lambda_{\max} + \lambda_{\min}}{2\sqrt{\lambda_{\max}\lambda_{\min}}} \geq 1, \tag{15}$$

i.e., the source is supported sufficiently far away from the absorbing layer, then the bound (13) *holds with $a = 0$ and some $m_t, m_s, C, p \geq 0$.*

Proof. Statement 1 is proven in Section 3.2, Cor. 3.7, and Statement 2 in Section 3.3.2, Cor. 3.19. □

The above result shows that the source of the observed numerical instability of radial PMLs is definitely not due to a lack of well-posedness. On the other hand, at the continuous level, the solution to the PML system (12) is stable for a particular class of sources which are located sufficiently far away from the PML. Since such sources are very special (while, perhaps, being the only "interesting" sources for the application of the PMLs), this does not imply that the corresponding problem is stable. Indeed, instabilities manifest themselves at the discrete level, independently of the support of the source term, as illustrated in Section 2.3.1 (it is easily verified that in the setting of Section 2.3.1 $\mu_* = 5/3$ while $|f|$ is far smaller than machine precision outside of $B_{3/5}$, and thus the conditions of Theorem 3.4 are met).

A possible origin of time-domain instabilities is the presence of singularities in $\mathbb{C}^+$ of the Laplace transform $s \mapsto \hat{u}^\sigma(s) \in L^2(\mathbb{R}^2)$ of the time-domain solution u^σ. These singularities are related to the points s where the operator corresponding to (16) is not invertible. The existence of such a spectrum is stated in the following theorem (with the notation $\langle u, u^\dagger \rangle = \int_{\mathbb{R}^2} u(\mathbf{x})\overline{u^\dagger(\mathbf{x})}d\mathbf{x}$).

Theorem 3.5. *Let σ be non-decreasing and continuous for $r \geq R_{\mathrm{pml}}$ (not necessarily piecewise-constant). For $s \in \mathbb{C}$ let the sesquilinear form $a^s_\sigma(\cdot,\cdot)$ be defined by*

$$a^s_\sigma(u, u^\dagger) := \langle \mathbf{A}_\sigma \nabla u, \nabla u^\dagger \rangle + s^2 \langle \tilde{d}_\sigma d_\sigma u, u^\dagger \rangle, \quad u, u^\dagger \in H^1(\mathbb{R}^2). \tag{16}$$

Then there exists $s_0 \in \mathbb{C}^+$, s.t. the Riesz representation $\mathcal{A}_\sigma(s_0) \in \mathcal{L}(H^1(\mathbb{R}^2))$ of $a^{s_0}_\sigma(\cdot,\cdot)$ is not Fredholm. Therefore, the essential spectrum of $\mathcal{A}_\sigma(\cdot)$ in $\mathbb{C}^+$ (the set $s \in \mathbb{C}^+$ where $\mathcal{A}_\sigma(s)$ is not Fredholm) is non-empty.

This theorem is proven in Section 3.4. The above result implies that, in general, for suitably chosen sources, $s \mapsto \hat{u}^\sigma(s)$ is not $H^1(\mathbb{R}^2)$-holomorphic in $\mathbb{C}^+$ (see [42, p.365]). We believe that it is not $L^2(\mathbb{R}^2)$-holomorphic either. A theoretical justification to this is out of scope of the present article. This lack of analyticity then indicates that we cannot bound the time-domain solution $t \mapsto u^\sigma(t) \in L^2(\mathbb{R}^2)$ by a polynomial in time bound, uniformly for any admissible source $\boldsymbol{f}$.

3.1. A remark on the analysis

The sections that follow are dedicated to the proofs of Theorems 3.4 (Sections 3.2 and 3.3.2) and 3.5 (Section 3.4). A direct time-domain analysis of well-posedness and stability is quite complicated, and thus we will work using Laplace domain arguments. For this we consider the system (12), with non-vanishing sources $(f, f_v, \boldsymbol{f}_p, \boldsymbol{f}_q)$ in the right-hand side. We further rewrite it in the Laplace domain w.r.t. the unknown u^σ, more precisely, we replace (6) by:

$$s^2 \tilde{d}_\sigma d_\sigma \hat{u}^\sigma - \operatorname{div}_{r,\phi}(\mathbf{A}^\phi_\sigma \nabla_{r,\phi} \hat{u}^\sigma) = \hat{F}, \tag{17}$$

where $\hat{F} = D(s, d_\sigma(s), \tilde{d}_\sigma(s), \partial_x, \partial_y)(\hat{f}, \hat{f}_v, \hat{\boldsymbol{f}}_p, \hat{\boldsymbol{f}}_q)^\top$, with the operator D being defined as $D(a_1, a_2, a_3, a_4, a_5)$ $= \sum_{j=1}^{5} \boldsymbol{b}_j^\top a_j$, for some $\boldsymbol{b}_j \in \mathbb{R}^{6\times 1}$. Assuming that $\hat{F} \in L^2(\mathbb{R}^2)$, we will look for a solution of (17) belonging to $H^1(\mathbb{R}^2)$. In terms of the Laplace domain analysis, one can establish the following *sufficient* conditions:

- If there exists $\alpha > 0$, s.t. the solution $s \mapsto \hat{u}^\sigma(s)$ is an $L^2(\mathbb{R}^2)$-valued analytic function in $\mathbb{C}^+_\alpha$, and satisfies the following bound

$$\|\hat{u}^\sigma(s)\|_{L^2(\mathbb{R}^2)} \leq C \max(1, (\operatorname{Re} s)^{-m})(1+|s|)^p \|\hat{F}\|_{L^2(\mathbb{R}^2)}, \quad C > 0, \quad m, p \geq 0,$$

  then the corresponding time-domain problem is well-posed. See, e.g., [6] for more details.

- If the above holds true with $\alpha = 0$, the respective time-domain problem is also stable.

More details on this type of analysis can be found in the monograph by F.-J. Sayas [56]; it was used in the PML context in e.g. [19],[35], [6], [28], [8], [13], and also in the time-domain BIE community, cf., e.g., [5].

3.2. Radial PMLs are well-posed

Let us consider the problem (17) in the variational form and establish the following bound:

$$\|\hat{u}^\sigma(s)\|_{H^1(\mathbb{R}^2)} \leq C(1+|s|)^p \|\hat{F}\|_{H^{-1}(\mathbb{R}^2)}, \quad s \in \mathbb{C}^+_\alpha, \quad \alpha > 0. \tag{18}$$

Lemma 3.6. *Under Assumption 2.1, there exists $\alpha > 0$ depending on $\|\sigma\|_{L^\infty(\mathbb{R}^+)}, \|\tilde{\sigma}\|_{L^\infty(\mathbb{R}^+)}, \mathbf{A}$, such that $\operatorname{Re} a^s_\sigma(u, su) \geq \|su\|^2_{L^2(\mathbb{R}^2)} + \|\nabla u\|^2_{L^2(\mathbb{R}^2)}$ for all $s \in \mathbb{C}^+_\alpha$.*

Proof. The main idea of the proof is to use the fact that, as $|s| \to +\infty$, the sesquilinear form $a_\sigma(\cdot,\cdot)$ becomes close to the sesquilinear form without the PML (i.e., $a_0(\cdot,\cdot)$). First of all, remark that

$$\operatorname{Re}(s^2 \langle \tilde{d}_\sigma d_\sigma u, su\rangle) = |s|^2 \operatorname{Re} s \|u\|^2_{L^2(\mathbb{R}^2)} + |s|^2 \|(\tilde{\sigma}+\sigma)^{1/2} u\|^2_{L^2(\mathbb{R}^2)} + \operatorname{Re} s \|(\tilde{\sigma}\sigma)^{1/2} u\|^2_{L^2(\mathbb{R}^2)}. \tag{19}$$

For the remaining term, we use the definition of the matrix $\mathbf{A}_\sigma = \mathbf{J}_\sigma^{-1} \mathbf{A} \mathbf{J}_\sigma^{-\top} \det \mathbf{J}_\sigma$ as per (7), (8). In particular, for all $s \in \mathbb{C}^+_1$, with a constant C depending only on $\|\sigma\|_\infty, \|\tilde{\sigma}\|_\infty, \mathbf{A}$, we have that

$$|\langle (\mathbf{A}_\sigma - \mathbf{A}) \nabla u, s \nabla u \rangle| \leq C \|\nabla u\|^2_{L^2(\mathbb{R}^2)}, \tag{20}$$

because $\mathbf{A}_\sigma - \mathbf{A} = \mathcal{O}(|s|^{-1})$ as $|s| \to \infty$ (since $\mathbf{J}_\sigma = \Pi_\parallel + \Pi_\perp + O(|s|^{-1})$, as $|s| \to +\infty$). Therefore,

$$\begin{aligned} \operatorname{Re}\langle \mathbf{A}_\sigma \nabla u, s \nabla u \rangle &= \operatorname{Re}\langle (\mathbf{A}_\sigma - \mathbf{A}) \nabla u, s \nabla u \rangle + \operatorname{Re}\langle \mathbf{A} \nabla u, s \nabla u \rangle \\ &\geq \operatorname{Re} s \lambda^{-1}_{\max} \|\nabla u\|^2_{L^2(\mathbb{R}^2)} - C \|\nabla u\|^2_{L^2(\mathbb{R}^2)}, \end{aligned}$$

where in the last inequality we used (20). Finally, taking $\alpha = \lambda_{\max}(C+1)$, and combining the above lower bound with the identity (19), we arrive at the conclusion in the statement of the lemma. □

With the Lax-Milgram lemma, we conclude that the bound (18) holds true. This, together with the arguments of the extended version [7, Proposition 3.3] of [6], implies the following result.

Corollary 3.7. *The problem* (12) *is well-posed.*

3.3. Radial PMLs are stable if the source is located far away from the absorbing layer

All over this section we consider σ that satisfies Assumption 3.3, which is not necessary, but simplifies some computations. Moreover, we use the principal definition of the square root ($\operatorname{Re}\sqrt{z} > 0$, $z \in \mathbb{C}\backslash(-\infty, 0]$).

3.3.1. The fundamental solution of the PML problem (12) *in the Laplace domain and its properties*

Because the PML problem (12) is well-posed, its solution can be expressed with the help of the associated fundamental solution. Analytic expressions of such fundamental solutions in the time domain are difficult to obtain, cf. [24] for the Cartesian PMLs in two dimensions, and therefore we are going to work purely in the Laplace domain. First of all, as expected, the fundamental solution for the PML problem coincides with the fundamental solution of the original wave equation with the PML change of variables applied to it.

Proposition 3.8 (Fundamental solution of the PML problem)**.** *Let $\hat{F} \in L^2(\mathbb{R}^2)$, and let $s \in \mathbb{C}^+_\alpha$, where $\alpha > 0$ is sufficiently large. Then the unique solution $\hat{u}^\sigma \in H^1(\mathbb{R}^2)$ to* (17) *is given by*

$$\hat{u}^\sigma(s, \mathbf{x}) := \int_{\mathbb{R}^2} G_\sigma(s; \mathbf{x}, \mathbf{y}) \hat{F}(\mathbf{y}) d\mathbf{y}, \quad \mathbf{x} \in \mathbb{R}^2, \tag{21}$$

where G_σ is a fundamental solution of the PML problem (17) *defined by*

$$G_\sigma(s; \mathbf{x}, \mathbf{y}) := \frac{1}{2\pi\sqrt{\det \mathbf{A}}} K_0\left(s\sqrt{(\mathbf{x}_\sigma(s) - \mathbf{y}_\sigma(s))^\top \mathbf{B}(\mathbf{x}_\sigma(s) - \mathbf{y}_\sigma(s))}\right), \qquad \mathbf{B} = \mathbf{A}^{-1}, \tag{22}$$

and $\mathbf{y}_\sigma$ is defined similarly to $\mathbf{x}_\sigma$ (see (5)*). In the above K_0 is the McDonald function, defined as in [25, 10.25], with the branch cut $\mathbb{R}^-_0 := \{t \in \mathbb{R} : t \leq 0\}$.*

The proof of this result can be found in the extended version of the present article [34].To show how the properties of the fundamental solution in the Laplace domain translate to time-domain bounds on $u^\sigma(t, \mathbf{x})$, we will study the behaviour of $s \mapsto G_\sigma(s; \mathbf{x}, \mathbf{y})$ in the complex plane.

Remark 3.9. As we will see further, the use of the fundamental solution enables us to show stronger stability results than the ones provided by the study of the PML sesquilinear form in Section 3.2.

Properties of $s \mapsto (\mathbf{x}_\sigma - \mathbf{y})^\top \mathbf{B}(\mathbf{x}_\sigma - \mathbf{y})$. First of all, we are interested in the analyticity of the argument of K_0 in Proposition 3.8. Clearly, the case $\mathbf{x}, \mathbf{y} \in \Omega_{\text{int}}$ reduces to the analysis of the fundamental solution without the PML. The case $\mathbf{x}, \mathbf{y} \in \Omega^\infty_{\text{pml}}$ is less interesting, since in applications the source $\hat{F}$ in (21) is supported inside Ω_{int}. Therefore, we fix $\mathbf{x} \in \Omega^\infty_{\text{pml}}$ and $\mathbf{y} \in \Omega_{\text{int}}$, and introduce (recall) the following definitions:

$$d_\sigma(s) = 1 + \frac{\sigma_c}{s}, \quad \boldsymbol{c}(\hat{\mathbf{x}}, \mathbf{y}) := R_{\text{pml}}\hat{\mathbf{x}} - \mathbf{y}, \quad \xi(\|\mathbf{x}\|) := \|\mathbf{x}\| - R_{\text{pml}}. \tag{23}$$

In the above and what follows, we denote by $\hat{\mathbf{x}} := \frac{\mathbf{x}}{\|\mathbf{x}\|}$. Remark that for $\mathbf{x}$ inside the PMLs $d_\sigma(s, \|\mathbf{x}\|)$ is constant, therefore we use the notation $d_\sigma(s)$ instead. With these definitions, we have in particular that

$$\mathbf{x}_\sigma = \left(\|\mathbf{x}\| + \frac{\sigma_c}{s}(\|\mathbf{x}\| - R_{\text{pml}})\right)\hat{\mathbf{x}} = \left(1 + \frac{\sigma_c}{s}\right)\xi(\|\mathbf{x}\|)\hat{\mathbf{x}} + R_{\text{pml}}\hat{\mathbf{x}}.$$

Therefore, the quantity that we wish to study can be rewritten as follows:

$$\begin{aligned} h_\sigma(s; \mathbf{x}, \mathbf{y}) := (\mathbf{x}_\sigma - \mathbf{y})^\top \mathbf{B}(\mathbf{x}_\sigma - \mathbf{y}) &= (\boldsymbol{c} + \hat{\mathbf{x}}\xi d_\sigma)\mathbf{B}(\boldsymbol{c} + \hat{\mathbf{x}}\xi d_\sigma) \\ &= \boldsymbol{c}^\top \mathbf{B}\boldsymbol{c} + d_\sigma^2(s)\xi^2 \hat{\mathbf{x}}^\top \mathbf{B}\hat{\mathbf{x}} + 2d_\sigma(s)\xi \boldsymbol{c}^\top \mathbf{B}\hat{\mathbf{x}}. \end{aligned} \tag{24}$$

With $\hat{\boldsymbol{c}} = \boldsymbol{c}\|\boldsymbol{c}\|^{-1}$, we define the following quantities:

$$\gamma_{11}(\hat{\mathbf{x}}, \mathbf{y}) := \hat{\boldsymbol{c}}^\top \mathbf{B}\hat{\boldsymbol{c}}, \quad \gamma_{22}(\hat{\mathbf{x}}) := \hat{\mathbf{x}}^\top \mathbf{B}\hat{\mathbf{x}}, \quad \text{and} \quad \gamma_{12}(\hat{\mathbf{x}}, \mathbf{y}) := \hat{\mathbf{x}}^\top \mathbf{B}\hat{\boldsymbol{c}}. \tag{25}$$

This allows us to rewrite $h_\sigma(s; \mathbf{x}, \mathbf{y})$ as follows:

$$h_\sigma = \|\boldsymbol{c}\|^2\gamma_{11} + 2d_\sigma\xi\|\boldsymbol{c}\|\gamma_{12} + d_\sigma^2\xi^2\gamma_{22}.$$

An illustration to the notation (23) is given in Figure 3. We are interested in the behaviour of h_σ for $s \in \mathbb{C}^+$ and $\xi \geq 0$, in particular in the points where $h_\sigma(s; \mathbf{x}, \mathbf{y}) \in \mathbb{R}^-_0$, so that the argument of the fundamental solution is not analytic. Remark that for $s \in \mathbb{C}^+$ s.t. $h_\sigma(s; \mathbf{x}, \mathbf{y}) \notin \mathbb{R}^-_0$, it also holds that $s\sqrt{h_\sigma(s; \mathbf{x}, \mathbf{y})} \notin (-\infty, 0]$, and the fundamental solution is well-defined in these points. We then have the following result.

Lemma 3.10. *Let $\mathbf{x} \in \Omega^\infty_{\text{pml}}$ and $\mathbf{y} \in \Omega_{\text{int}}$ be fixed. Then $h_\sigma(s; \mathbf{x}, \mathbf{y}) \leq 0$ if and only if $s \in \mathbb{C}^+$ is s.t. the following two conditions hold true:*

$$(a)\ \operatorname{Re} d_\sigma(s) = -\frac{\|R_{\text{pml}}\hat{\mathbf{x}} - \mathbf{y}\|}{\|\mathbf{x}\| - R_{\text{pml}}} \frac{\gamma_{12}(\hat{\mathbf{x}}, \mathbf{y})}{\gamma_{22}(\hat{\mathbf{x}})}; \quad (b)\ \cos^2(\arg d_\sigma(s)) \leq \frac{\gamma_{12}^2(\hat{\mathbf{x}}, \mathbf{y})}{\gamma_{11}(\hat{\mathbf{x}}, \mathbf{y})\gamma_{22}(\hat{\mathbf{x}})}. \tag{26}$$

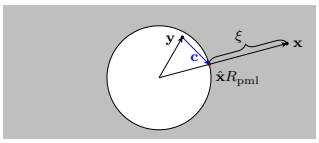

Figure 3: An illustration to the notation (23). The PML medium is marked in gray and the physical medium in white.

Proof. Computing the real and imaginary part of h_σ explicitly yields with $d_{\sigma,r} := \operatorname{Re} d_\sigma$, $d_{\sigma,i} := \operatorname{Im} d_\sigma$ and the notation from (25)

$$h_\sigma = \|\boldsymbol{c}\|^2\gamma_{11} + 2d_{\sigma,r}\xi\|\boldsymbol{c}\|\gamma_{12} + \left(d_{\sigma,r}^2 - d_{\sigma,i}^2\right)\xi^2\gamma_{22} + 2id_{\sigma,i}\xi\left(\|\boldsymbol{c}\|\gamma_{12} + d_{\sigma,r}\xi\gamma_{22}\right). \tag{27}$$

Thus $\operatorname{Im} h_\sigma(s;\mathbf{x},\mathbf{y}) = 0$ if and only if $d_{\sigma,i} = 0$ or (a) is satisfied, i.e.,

$$d_{\sigma,r}(s) = -\frac{\|\boldsymbol{c}\|}{\xi}\frac{\gamma_{12}}{\gamma_{22}}. \tag{28}$$

The identity $d_{\sigma,i} = 0$ is equivalent to $s \in \mathbb{R}^+$ which implies $h_\sigma(s;\mathbf{x},\mathbf{y}) > 0$. This leaves us with (a). For $h_\sigma(s;\mathbf{x},\mathbf{y}) \leq 0$, it is further necessary that

$$\|\boldsymbol{c}\|^2\gamma_{11} + 2d_{\sigma,r}\xi\|\boldsymbol{c}\|\gamma_{12} + (d_{\sigma,r}^2 - d_{\sigma,i}^2)\xi^2\gamma_{22} \leq 0.$$

Re-expressing ξ via $d_{\sigma,r}$ from (28) (or (26)(a)) yields

$$\gamma_{11} - 2\frac{\gamma_{12}^2}{\gamma_{22}} + d_{\sigma,r}^{-2}(d_{\sigma,r}^2 - d_{\sigma,i}^2)\frac{\gamma_{12}^2}{\gamma_{22}} \leq 0.$$

This can be rewritten as

$$\frac{d_{\sigma,i}^2}{d_{\sigma,r}^2} + 1 \geq \frac{\gamma_{11}\gamma_{22}}{\gamma_{12}^2}. \tag{29}$$

The above is equivalent to the condition (26)(b). □

To understand the statement of Lemma 3.10, remark that the condition (b) is a condition on a 'source' point $\mathbf{y}$ and on the direction $\hat{\mathbf{x}} \in \mathbb{S}^2$. The condition (a) is more involved, and involves the distance between the point $\mathbf{x}$ inside the PML and the interface between the PML and the physical media.

Let us now study the validity of the conditions (a), (b) for arbitrary points $\mathbf{x} \in \Omega_{\text{pml}}^{\infty}$ and $\mathbf{y} \in \Omega_{\text{int}}$. It appears that the condition (b) always holds true for some $s \in \mathbb{C}^+$ and almost all directions $\hat{\mathbf{x}}$.

Lemma 3.11. *Let $\mathbf{y} \in \Omega_{\text{int}}$ and $\hat{\mathbf{x}} \in \mathbb{S}^2$ be s.t. $\gamma_{12}(\hat{\mathbf{x}},\mathbf{y}) \neq 0$. Then there exists $s \in \mathbb{C}^+$, s.t. the condition (b) in* (26) *holds true.*

Proof. First, the right-hand side of (b) in (26) is strictly positive. Next, remark that $s \mapsto d_\sigma(s) = 1 + \frac{\sigma_c}{s}$ is a bijection from $\mathbb{C}^+$ to $\mathbb{C}_1^+$. Thus, $s \mapsto \arg d_\sigma(s)$ takes all the values in $\left(-\frac{\pi}{2},\frac{\pi}{2}\right)$, hence the conclusion. □

The validity of the condition (a), however, depends on whether the medium is isotropic or anisotropic. In particular, for isotropic media, the condition (a) never holds true, and we have that $h_\sigma(s;\mathbf{x},\mathbf{y}) \notin \mathbb{R}_0^-$.

Lemma 3.12. *For the isotropic medium ($\mathbf{B} = a\,\mathrm{Id}$, $a > 0$), for all $\hat{\mathbf{x}} \in \mathbb{S}^2$ and $\mathbf{y} \in \Omega_{\text{int}}$, it holds that $\gamma_{12} = \gamma_{12}(\hat{\mathbf{x}},\mathbf{y}) > 0$. Therefore, for all $s \in \mathbb{C}^+$, $h_\sigma(s;\mathbf{x},\mathbf{y}) \notin \mathbb{R}_0^-$.*

Proof. Since for isotropic media $\mathbf{B} = a\,\mathrm{Id}$, $a > 0$, we have that

$$\operatorname{sign}\gamma_{12}(\hat{\mathbf{x}},\mathbf{y}) = \operatorname{sign}\left(\hat{\mathbf{x}}^\top(R_{\text{pml}}\hat{\mathbf{x}} - \mathbf{y})\right) = \operatorname{sign}\left(\hat{\mathbf{x}}^\top\boldsymbol{c}\right).$$

The condition $\|\mathbf{y}\| < R_{\text{pml}}$ is equivalent to $\|R_{\text{pml}}\hat{\mathbf{x}} - \boldsymbol{c}\|^2 < R_{\text{pml}}^2$, which, after straightforward computations yields $\|\boldsymbol{c}\|^2 - 2R_{\text{pml}}\hat{\mathbf{x}}^\top\boldsymbol{c} < 0$. Thus $\hat{\mathbf{x}}^\top\boldsymbol{c} > \|\boldsymbol{c}\|^2/(2R_{\text{pml}}) > 0$ and hence $\gamma_{12}(\hat{\mathbf{x}},\mathbf{y}) > 0$. Since the left hand-side of (26)(a) is always positive, we conclude with Lemma 3.10. □

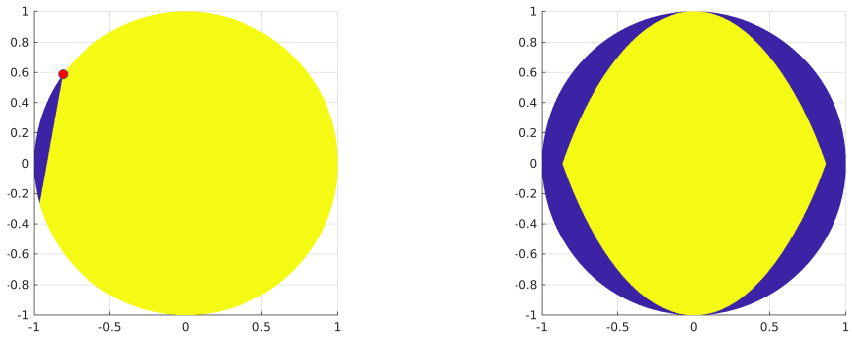

Figure 4: Left: the quantity $\operatorname{sign}\gamma_{12}(\hat{\mathbf{x}},\mathbf{y})$ as defined in (25) depending on $\mathbf{y}\in B(0,1)$, for a fixed $\mathbf{x}=(\cos 0.8\pi,\sin 0.8\pi)$, $R_{\mathrm{pml}}=1$. In dark blue we mark $\mathbf{y}$, s.t. $\operatorname{sign}\gamma_{12}(\hat{\mathbf{x}},\mathbf{y})=-1$, while in yellow $\mathbf{y}$ with $\operatorname{sign}\gamma_{12}(\hat{\mathbf{x}},\mathbf{y})=1$. The point $\mathbf{x}$ is marked in red. Right: the dependence of the quantity $\min_{\hat{\mathbf{x}}\in\mathbb{S}^2}\operatorname{sign}\gamma_{12}(\hat{\mathbf{x}},\mathbf{y})$ on $\mathbf{y}$ (with yellow marking positive values and blue negative ones). In all the experiments, the matrix $\mathbf{B}=\operatorname{diag}(1,1/4)$.

For an anisotropic medium, the above result for the sign of $\gamma_{12}(\hat{\mathbf{x}},\mathbf{y})$ does not hold true. Indeed,

$$\operatorname{sign}\gamma_{12}(\hat{\mathbf{x}},\mathbf{y})=\operatorname{sign}\left(\hat{\mathbf{x}}^\top\mathbf{B}\boldsymbol{c}\right),$$

and the positivity of $\hat{\mathbf{x}}^\top\boldsymbol{c}$ does not imply that the above quantity is positive. This is illustrated in Figure 4.

Remark 3.13. It is possible to prove that when eigenvalues of $\mathbf{B}$ differ, i.e. $\lambda_{\min}\neq\lambda_{\max}$, then there always exists $\mathbf{y}\in\Omega_{\mathrm{int}}$ and a direction $\hat{\mathbf{x}}_0$, s.t. $\gamma_{12}(\hat{\mathbf{x}}_0,\mathbf{y})<0$.

The condition on the sign of γ_{12} is of utmost importance. Indeed, we show below that if there exists a direction $\hat{\mathbf{x}}_0$ and the point $\mathbf{y}\in\Omega_{\mathrm{int}}$, s.t. $\gamma_{12}(\hat{\mathbf{x}}_0,\mathbf{y})<0$, the condition (a) of Lemma 3.10 holds necessarily true for some $s\in\mathbb{C}^+$ and $\mathbf{x}\in\Omega^\infty_{\mathrm{pml}}$.

Lemma 3.14. *Assume that there exist $\hat{\mathbf{x}}_0\in\mathbb{S}^2$ and $\mathbf{y}\in\Omega_{\mathrm{int}}$, s.t. $\gamma_{12}(\hat{\mathbf{x}}_0,\mathbf{y})<0$. Then for any $s\in\mathbb{C}^+$, the condition (a) of (26) holds true for $\mathbf{x}\in\Omega^\infty_{\mathrm{pml}}$ defined by $\mathbf{x}=\rho\hat{\mathbf{x}}_0$ with*

$$\rho=R_{\mathrm{pml}}-\|R_{\mathrm{pml}}\hat{\mathbf{x}}_0-\mathbf{y}\|\frac{\gamma_{12}(\hat{\mathbf{x}}_0,\mathbf{y})}{\operatorname{Re}d_\sigma(s)\gamma_{22}(\hat{\mathbf{x}}_0)}R_{\mathrm{pml}}>R_{\mathrm{pml}}.$$

The proof of this lemma is left to the reader. It also implies the following positive result.

Corollary 3.15. *Let $\mathbf{y}\in\Omega_{\mathrm{int}}$. If $\gamma_{12}(\hat{\boldsymbol{z}},\mathbf{y})\geq 0$ for all $\hat{\boldsymbol{z}}\in\mathbb{S}^2$, then $h_\sigma(s;\mathbf{x},\mathbf{y})\notin\mathbb{R}_0^-$ for all $s\in\mathbb{C}^+$.*

Fig. 4 indicates that for $\mathbf{y}$ located sufficiently far from the boundary of the PML, it holds that $\gamma_{12}(\hat{\boldsymbol{z}},\mathbf{y})>0$ for all $\hat{\boldsymbol{z}}\in\mathbb{S}^2$. This is quantified below.

Lemma 3.16. *Let μ_* be like in (15). For all $\hat{\boldsymbol{z}}\in\mathbb{S}^2$ and $\mathbf{y}\in\Omega_{\mathrm{int}}$ s.t. $\|\mathbf{y}\|<R_{\mathrm{pml}}/\mu_*$, the function $\mathbb{S}^2\ni\hat{\boldsymbol{z}}\mapsto\gamma_{12}(\hat{\boldsymbol{z}},\mathbf{y})$ is strictly positive.*

This implies that for such $\mathbf{y}$, the function $h_\sigma(s;\mathbf{x},\mathbf{y})\in\mathbb{C}\setminus\mathbb{R}_0^-$ for all $s\in\mathbb{C}^+$ and $\mathbf{x}\in\Omega^\infty_{\mathrm{pml}}$. Also, for all such $\mathbf{y}$ and all $\mathbf{x}\in\Omega^\infty_{\mathrm{pml}}$, the function $\mathbb{C}^+\ni s\mapsto G_\sigma(s;\mathbf{x},\mathbf{y})$ is analytic.

Proof. By Corollary 3.15, to have that $h_\sigma(s;\mathbf{x},\mathbf{y})\in\mathbb{C}\setminus\mathbb{R}_0^-$ it is sufficient to ensure that $\mathbf{y}$ is s.t. $\mathbb{S}^2\ni\hat{\boldsymbol{z}}\mapsto\gamma_{12}(\hat{\boldsymbol{z}},\mathbf{y})$ is strictly positive. We have that

$$\operatorname{sign}\gamma_{12}(\hat{\boldsymbol{z}},\mathbf{y})=\operatorname{sign}\left(R_{\mathrm{pml}}\hat{\boldsymbol{z}}^\top\mathbf{B}\hat{\boldsymbol{z}}-\|\mathbf{y}\|\hat{\boldsymbol{z}}^\top\mathbf{B}\hat{\mathbf{y}}\right).$$

By straighforward calculations carried out in [34, Lemma C.1], for any $\hat{\boldsymbol{z}}_1$, $\hat{\boldsymbol{z}}_2\in\mathbb{S}^2$,

$$\left|\frac{\hat{\boldsymbol{z}}_1^\top\mathbf{B}\hat{\boldsymbol{z}}_2}{\hat{\boldsymbol{z}}_1^\top\mathbf{B}\hat{\boldsymbol{z}}_1}\right|\leq\mu_*,$$

where μ_* is defined as in the statement of the present lemma. Then it follows immediately that $\mathbb{S}^2 \ni \hat{\boldsymbol{z}} \mapsto \gamma_{12}(\hat{\boldsymbol{z}}, \mathbf{y}) > 0$. The analyticity of $s \mapsto G_\sigma(s; \mathbf{x}, \mathbf{y})$ follows then from $h_\sigma(s; \mathbf{x}, \mathbf{y}) \in \mathbb{C} \setminus \mathbb{R}_0^-$. Indeed, remark first of all that $z \mapsto K_0(z)$ is analytic on $\mathbb{C} \setminus \mathbb{R}_-$, and therefore, it is sufficient to check that $\arg s\sqrt{h_\sigma(s; \mathbf{x}, \mathbf{y})} \in (-\pi, \pi)$, for all $s \in \mathbb{C}^+$. This follows from $\arg \sqrt{h_\sigma(s; \mathbf{x}, \mathbf{y})} \in (-\pi/2, \pi/2)$. □

In what follows, we will need a finer result on $h_\sigma(s; \mathbf{x}, \mathbf{y})$, summarized in the following lemma.

Lemma 3.17. *Let* $\mathbf{y}$ *be s.t.* $\|\mathbf{y}\| \le R_{\rm pml}/\mu_* - \delta$, *where* μ_* *is like in* (15) *and* $\delta > 0$. *There exists* $C > 0$, *which depends only on* $R_{\rm pml}$, *the matrix* $\mathbf{B}$ *and* $\delta > 0$, *s.t. for all* $s \in \mathbb{C}^+$, *we have that,*

$$\operatorname{Re}(s\sqrt{h_\sigma(s; \mathbf{x}, \mathbf{y})}) \ge C \operatorname{Re} s \|\mathbf{x}\|, \quad \text{for } \|\mathbf{x}\| \ge R_{\rm pml}.$$

Proof. We start with the identity $\operatorname{Re}(s\sqrt{h_\sigma}) = \operatorname{Re} s \operatorname{Re}\sqrt{h_\sigma} - \operatorname{Im} s \operatorname{Im}\sqrt{h_\sigma}$. Let us first prove that $\operatorname{Im}\sqrt{h_\sigma}$ is of the same sign as $-\operatorname{Im} s$. For this let us recall that by (27)

$$\operatorname{Im} h_\sigma(s; \mathbf{x}, \mathbf{y}) = 2 \operatorname{Im} d_\sigma(s) \left(\xi \|\mathbf{x} - \mathbf{y}\| \gamma_{12} + \operatorname{Re} d_\sigma(s) \xi^2 \gamma_{22}\right),$$

and as $\gamma_{12} \ge 0$ (cf. Lemma 3.16) and $\operatorname{Re} d_\sigma(s) > 0$, we conclude that $\operatorname{sign} \operatorname{Im} h_\sigma(s; \mathbf{x}, \mathbf{y}) = \operatorname{sign} \operatorname{Im} d_\sigma(s) = \operatorname{sign} \operatorname{Im}(\sigma/s) = -\operatorname{sign} \operatorname{Im} s$ if $\xi \neq 0$, and $\operatorname{Im} h_\sigma(s; \mathbf{x}, \mathbf{y}) = 0$ otherwise. Therefore,

$$\operatorname{Re}(s\sqrt{h_\sigma(s; \mathbf{x}, \mathbf{y})}) \ge \operatorname{Re} s \operatorname{Re}\sqrt{h_\sigma(s; \mathbf{x}, \mathbf{y})}. \tag{30}$$

Let us now define $H \colon \mathbb{C}^+ \times \mathbb{C}^2 \times \mathbb{R}^2 \to \mathbb{C}$ by $H(s; \mathbf{x}, \mathbf{y}) := h_\sigma(s; \tilde{d}_\sigma^{-1}\mathbf{x}, \mathbf{y})$, so that $H(s; \mathbf{x}_\sigma, \mathbf{y}) = h_\sigma(s; \mathbf{x}, \mathbf{y})$, see the expression (24). For $(\mathbf{x}_\sigma, \mathbf{y})$ belonging to a compact set K, $\operatorname{Re} H(s; \mathbf{x}_\sigma, \mathbf{y}) > c_K > 0$, since $H(s; \mathbf{x}_\sigma, \mathbf{y}) = h_\sigma(s; \mathbf{x}, \mathbf{y})$ does not vanish. For large $\|\mathbf{x}_\sigma\| \to +\infty$, we have that, uniformly in $\|\mathbf{y}\| \le R_{\rm pml}/\mu_* - \delta$,

$$\sqrt{H(s; \mathbf{x}_\sigma, \mathbf{y})} = \sqrt{\mathbf{x}_\sigma^\top \mathbf{B} \mathbf{x}_\sigma}\,(1 + o(1)) = \left(1 + \frac{\sigma_c}{s}\right)\sqrt{\mathbf{x}^\top \mathbf{B} \mathbf{x}}\,(1 + o(1)).$$

We then have

$$\operatorname{Re}\left(1 + \frac{\sigma_c}{s}\right)\sqrt{\mathbf{x}^\top \mathbf{B} \mathbf{x}} \ge \sqrt{\lambda_{\min}}\|\mathbf{x}\|,$$

which yields the result in the statement of the lemma. □

3.3.2. Proof of Theorem 3.4.(2)

This section is dedicated to proving that radial PMLs for anisotropic media are stable, as long as the support of the source is sufficiently separated from the PML. We start with the following auxiliary result.

Lemma 3.18 (The source far from the PML)**.** *Let* $r_* := R_{\rm pml}/\mu_* - \delta$, *where* μ_* *is defined in* (15) *and* $\delta > 0$. *We have the following bound for all* $s \in \mathbb{C}^+$*:*

$$\int_{\mathbb{R}^2} \int_{B(0, r_*)} |G_\sigma(s; \mathbf{x}, \mathbf{y})|^2 d\mathbf{y}\, d\mathbf{x} \le C \max\left(1, \left(\frac{1}{\operatorname{Re} s}\right)^2\right), \tag{31}$$

where the constant C *depends only on* $R_{\rm pml}$, δ, *and the matrix* $\mathbf{B}$.

Proof. We split the integral in the left-hand side of (31) as $I_0 + I_\sigma$, where

$$I_0 = \int_{\Omega_{\rm int}} \int_{B(0, r_*)} |G_\sigma(s; \mathbf{x}, \mathbf{y})|^2 d\mathbf{y}\, d\mathbf{x}, \quad I_\sigma = \int_{\Omega_{\rm pml}^\infty} \int_{B(0, r_*)} |G_\sigma(s; \mathbf{x}, \mathbf{y})|^2 d\mathbf{y}\, d\mathbf{x}.$$

Next, let us bound the above two integrals by the right-hand side of (31). We start with a less classical one, namely I_σ, and next argue that the corresponding estimate can be extended to I_0.

Step 1. A bound on I_σ. Recall an explicit expression for G_σ given in Proposition 3.8. We start by bounding G_σ. First of all, remark that the function $z \mapsto K_0(z)$ is analytic in $\mathbb{C} \setminus \mathbb{R}^-$. By [25, 10.32.9], it holds that

$$K_0(z) = \int_0^\infty \mathrm{e}^{-z\cosh t} dt, \quad z \in \mathbb{C}^+, \text{ therefore } |K_0(z)| \leq |K_0(\operatorname{Re} z)| \text{ in } \mathbb{C}^+.$$

Moreover, from the above representation it follows that the function $\mathbb{R}^+ \ni \lambda \mapsto K_0(\lambda)$ is decreasing. Therefore, by the above considerations and Lemma 3.17, we have that

$$|G_\sigma(s;\mathbf{x},\mathbf{y})| \leq \frac{1}{2\pi\sqrt{\det \mathbf{A}}} |K_0(\operatorname{Re}(s\sqrt{h_\sigma(s;\mathbf{x},\mathbf{y})}))| \leq \frac{1}{2\pi\sqrt{\det \mathbf{A}}} |K_0(C \operatorname{Re} s \|\mathbf{x}\|)|.$$

This allows to rewrite

$$\begin{aligned} I_\sigma &\leq \frac{1}{4\pi^2 \det \mathbf{A}} \int_{\Omega^\infty_{\mathrm{pml}}} \int_{B(0,r_*)} |K_0(C \operatorname{Re} s \|\mathbf{x}\|)|^2 d\mathbf{x} d\mathbf{y} \leq \frac{r_*^2}{4\pi \det \mathbf{A}} \int_{\Omega^\infty_{\mathrm{pml}}} |K_0(C \operatorname{Re} s \|\mathbf{x}\|)|^2 d\mathbf{x} \\ &\leq \frac{r_*^2}{4\pi \det \mathbf{A}} \int_{\mathbb{R}^2} |K_0(C \operatorname{Re} s \|\mathbf{x}\|)|^2 d\mathbf{x} = \frac{r_*^2}{4\pi (\operatorname{Re} s)^2 C^2 \det \mathbf{A}} \int_{\mathbb{R}^2} |K_0(\|\mathbf{x}\|)|^2 d\mathbf{x}. \end{aligned}$$

By [25, 10.30], for any $a > 0$ (where the constant $C_a > 0$ in the bound depends on $a > 0$), it holds that

$$|K_0(z)| \leq C_a \begin{cases} \max(1, |\log|z||) & |z| < a, \\ \mathrm{e}^{-\operatorname{Re} z}, & |z| \geq a. \end{cases} \tag{32}$$

The above bound shows that $\mathbf{x} \mapsto K_0(\|\mathbf{x}\|) \in L^2(\mathbb{R}^2)$. This yields the desired bound for I_σ.
Step 2. A bound on I_0. First, we remark that $I_0 \leq \|G_\sigma(s;.,.)\|^2_{L^2(\Omega_{\mathrm{int}} \times \Omega_{\mathrm{int}})}$. Next, recall that for $\mathbf{x}, \mathbf{y} \in \Omega_{\mathrm{int}}$, it holds that $G_\sigma(s;\mathbf{x},\mathbf{y}) = \frac{1}{2\pi\sqrt{\det \mathbf{A}}} K_0(s\|\mathbf{x}-\mathbf{y}\|_{\mathbf{B}})$, where $\|\mathbf{x}\|^2_{\mathbf{B}} = \mathbf{x}^\top \mathbf{B} \mathbf{x}$. Like before, we conclude that $|G_\sigma(s;\mathbf{x},\mathbf{y})| \leq \frac{1}{2\pi\sqrt{\det \mathbf{A}}} |K_0(\operatorname{Re} s \|\mathbf{x}-\mathbf{y}\|_{\mathbf{B}})|$. The remainder of the proof is left to the reader. □

We immediately obtain from the above the following corollary, which is the principal result of this section.

Corollary 3.19. *Consider the PML problem* (12) *with the source terms* $(f, f_v, \boldsymbol{f}_p, \boldsymbol{f}_q) \in L^2(\mathbb{R}^+; L^2(\mathbb{R}^2))$ *and vanishing initial conditions. Let the source term F, defined after* (17)*, be s.t. $F \in H^1(\mathbb{R}^+; L^2(\mathbb{R}^2))$, and $F(0) = 0$. Let, additionally, for all $t > 0$,* $\operatorname{supp} F(t) \subset B(0, r_*)$*, with r_* being like in Lemma 3.18.*

Then, for all $T > 0$, (12) *admits a unique solution $u^\sigma \in L^\infty(0,T;L^2(\mathbb{R}^2))$. This solution satisfies the following bound, with the constant $C > 0$ depending on r_*, R_{pml} and the matrix $\mathbf{B}$, but independent of σ_c:*

$$\|u^\sigma\|_{L^\infty(0,T;L^2(\mathbb{R}^2))} \leq C T^{1/2}(1+T) \|F\|_{H^1(0,T;L^2(\mathbb{R}^2))}.$$

Proof. First of all, as shown in Section 3.2, the solution to the PML problem is unique, and its Fourier-Laplace transform is given by, cf. Proposition 3.8,

$$\hat{u}^\sigma(s,\mathbf{x}) = \int_{\mathbb{R}^2} G_\sigma(s,\mathbf{x},\mathbf{y}) \hat{F}(s,\mathbf{y}) d\mathbf{y}. \tag{33}$$

We remark that for $\|\mathbf{x}\| < R_{\mathrm{pml}}$, $\hat{u}^\sigma(s,\mathbf{x}) = \hat{u}(s,\mathbf{x})$ (i.e., equal to the solution without the PML), and therefore is $L^2(\Omega_{\mathrm{int}})$-valued analytic function. As for the $\Omega^\infty_{\mathrm{pml}}$, let us fix $\mathbf{x} \in \Omega^\infty_{\mathrm{pml}}$, $\mathbf{y} \in B(0, r_*)$. Remark that $s \mapsto G_\sigma(s;\mathbf{x},\mathbf{y})$ can be extended by analyticity to $\mathbb{C}^+$. With the Lebesgue's dominated convergence theorem, it is possible to prove that $s \mapsto \hat{u}^\sigma(s) \in L^2(\mathbb{R}^2 \setminus B(0, R_{\mathrm{pml}}))$ is analytic in $\mathbb{C}^+$ (recall that analyticity amounts to weak analyticity, cf. [42, Chapter 7]). With the Cauchy-Schwarz inequality and Lemma 3.18,

$$\text{for all } s \in \mathbb{C}^+, \quad \|\hat{u}^\sigma(s)\|_{L^2(\mathbb{R}^2)} \leq C \|\hat{F}(s)\|_{L^2(\mathbb{R}^2)} \max(1, (\operatorname{Re} s)^{-1}), \quad C > 0.$$

In the above the constant C is independent of s. It remains to use the Plancherel inequality and the causality argument to obtain the desired stability bound, see [8, Theorem 4.1], [13, Theorem 2.11]. □

3.4. The origin of the instabilities: presence of the essential spectrum for small frequencies

The goal of this section is to prove Theorem 3.5. Its proof relies on the following lemma, which shows that the principal symbol of the PDE associated to the frequency-domain PML problem (6) may vanish for some $s_0 \in \mathbb{C}^+$ and $\mathbf{x}_0 \in \Omega^\infty_{\mathrm{pml}}$. As a corollary, the underlying operator $\mathcal{A}_\sigma$ is no longer Fredholm. To prove this result, it is sufficient to show the existence of a singular sequence, i.e., $(v_n)_{n\in\mathbb{N}} \subset H^1(\mathbb{R}^2)$, s.t. $\|v_n\|_{H^1(\mathbb{R}^2)} = 1$, (v_n) does not have a convergent subsequence, and $\|\mathcal{A}_\sigma(s)v_n\| \to 0$, see [30, Thm. 3.3]. In order to construct such a sequence, we will use (truncated) plane waves $\mathrm{e}^{in\boldsymbol{\xi}_0\cdot\mathbf{x}}$, with a well-chosen phase $\boldsymbol{\xi}_0$. The choice of the phase is given by the following lemma.

Lemma 3.20. *Let σ be continuous for $r > R_{\mathrm{pml}}$ and non-decreasing (not necessarily constant). Let additionally $\lambda_{\max} \neq \lambda_{\min}$. Then there exist $\mathbf{x}_0 \in \Omega^\infty_{\mathrm{pml}}$, $s_0 \in \mathbb{C}^+$ and $\boldsymbol{\xi}_0 \in \mathbb{R}^2 \setminus \{0\}$ such that $\boldsymbol{\xi}_0^\top \mathbf{A}_\sigma(s_0, \mathbf{x}_0)\boldsymbol{\xi}_0 = 0$.*

Proof. Remark that it is sufficient to show the existence of $\boldsymbol{\xi} \neq 0$ s.t. $\boldsymbol{\xi}^\top \mathbf{A}^\phi_\sigma(s_0, \mathbf{x}_0)\boldsymbol{\xi} = 0$, as $\mathbf{A}_\sigma = \mathbf{R}_\phi \mathbf{A}^\phi_\sigma \mathbf{R}_\phi^\top$, see Section 2.1.2 for respective definitions of the matrices (and in particular (6)).

Let $\mathbf{x} = r(\cos\phi, \sin\phi)^\top \in \Omega^\infty_{\mathrm{pml}}$ be an arbitrary vector (such that $\sigma(r), \tilde{\sigma}(r) > 0$), and $s \in \mathbb{C}^+$, both quantities to be fixed later. Following [31, p. 2721], we express $\mathbf{A}^\phi_\sigma(s, \mathbf{x})$ via the entries of $\mathbf{A}^\phi = (A^\phi_{ij})_{i,j}$:

$$\mathbf{A}^\phi_\sigma(s, \mathbf{x}) = \begin{pmatrix} e^{-i\tau} c_d^{-1} A^\phi_{11} & A^\phi_{12} \\ A^\phi_{12} & e^{i\tau} c_d A^\phi_{22} \end{pmatrix}, \quad \tau := \arg(d_\sigma(s,r)/\tilde{d}_\sigma(s,r)), \quad c_d := |d_\sigma(s,r)/\tilde{d}_\sigma(s,r)|.$$

Recall that $\mathbf{A} = \mathrm{diag}(\lambda_{\max}^{-1}, \lambda_{\min}^{-1})$, and that under the condition $\lambda_{\max} \neq \lambda_{\min}$, for $\phi \neq \pi n/2$, $n \in \mathbb{Z}$, it holds that $A^\phi_{12} \neq 0$. From now on we restrict ourselves to this range of ϕ. Next we plug $\boldsymbol{\xi} = (\xi_1, \xi_2)^\top \in \mathbb{R}^2$ into the equation $\boldsymbol{\xi}^\top \mathbf{A}^\phi_\sigma(s, \mathbf{x})\boldsymbol{\xi} = 0$. The imaginary part of the left-hand side vanishes if $\xi_1^2 = c_d^2 \xi_2^2 A^\phi_{22}/A^\phi_{11}$. Plugging in $\boldsymbol{\xi} = (c_d^{1/2}\sqrt{A^\phi_{22}}, -c_d^{-1/2}\sqrt{A^\phi_{11}}\,\mathrm{sign}\, A^\phi_{12})^\top$ into $\boldsymbol{\xi}^\top \mathbf{A}^\phi_\sigma(s, \mathbf{x})\boldsymbol{\xi} = 0$ yields the identity

$$\cos\tau = |A^\phi_{12}|/(A^\phi_{11}A^\phi_{22})^{1/2} =: a_0. \tag{34}$$

It remains to show that there exist $\mathbf{x}$ and $s \in \mathbb{C}^+$, s.t. the above holds true. This will be the values $\mathbf{x}_0$ and s_0 as in the statement of the lemma. First, as $\mathbf{A}^\phi$ is positive definite, and by the restriction on ϕ, we have that $0 < a_0 < 1$. Next, we remark that

$$\arg\tau = \arg z(\eta, \omega, r), \qquad z(\eta, \omega, r) = \eta^2 + \omega^2 + (\widetilde{\sigma} + \sigma)\eta + \sigma\widetilde{\sigma} + i(\widetilde{\sigma} - \sigma)\omega,$$

where z depends on r through σ, $\tilde{\sigma}$. Let us consider the above expression on the lines $\omega = \mathrm{const}$. For $\eta = 0$, $z = \omega^2 + i(\widetilde{\sigma} - \sigma)\omega$. Moreover, since σ is non-decreasing, we have that $\widetilde{\sigma}(r) \leq \frac{r - R_{\mathrm{pml}}}{r}\sigma(r)$, and thus $\widetilde{\sigma} - \sigma \neq 0$ for any $r > R_{\mathrm{pml}}$. From this it follows that there exists $\omega = \omega_0$ (sufficiently small) and $r = r_0$, s.t. $\cos\arg z(0, \omega_0, r_0) < a_0$. By the continuity argument, this inequality holds true for sufficiently small $\eta > 0$. As $\eta \to +\infty$, $\cos\arg z(\eta, \omega_0, r_0) \to 1$. By the mean-value theorem, we conclude that there exists $\eta_0 > 0$, s.t. $\cos\arg z(\eta_0, \omega_0, r_0) = a_0$. Thus, we fix $s_0 = \eta_0 + i\omega_0$ and choose r_0, ϕ_0, $\boldsymbol{\xi}_0$ as discussed above. □

Remark 3.21. The condition $\boldsymbol{\xi}_0^\top \mathbf{A}_\sigma(s_0, \mathbf{x}_0)\boldsymbol{\xi}_0 = 0$ with $\boldsymbol{\xi}_0 \in \mathbb{R}^2$ is stronger than $\boldsymbol{\xi}_0^* \mathbf{A}_\sigma(s_0, \mathbf{x}_0)\boldsymbol{\xi}_0 = 0$, $\boldsymbol{\xi}_0 \in \mathbb{C}^2$.

With the help of the above lemma, we can prove Theorem 3.5.

Proof of Theorem 3.5. Assume that $\mathcal{A}_\sigma$ is Fredholm. We are going to derive a contradiction. Let $\mathbf{x}_0$, s_0 and $\boldsymbol{\xi}_0$ be like in Lemma 3.20. For $\delta > 0$ let

$$\mathbf{A}_{\sigma,\delta}(s, \mathbf{x}) := \begin{cases} \mathbf{A}_\sigma(s, \mathbf{x}), & \|\mathbf{x} - \mathbf{x}_0\| > \delta, \\ \mathbf{A}_\sigma(s, \mathbf{x}_0), & \|\mathbf{x} - \mathbf{x}_0\| \leq \delta. \end{cases}$$

Let $a^s_{\sigma,\delta}(\cdot,\cdot)$ be defined as $a^s_\sigma(\cdot,\cdot)$ with $\mathbf{A}_\sigma$ being replaced by $\mathbf{A}_{\sigma,\delta}$. Since $\mathbf{A}_\sigma(s_0, \mathbf{x})$ is continuous at $\mathbf{x}_0$, for a fixed $\epsilon > 0$, we can find $\delta > 0$ such that $\|\mathbf{A}_\sigma(s_0, .) - \mathbf{A}_{\sigma,\delta}(s_0, .)\|_{L^\infty(\mathbb{R}^2)} < \epsilon$. Hence there exists $\delta > 0$ such

that the Riesz representation $\mathcal{A}_{\sigma,\delta}(s_0)$ of $a^{s_0}_{\sigma,\delta}(\cdot,\cdot)$ is Fredholm. We are going to construct a singular sequence for $\mathcal{A}_{\sigma,\delta}(s_0)$ in a similar fashion as in the proof of [2, Thm. 6.2.1], and thus arrive at a contradiction.

Let χ be a C^2 cut-off function with $\chi(\mathbf{x}_0) = 1$, $\operatorname{supp}\chi \subset B_\delta(\mathbf{x}_0)$. Consider the sequence of functions $u_n(\mathbf{x}) := \chi(\mathbf{x})\exp(in\boldsymbol{\xi}_0\cdot\mathbf{x})$, $n \in \mathbb{N}$, for which $\|u_n\|_{H^1(\mathbb{R}^2)} \approx n$. It is not difficult to check that $u_n/\|u_n\|_{H^1} \rightharpoonup 0$ in $L^2(\mathbb{R}^2)$, therefore, $u_n/\|u_n\|_{H^1}$ has no convergent in H^1 subsequence. Next, let us verify that there exists a constant $C > 0$, s.t. $|a^{s_0}_{\sigma,\delta}(u_n, u^\dagger)| \le C\|u^\dagger\|_{H^1(\mathbb{R}^2)}$ uniformly in n. We compute

$$\begin{aligned}
&\left\langle \mathbf{A}_{\sigma,\delta}(s_0,\mathbf{x})\nabla u_n, \nabla u^\dagger\right\rangle_{L^2} = \left\langle \mathbf{A}_{\sigma,\delta}(s_0,\mathbf{x}_0)\nabla u_n, \nabla u^\dagger\right\rangle_{L^2} = I_1^{(n)} + I_2^{(n)},\\
&I_1^{(n)} = \left\langle \exp(in\boldsymbol{\xi}_0\cdot\mathbf{x})\mathbf{A}_\sigma(s_0,\mathbf{x}_0)\nabla\chi, \nabla u^\dagger\right\rangle, \quad I_2^{(n)} = \left\langle in\chi\exp(in\boldsymbol{\xi}_0\cdot\mathbf{x})\mathbf{A}_\sigma(s_0,\mathbf{x}_0)\boldsymbol{\xi}_0, \nabla u^\dagger\right\rangle.
\end{aligned}$$

Clearly, $|I_1^{(n)}| \le C(\chi, \mathbf{A}_\sigma(s_0,\mathbf{x}_0))\|u^\dagger\|_{H^1(\mathbb{R}^2)}$. It remains to show that the same holds true for $I_2^{(n)}$. We rewrite it by using the integration by parts

$$I_2^{(n)} = -\left\langle (in)^2\chi\exp(in\boldsymbol{\xi}_0\cdot\mathbf{x})\boldsymbol{\xi}_0^\top\mathbf{A}_\sigma(s_0,\mathbf{x}_0)\boldsymbol{\xi}_0, u^\dagger\right\rangle - \left\langle in\exp(in\boldsymbol{\xi}_0\cdot\mathbf{x})\nabla\chi^\top\mathbf{A}_\sigma(s_0,\mathbf{x}_0)\boldsymbol{\xi}_0, u^\dagger\right\rangle.$$

By Lemma 3.20, the first term in the right-hand side of the above vanishes. To deal with the second term, we rewrite $in\exp(in\boldsymbol{\xi}_0\cdot\mathbf{x})\boldsymbol{\xi}_0 = \nabla\exp(in\boldsymbol{\xi}_0\cdot\mathbf{x})$ and integrate by parts again, which yields the following identity:

$$\begin{aligned}
I_2^{(n)} &= -\left\langle \nabla\exp(in\boldsymbol{\xi}_0\cdot\mathbf{x}), u^\dagger\mathbf{A}_\sigma(s_0,\mathbf{x}_0)^*\nabla\chi\right\rangle\\
&= \left\langle \exp(in\boldsymbol{\xi}_0\cdot\mathbf{x}), (\nabla u^\dagger)^\top\mathbf{A}_\sigma(s_0,\mathbf{x}_0)^*\nabla\chi + u^\dagger\operatorname{div}(\mathbf{A}_\sigma(s_0,\mathbf{x}_0)^*\nabla\chi)\right\rangle.
\end{aligned}$$

The absolute value of the latter expression can be bounded from above by $C(\chi, \mathbf{A}_\sigma(\mathbf{x}_0))\|u^\dagger\|_{H^1}$. Hence $u_n/\|u_n\|_{H^1}$ is a singular sequence for $\mathcal{A}^{s_0}_{\sigma,\delta}$ and thus $\mathcal{A}_{\sigma,\delta}(s_0)$ is not Fredholm. This is a contradiction to the Fredholmness of $\mathcal{A}_\sigma(s_0)$. This implies that the essential spectrum of $s \mapsto \mathcal{A}_\sigma(s)$ is non-empty in $\mathbb{C}^+$. □

Remark 3.22. Alternatively, one can prove Theorem 3.5 by constructing a singular sequence based on the localized fundamental solution around the points $\mathbf{x}$ where its argument vanishes, see Lemma 3.10. Yet another approach in the isotropic time-harmonic context is presented in [58, Section 5.3.1] based on a decomposition into polar coordinates and a singular sequence based on spherical Hankel functions with increasing index.

Remark 3.23. The analysis in the proofs of Theorem 3.5 and Lemma 3.20 are in accordance with previous observations: The supports of $(u_n)_{n\in\mathbb{N}}$ are localized in the absorbing layer and hence cannot be 'triggered' by the data with a sufficient distance to the absorbing layer, cf. Theorem 3.4. Additionally, the functions $(u_n)_{n\in\mathbb{N}}$ are increasingly oscillating and hence coarse discretizations do not capture the part of the spectrum in $\mathbb{C}^+$, cf., the numerical experiments in Section 2.3.

Now we have proven Theorems 3.4 and 3.5. These results show that radial PMLs in general fail when applied to anisotropic problems. Thus in the next section we will seek a remedy for this issue.

4. A possible remedy: shifted change of variables?

In Section 3.4 we have observed that $\mathcal{A}_\sigma$ can loose its Fredholmness when $\cos\arg(\tilde{d}_\sigma/d_\sigma)$ is not bounded far enough away from zero. Indeed, in the isotropic case ($\lambda_{\max} = \lambda_{\min}$) the condition (34), sufficient for the loss of Fredholmness, becomes $\cos\arg(d_\sigma/\tilde{d}_\sigma) = 0$ (which never holds true for $s \in \mathbb{C}^+$). In the anisotropic case ($\lambda_{\min} \ne \lambda_{\max}$) (34) can be written as

$$\cos\arg(d_\sigma/\tilde{d}_\sigma) = \frac{|(\lambda_{\max} - \lambda_{\min})\sin\phi\cos\phi|}{(\lambda_{\max}\cos^2\phi + \lambda_{\min}\sin^2\phi)^{1/2}(\lambda_{\min}\cos^2\phi + \lambda_{\max}\sin^2\phi)^{1/2}}. \tag{35}$$

This condition can be fulfilled because $d_\sigma(s,r)/\tilde{d}_\sigma(s,r) \sim (1 + \frac{\sigma}{s})$ in the vicinity of the PML interface inside the PML (i.e. when $r = R_{\text{pml}} + \varepsilon$, with ε being sufficiently small). Then it is always possible to choose $s \in \mathbb{C}^+$, s.t. $\arg(1 + \frac{\sigma}{s}) = \arctan\frac{\sigma\operatorname{Im} s}{|s|^2 + \sigma\operatorname{Re} s}$ can take any assigned value $(-\frac{\pi}{2}, \frac{\pi}{2})$, which ensures the validity

of the identity (35) for a range of ϕ. Therefore, we will look for an alternative PML change of variables, as suggested in the frequency-domain work [31, p. 2723]. This new PML change of variables reads:

$$r \mapsto r + \frac{\int_{R_{\text{pml}}}^{r} \sigma(\tilde{r}) d\tilde{r}}{s+\gamma}. \tag{36}$$

The parameter $\gamma > 0$ is then chosen to ensure that $\cos\arg \frac{d_\sigma}{\tilde{d}_\sigma}$ exceeds the quantity in the right hand side of (35) for all ϕ and all $s \in \mathbb{C}^+$. Then it is possible to ensure that $\mathcal{A}_\sigma(s)$ is Fredholm for all $s \in \mathbb{C}^+$, in the spirit of [31, Thm. 3.6]. Indeed, since $\cos\arg(z_1/z_2) > \cos\arg z_1$ when $\arg z_1, \arg z_2, \arg z_1 - \arg z_2 \in (0, \pi/2)$ (resp. in $(-\pi/2, 0)$), we have that

$$\begin{aligned}\cos\arg(d_\sigma(s+\gamma)/\tilde{d}_\sigma(s+\gamma)) &\geq \cos\arg(d_\sigma(s+\gamma)) = \cos\arg\left(1 + \frac{\sigma_c}{s+\gamma}\right) \\ &\geq \cos\arctan\operatorname{Im}\left(1+\frac{\sigma_c}{s+\gamma}\right) = \cos\arctan\left(\frac{\sigma_c}{\gamma}\operatorname{Im}\left(\frac{1}{s\gamma^{-1}+1}\right)\right)\end{aligned}$$

for all $s \in \mathbb{C}^+$. Since

$$\left|\operatorname{Im}\frac{1}{s\gamma^{-1}+1}\right| = \frac{\gamma^{-1}|\operatorname{Im}(s)|}{(\operatorname{Re}(s\gamma^{-1})+1)^2 + \gamma^{-2}(\operatorname{Im} s)^2} \leq \frac{\gamma^{-1}|\operatorname{Im}(s)|}{1+\gamma^{-2}(\operatorname{Im} s)^2} \leq \frac{1}{2}$$

for all $s \in \mathbb{C}^+$, we deduce that

$$\inf_{s\in\mathbb{C}^+} \cos\arg\left(\frac{d_\sigma(s+\gamma)}{\tilde{d}_\sigma(s+\gamma)}\right) \geq \cos\arctan\left(\frac{\sigma_c}{2\gamma}\right) = \frac{1}{\sqrt{1+(\sigma_c/(2\gamma))^2}}.$$

Thus by choosing $\sigma_c/2\gamma$ small enough we can ensure that $\inf_{s\in\mathbb{C}^+}\cos\arg(d_\sigma(s+\gamma)/\tilde{d}_\sigma(s+\gamma))$ is larger than the right hand side of (35) for all ϕ, which yields that $\mathcal{A}_\sigma(s)$ is Fredholm for all $s \in \mathbb{C}^+$ [31, Thm. 3.6]. In order to obtain a more precise stability condition on γ, we will examine the behaviour of the fundamental solution of the respective problem, in the spirit of Section 3.3.1.

Remark 4.1. The idea of using the complex shift in order to stabilize the PMLs for anisotropic media is not new, and, to the best of our knowledge, first appeared in the works of K. Duru and G. Kreiss [26], [43]. However, *complex-frequency shifted* PMLs were introduced already much earlier, e.g., in [52]. See the discussion in the introduction of [10] for more details.

4.1. A stability condition on γ

Let us introduce the fundamental solution $G_{\sigma,\gamma}$ corresponding to the new PML change of variables:

$$\begin{aligned}G_{\sigma,\gamma}(s,\mathbf{x},\mathbf{y}) &:= \frac{1}{2\pi\sqrt{\det\mathbf{A}}} K_0\left(s\sqrt{(\mathbf{x}_{\sigma,\gamma}(s)-\mathbf{y}_{\sigma,\gamma}(s))^\top \mathbf{B}(\mathbf{x}_{\sigma,\gamma}(s)-\mathbf{y}_{\sigma,\gamma}(s))}\right), \quad \mathbf{B}=\mathbf{A}^{-1}, \\ \mathbf{x}_{\sigma,\gamma}(s) &:= \hat{\mathbf{x}}\big(\|\mathbf{x}\| + \frac{1}{s+\gamma}\int_{R_{\text{pml}}}^{\|\mathbf{x}\|}\sigma(r')dr'\big) = \mathbf{x}\left(1+\frac{\sigma_c}{s+\gamma}\frac{\|\mathbf{x}\|-R_{\text{pml}}}{\|\mathbf{x}\|}\right) = \mathbf{x}\,\tilde{d}_\sigma(s+\gamma,\|\mathbf{x}\|),\end{aligned} \tag{37}$$

and $\mathbf{y}_{\sigma,\gamma}$ is defined similarly to $\mathbf{x}_{\sigma,\gamma}$. The proof of the counterpart of Proposition 3.8 with γ-shifted change of variables follows the same steps as the proof of Proposition 3.8 in [34], and thus we leave it to the reader. To study the behaviour of the fundamental solution, we can proceed as in Section 3.3.1. Remark that instead of $h_\sigma(s;\mathbf{x},\mathbf{y})$ as defined in (24), we now study $h_\sigma(s+\gamma;\mathbf{x},\mathbf{y})$. Our goal is to choose γ so that Lemma 3.17 holds true for any source term, and not only for the data supported far enough from the interface. For this we will require in particular that $h_\sigma(s+\gamma;\mathbf{x},\mathbf{y}) \notin (-\infty, 0]$ for all $s \in \mathbb{C}^+$, **all** $\mathbf{y} \in \Omega_{\text{int}}$ and $\mathbf{x} \in \Omega_{\text{pml}}$. By Lemma 3.10, this requires that one of the following holds true:

$$(a)\ \operatorname{Re} d_\sigma(s+\gamma) \neq -\frac{\|R_{\text{pml}}\hat{\mathbf{x}}-\mathbf{y}\|}{\|\mathbf{x}\|-R_{\text{pml}}}\frac{\gamma_{12}(\hat{\mathbf{x}},\mathbf{y})}{\gamma_{22}(\hat{\mathbf{x}})}; \quad (b)\ \cos^2(\arg d_\sigma(s+\gamma)) > \frac{\gamma_{12}^2(\hat{\mathbf{x}},\mathbf{y})}{\gamma_{11}(\hat{\mathbf{x}},\mathbf{y})\gamma_{22}(\hat{\mathbf{x}})}. \tag{38}$$

Let us define the following ratio which will play an important role in the analysis that follows:

$$\nu := \frac{\sigma_c}{\gamma}. \tag{39}$$

Observe that the image of $\mathbb{C}^+$ under the mapping $d_\sigma(\cdot+\gamma)$ depends on this ratio only (rather than on γ, σ_c separately). It is the circle centered in the point $\mathbf{s}_\nu = \left(1+\frac{\nu}{2},0\right)^\top \in \mathbb{R}^2$ and of radius $\nu/2$; indeed,

$$\begin{aligned} B_{\nu/2}(\boldsymbol{s}_\nu) &= \{z\in\mathbb{C}\colon (\operatorname{Re} z - 1 - \nu/2)^2 + (\operatorname{Im} z)^2 < \nu^2/4\} = \{1+z\colon z\in\mathbb{C},\ (\operatorname{Re} z - \nu/2)^2 + (\operatorname{Im} z)^2 < \nu^2/4\} \\ &= \{1+z\colon z\in\mathbb{C},\ |z|^2 < \nu \operatorname{Re} z\} = \{1+z\colon z\in\mathbb{C},\ \operatorname{Re}(z^{-1}-\nu^{-1})>0\} \\ &= \{1+z\colon\ z = \frac{1}{s+\nu^{-1}},\quad s\in\mathbb{C}^+\} = \{1+z\colon\ z=\frac{\sigma_c}{s+\gamma},\quad s\in\mathbb{C}^+\}. \end{aligned} \tag{40}$$

Let us now study under which condition on ν (38)(a) or (b) holds true. First of all, the result below shows that the condition (38)(a) necessarily fails for some $(\mathbf{y},\mathbf{x})\in\Omega_{\mathrm{int}}\times\Omega_{\mathrm{pml}}$ (see Remark 3.13).

Lemma 4.2. *Let $\mathbf{y}\in\Omega_{\mathrm{int}}$, $\hat{\boldsymbol{z}}\in\mathbb{S}^2$ be s.t. $\gamma_{12}(\hat{\boldsymbol{z}},\mathbf{y})<0$. Let ν, $\gamma>0$. Then, for $s=\gamma$ and $\mathbf{x}=\rho\hat{\boldsymbol{z}}\in\Omega^\infty_{\mathrm{pml}}$, where ρ is given by*

$$\rho = R_{\mathrm{pml}} - \left(1+\frac{\nu}{2}\right)^{-1} \|R_{\mathrm{pml}}\hat{\boldsymbol{z}} - \mathbf{y}\| \frac{\gamma_{12}(\hat{\boldsymbol{z}},\mathbf{y})}{\gamma_{22}(\hat{\boldsymbol{z}},\mathbf{y})} > R_{\mathrm{pml}},$$

the condition (38)*(a)* ***does not*** *hold true.*

The proof of this result is left to the reader. Therefore, in our choice of ν, we will enforce (38)(b), for all $\mathbf{y}\in\Omega_{\mathrm{int}}$ and $\hat{\mathbf{x}}\in\mathbb{S}^2$. Let us define

$$\beta^2 := \max_{\hat{\mathbf{x}}\in\mathbb{S}^2,\,\mathbf{y}\in\Omega_-(\hat{\mathbf{x}})} \frac{\gamma_{12}^2(\hat{\mathbf{x}},\mathbf{y})}{\gamma_{11}(\hat{\mathbf{x}},\mathbf{y})\gamma_{22}(\hat{\mathbf{x}})},\quad \Omega_-(\hat{\mathbf{x}}) := \{\mathbf{y}\in\Omega_{\mathrm{int}} : \gamma_{12}(\hat{\mathbf{x}},\mathbf{y})<0\}.$$

Then we would like that

$$\cos^2(\arg d_\sigma(s+\gamma)) > \beta^2,\ \text{for all } s\in\mathbb{C}^+. \tag{41}$$

By Lemma C.2 in the report [34], $\beta<1$ and equals $\beta=\frac{\lambda_{\max}-\lambda_{\min}}{\lambda_{\max}+\lambda_{\min}}$. It remains to rewrite (41), cf. (29):

$$\tan^2\arg d_\sigma(s+\gamma) < \frac{1}{\beta^2}-1,\quad s\in\mathbb{C}^+. \tag{42}$$

In view of the definition of the image of $d_\sigma(\cdot+\gamma)$, given in (40), we have that [2]

$$\max\nolimits_{z\in\mathcal{B}_{\nu/2}(\mathbf{s}_\nu)} \tan^2\arg z = \frac{\nu^2}{4(\nu+1)}.$$

Therefore, (42) is equivalent to

$$\frac{\nu^2}{4\nu+4} < \frac{1}{\beta^2}-1 \iff \nu<\nu_* := 2\sqrt{\frac{1}{\beta^2}-1}\left(\sqrt{\frac{1}{\beta^2}-1}+\frac{1}{\beta}\right). \tag{43}$$

Remark that as $\beta\to 1$ (which amounts to $\lambda_{\max}/\lambda_{\min}\to+\infty$), the above upper bound requires that $\nu\to 0$.

[2] Because the maximum of $\tan\arg z$ is achieved on the boundary of the circle $\mathcal{B}_{\nu/2}(\mathbf{s}_\nu)$, it suffices to find the supremum of the function $f(x)=\frac{\nu^2/4-(x-1-\nu/2)^2}{x^2}$ on the interval $(1,1+\nu)$.

Our next step would be to show that the condition (43) ensures the stability of the PML system. However, this condition per se is not sufficient. Indeed, a complete stability result would also require the analysis of the problem when the sources are located **inside** the perfectly matched layers. Otherwise we can expect that the instabilities will manifest themselves on the discrete level, just like they did in the case when the source was supported far away from the PMLs, and the corresponding continuous problem was stable. Indeed, recall the numerical experiments of Section 2.3.1, where the parameters are chosen so that Theorem 3.4 yields the stability of the continuous solution, and yet the discrete solution is unstable.

Since such an analysis is fairly technical, and, moreover, it will not allow us to relax [3] the requirement $\sigma_c/\gamma < \nu_*$, we proceed as follows. We will prove a somewhat weaker stability result, where ν_* is replaced by a sufficiently small number. We start by formulating the time-domain system that we are going to study.

4.2. The frequency-shifted first-order system

Up to this point all our reasoning was solely based on the frequency-domain fundamental solution. The corresponding time-domain system (cf., (12)) needs yet to be derived. We do this along the lines of the paragraphs preceding (12) to obtain the frequency shifted first-order in time system (44). Note that, to this end we merely have to replace the arguments of $d_\sigma, \tilde{d}_\sigma$ by $s+\gamma$ in (9) to obtain

$$
\begin{aligned}
s\tilde{d}_\sigma(s+\gamma)d_\sigma(s+\gamma) &= s+\sigma+\tilde{\sigma}+\frac{\sigma\tilde{\sigma}-\gamma(\sigma+\tilde{\sigma})}{s+\gamma}-\frac{\gamma\sigma\tilde{\sigma}}{(s+\gamma)^2},\\
s\frac{d_\sigma(s+\gamma)}{\tilde{d}_\sigma(s+\gamma)} &= s+\sigma-\tilde{\sigma}-\frac{(\sigma-\tilde{\sigma})(\gamma+\tilde{\sigma})}{s+\gamma+\tilde{\sigma}},\\
s\frac{\tilde{d}_\sigma(s+\gamma)}{d_\sigma(s+\gamma)} &= s-(\sigma-\tilde{\sigma})+\frac{(\sigma-\tilde{\sigma})(\gamma+\sigma)}{s+\gamma+\sigma}.
\end{aligned}
$$

With $\mathbf{J}_{\sigma,\gamma}(s,\mathbf{x}) = \mathbf{J}_\sigma(s+\gamma,\mathbf{x})$, the frequency-shifted counterparts to (10) and (11) are given by

$$
\begin{aligned}
s\det\mathbf{J}_{\sigma,\gamma}\hat{u}^\sigma &= (s+\sigma+\tilde{\sigma})\hat{u}^\sigma+\frac{\sigma\tilde{\sigma}-\gamma(\sigma+\tilde{\sigma})}{s+\gamma}\hat{u}^\sigma-\frac{\gamma\sigma\tilde{\sigma}}{(s+\gamma)^2}\hat{u}^\sigma,\\
s\det\mathbf{J}_{\sigma,\gamma}^{-1}\mathbf{J}_{\sigma,\gamma}^{\top}\mathbf{A}^{-1}\mathbf{J}_{\sigma,\gamma}\hat{\mathbf{p}}^\sigma &= s\mathbf{A}^{-1}\hat{\mathbf{p}}^\sigma+\left(\sigma-\tilde{\sigma}-\frac{(\sigma-\tilde{\sigma})(\gamma+\tilde{\sigma})}{s+\tilde{\sigma}+\gamma}\right)\Pi_\parallel\mathbf{A}^{-1}\Pi_\parallel\hat{\mathbf{p}}^\sigma,\\
&\quad+\left(-(\sigma-\tilde{\sigma})+\frac{(\sigma-\tilde{\sigma})(\gamma+\sigma)}{s+\sigma+\gamma}\right)\Pi_\perp\mathbf{A}^{-1}\Pi_\perp\hat{\mathbf{p}}^\sigma.
\end{aligned}
$$

We introduce the auxiliary frequency-domain unknowns

$$
\hat{v} := \frac{1}{\gamma+s}\hat{u}^\sigma, \qquad \hat{w} := \frac{1}{\gamma+s}\hat{v}, \qquad \hat{\mathbf{q}} := \frac{\tilde{\sigma}+\gamma}{s+\gamma+\tilde{\sigma}}\Pi_\parallel\hat{\mathbf{p}}^\sigma+\frac{\sigma+\gamma}{s+\gamma+\sigma}\Pi_\perp\hat{\mathbf{p}}^\sigma.
$$

This leads to the first order time-domain system

$$
\begin{aligned}
\partial_t u^\sigma &= -(\sigma+\tilde{\sigma})u^\sigma+(\gamma(\sigma+\tilde{\sigma})-\sigma\tilde{\sigma})v+\gamma\sigma\tilde{\sigma}w+\operatorname{div}\mathbf{p}^\sigma+f,\\
\partial_t v &= u^\sigma-\gamma v,\\
\partial_t w &= v-\gamma w,\\
\mathbf{A}^{-1}\partial_t\mathbf{p}^\sigma &= (\sigma-\tilde{\sigma})\left(\Pi_\perp\mathbf{A}^{-1}\Pi_\perp\mathbf{p}^\sigma-\Pi_\parallel\mathbf{A}^{-1}\Pi_\parallel\mathbf{p}^\sigma-\Pi_\perp\mathbf{A}^{-1}\Pi_\perp\mathbf{q}+\Pi_\parallel\mathbf{A}^{-1}\Pi_\parallel\mathbf{q}\right)+\nabla u^\sigma,\\
\partial_t\mathbf{q} &= (\tilde{\sigma}+\gamma)\left(\Pi_\parallel\mathbf{p}^\sigma-\Pi_\parallel\mathbf{q}\right)+(\sigma+\gamma)\left(\Pi_\perp\mathbf{p}^\sigma-\Pi_\perp\mathbf{q}\right).
\end{aligned}
\tag{44}
$$

The above problem, equipped with initial conditions, source terms and posed in $\mathbb{R}^2$, can be proven to be well-posed, following the same arguments as in Section 3.2. We will not repeat them here, but rather concentrate on the stability question, which we again study by examining the fundamental solution.

Remark 4.3. Compared to the system (12), the above system requires the introduction of a single additional auxiliary scalar unknown in the PML layer.

[3] We will discuss later, in Section 4.4, why this requirement is disadvantageous for the PMLs.

4.3. Stability of the obtained PML system in the free space

The principal result of this section is a counterpart of Corollary 3.19, and reads as follows.

Theorem 4.4. *There exists $\nu_0 > 0$, s.t. for any $\sigma_c, \gamma > 0$, s.t. $\sigma_c/\gamma < \nu_0$, the following holds true. Let $F \in H^1(\mathbb{R}^+; L^2(\mathbb{R}^2))$ be s.t. $F(0) = 0$. Then*

$$\hat{u}^\sigma(s, \mathbf{x}) = \int_{\mathbb{R}^2} G_{\sigma,\gamma}(s, \mathbf{x}, \mathbf{y}) \hat{F}(s, \mathbf{y}) d\mathbf{y}$$

is a Fourier-Laplace transform of a $L^\infty_{loc}(\mathbb{R}^+; L^2(\mathbb{R}^2))$-function u^σ, which additionally satisfies the following stability bound for all $T > 0$:

$$\|u^\sigma\|_{L^\infty(0,T;L^2(\mathbb{R}^2))} \leq C_1(\mathbf{B}, R_{\text{pml}}) \mathrm{e}^{C_2(\mathbf{B})\sigma_c R_{\text{pml}}} T^{1/2} \max(1, T^2) \|F\|_{H^1(0,T;L^2(\mathbb{R}^2))},$$

with some non-negative constants $C_1(\mathbf{B}, R_{\text{pml}})$ and $C_2(\mathbf{B})$.

The proof of this theorem can be found in the end of the present section.

Remark 4.5. We believe that the dependence on R_{pml} in the above estimate can be waived. As for the dependence on σ_c, we did not manage to get rid of it.

Remark 4.6. At a first glance, an exponential increase of the above stability constant with respect to σ_c seems to indicate that it is impossible to ensure convergence of the complex frequency-shifted PMLs as $\sigma_c \to +\infty$. This is confirmed by the numerical experiments in the section that follows (Section 4.4). Instead, in Section 5, we propose an alternative, truncation-less perfectly matched layer, whose convergence does not rely on increasing σ_c. Thus, the non-uniformity of the stability estimate in σ_c does not seem to pose any problems for the class of methods that we propose in this manuscript.

Our considerations rely on the analysis of the fundamental solution. Remark that the argument of K_0 depends now on $(\mathbf{x}_{\sigma,\gamma} - \mathbf{y}_{\sigma,\gamma})^\top \mathbf{B} (\mathbf{x}_{\sigma,\gamma} - \mathbf{y}_{\sigma,\gamma}) \equiv h_\sigma(s + \gamma; \mathbf{x}, \mathbf{y})$, with h_σ as defined in (24). The key result in the proof of Theorem 4.4 is the following lemma, which is a counterpart of Lemma 3.17.

Lemma 4.7. *There exist constants ν_0, $C_\pm$, $c_\pm$, $C_{\mathbf{B}} > 0$ depending on $\mathbf{B}$ only, s.t. for all $\sigma_c, \gamma > 0$: $\sigma_c/\gamma < \nu_0$, the following bounds hold true.*
1. For $(\mathbf{x}, \mathbf{y}) \in \mathbb{R}^2 \times \mathbb{R}^2$,

$$C_+ |s| \|\mathbf{x} - \mathbf{y}\| \geq |s\sqrt{h_\sigma(s + \gamma; \mathbf{x}, \mathbf{y})}| \geq C_- |s| \|\mathbf{x} - \mathbf{y}\|. \tag{45}$$

2. For all $(\mathbf{x}, \mathbf{y}) \in \overline{\Omega^\infty_{\text{pml}}} \times \mathbb{R}^2$ with $\|\mathbf{x} - \mathbf{y}\| > \rho := C_{\mathbf{B}} R_{\text{pml}}$, it holds that

$$\operatorname{Re}\left(s\sqrt{h_\sigma(s + \gamma; \mathbf{x}, \mathbf{y})}\right) \geq c_+ \operatorname{Re} s \|\mathbf{x} - \mathbf{y}\|. \tag{46}$$

3. For $(\mathbf{x}, \mathbf{y}) \in \overline{\Omega^\infty_{\text{pml}}} \times \mathbb{R}^2$,

$$\operatorname{Re}(s\sqrt{h_\sigma(s + \gamma; \mathbf{x}, \mathbf{y})}) \geq (c_+ \operatorname{Re} s - c_- \sigma_c) \|\mathbf{x} - \mathbf{y}\|. \tag{47}$$

Remark 4.8. In the above, we believe that the dependence of ρ on R_{pml} can be waived, and is due to the non-optimality of the estimates.

For the proof of the above lemma please see Appendix A, where this lemma is re-stated as Proposition A.9. The above lemma allows to obtain Laplace-domain bounds on the solution of the shifted PML problem.

Proposition 4.9. *Assume that $g \in L^2(\mathbb{R}^2)$. Then, with $\nu_0 > 0$ like in Lemma 4.7, and for all $\sigma_c, \gamma > 0$, s.t. $\sigma_c/\gamma < \nu_0$, the function $v(s, \mathbf{x}) = \int_{\mathbb{R}^2} G_{\sigma,\gamma}(s; \mathbf{x}, \mathbf{y}) g(\mathbf{y}) d\mathbf{y}$ satisfies the following bound:*

$$\|v(s)\|_{L^2(\mathbb{R}^2)} \leq C_1(\mathbf{B}, R_{\text{pml}}) \mathrm{e}^{C_2(\mathbf{B})\sigma_c R_{\text{pml}}} \max(1, (\operatorname{Re} s)^{-2}) \|g\|_{L^2(\mathbb{R}^2)},$$

with some non-negative constants $C_1(\mathbf{B}, R_{\text{pml}})$ and $C_2(\mathbf{B})$.

Proof. Let us consider

$$\|v(s)\|^2_{L^2(\mathbb{R}^2)} = \int_{\mathbb{R}^2} \left| \int_{\mathbb{R}^2} G_{\sigma,\gamma}(s;\mathbf{x},\mathbf{y}) g(\mathbf{y}) d\mathbf{y} \right|^2 d\mathbf{x}.$$

We make use of the explicit expression of the fundamental solution (37) and the bound (32), which we repeat for the convenience of the reader below. For any $a > 0$, there exists $C(a) > 0$, s.t.

$$|K_0(z)| \leq C(a) \begin{cases} \max(1, |\log|z||), & |z| \leq a, \\ \mathrm{e}^{-\operatorname{Re} z}, & |z| > a. \end{cases} \tag{48}$$

For a fixed $\mathbf{x} \in \mathbb{R}^2$, we split, based on the elements of Lemma 4.7,

$$\begin{aligned} &\mathbb{R}^2 = \mathcal{O}_1(\mathbf{x}) \cup \mathcal{O}_2(\mathbf{x}) \cup \mathcal{O}_3(\mathbf{x}), \\ &\mathcal{O}_1(\mathbf{x}) := \{\mathbf{y} \in \mathbb{R}^2 \colon\ |s| \|\mathbf{x}-\mathbf{y}\| \leq 1\}, \\ &\mathcal{O}_2(\mathbf{x}) := \{\mathbf{y} \in \mathbb{R}^2 \colon\ |s| \|\mathbf{x}-\mathbf{y}\| > 1, \quad \|\mathbf{x}-\mathbf{y}\| \leq \rho\}, \\ &\mathcal{O}_3(\mathbf{x}) := \{\mathbf{y} \in \mathbb{R}^2 \colon\ |s| \|\mathbf{x}-\mathbf{y}\| > 1, \quad \|\mathbf{x}-\mathbf{y}\| > \rho\}. \end{aligned} \tag{49}$$

Let us now consider $G_{\sigma,\gamma}(s;\mathbf{x},\mathbf{y})$ in each of these regions. In $\mathcal{O}_1$, by the upper bound in (45), $|s\sqrt{h_\sigma(s+\gamma;\mathbf{x},\mathbf{y})}|$ $\leq C_+$, and therefore, by (48),

$$|G_{\sigma,\gamma}(s;\mathbf{x},\mathbf{y})| \leq \tilde{C}_1 \max(1, |s\sqrt{h_\sigma(s+\gamma;\mathbf{x},\mathbf{y})}|) \leq C_1 \left(1 + |\log(|s|\|\mathbf{x}-\mathbf{y}\|)|\right),$$

where in the last bound we exploited the lower bound in (45). In $\mathcal{O}_2$, $\left|s\sqrt{h_\sigma(s+\gamma;\mathbf{x},\mathbf{y})}\right| > C_-$, therefore, we employ (48) to show that

$$|G_{\sigma,\gamma}(s;\mathbf{x},\mathbf{y})| \leq C_2 \mathrm{e}^{-\operatorname{Re}(s\sqrt{h_\sigma(s+\gamma;\mathbf{x},\mathbf{y})})}.$$

We then use (47) to further bound

$$|G_{\sigma,\gamma}(s;\mathbf{x},\mathbf{y})| \leq C_2 \mathrm{e}^{-c_+ \operatorname{Re} s\|\mathbf{x}-\mathbf{y}\| + c_- \sigma_c \|\mathbf{x}-\mathbf{y}\|} \leq C_2 \mathrm{e}^{c_- \sigma_c \rho}.$$

Finally, in $\mathcal{O}_3$, we have again that $\left|s\sqrt{h_\sigma(s+\gamma;\mathbf{x},\mathbf{y})}\right| \geq C_-$, and thus use the bound of (48), combined with the bound (46), which yields

$$|G_{\sigma,\gamma}(s;\mathbf{x},\mathbf{y})| \leq C_3 \mathrm{e}^{-c_+ \operatorname{Re} s\|\mathbf{x}-\mathbf{y}\|}.$$

The splitting (49) and the above bounds allow us to rewrite

$$\|v(s)\|^2_{L^2(\mathbb{R}^2)} \leq 3 \sum_{i=1}^{3} S_i, \quad S_i = \int_{\mathbb{R}^2} \left| \int_{\mathcal{O}_i(\mathbf{x})} G_{\sigma,\gamma}(s;\mathbf{x},\mathbf{y}) g(\mathbf{y}) d\mathbf{y} \right|^2 d\mathbf{x} \leq \int_{\mathbb{R}^2} \left| \int_{\mathbb{R}^2} H_i(\mathbf{x}-\mathbf{y}) |g(\mathbf{y})| d\mathbf{y} \right|^2 d\mathbf{x}, \tag{50}$$

$$H_1(\mathbf{x}) = C_1 \left(1 - \log\left(|s|\|\mathbf{x}\|\right)\right) \mathbb{1}_{|s|\|\mathbf{x}\| \leq 1}, \quad H_2(\mathbf{x}) = C_2 \mathrm{e}^{c_- \sigma_c \rho} \mathbb{1}_{1 < |s|\|\mathbf{x}\| \leq |s|\rho}, \quad H_3(\mathbf{x}) = C_3 \mathrm{e}^{-\operatorname{Re} s\|\mathbf{x}\|} \mathbb{1}_{|s|\|\mathbf{x}\| > \max(1, |s|\rho)}.$$

Next we recognize in the bound (50) for S_i the L^2-norm of a convolution product. With Young's inequality for convolutions we obtain $S_i \lesssim \|H_i\|^2_{L^1} \|g\|^2_{L^2}$. We end up with the following inequality:

$$\|v(s)\|^2_{L^2(\mathbb{R}^2)} \leq \|g\|^2_{L^2(\mathbb{R}^2)} \sum_{i=1}^{3} \|H_i\|^2_{L^1(\mathbb{R}^2)}.$$

It remains to estimate the L^1-norms of H_i, $1 \le i \le 3$. This yields

$$\|H_1\|_{L^1(\mathbb{R}^2)} = \int_{B_{\frac{1}{|s|}}} (1 - \log(|s|\|\mathbf{x}\|))d\mathbf{x} \lesssim \left(|s|^{-2} - |s|^{-2}\int_{B_1} \log\|\mathbf{x}\|d\mathbf{x}\right) \lesssim \max(1, (\operatorname{Re} s)^{-2}),$$

$$\|H_2\|_{L^1(\mathbb{R}^2)} \le \int_{B_\rho} \mathrm{e}^{c_- - \sigma_c\rho}d\mathbf{x} \lesssim \rho^2\mathrm{e}^{c_- - \sigma_c\rho}, \quad \|H_3\|_{L^1(\mathbb{R}^2)} \lesssim \int_{B_\rho^c} \mathrm{e}^{-c_- \operatorname{Re} s\|\mathbf{x}\|}d\mathbf{x} \lesssim C_\rho \max((\operatorname{Re} s)^{-2}, 1).$$

Recalling the definition of ρ from Lemma 4.7 allows to conclude with the desired estimate. □

We have the necessary ingredients to prove Theorem 4.4.

Proof of Theorem 4.4. Use Proposition 4.9, and the Plancherel theorem like in [8, Proposition 3.15]. □

4.4. Investigation of convergence

Recall that the convergence of the PMLs is quantified by two parameters: the absorption parameter σ and the width of the PML layer L, see [24, 13, 8]. In the classical, Bérenger's case, both in waveguides and in the free space, the error between the PML solution and the exact solution on the time interval $(0, T)$ decreases at least exponentially fast as $\sigma_c \to +\infty$ and L is fixed, or as $L \to +\infty$ and σ_c is fixed [24, 8, 13] Since from the computational viewpoint varying L can be quite expensive, much effort in recent years was dedicated to the choice of the optimal profiles of the damping functions σ [22, 47]. In this section we present the analysis for σ being piecewise constant (cf. Assumption 3.3).

Unfortunately, **when γ is chosen proportionally to σ_c, it seems impossible to ensure the PML convergence as $\sigma_c \to +\infty$ and the PML width L is kept constant**. The lack of convergence is easy to understand when considering the time-harmonic regime ($s = -i\omega$). Indeed, in one dimension, under the PML change of variables $x \mapsto x + \frac{\int_{R_{\mathrm{pml}}}^x \sigma(x)dx}{-i\omega+\gamma}$, the time-harmonic outgoing plane wave $u_{pw}(t, x) = \mathrm{e}^{-i\omega t+ikx}$ is transformed into an evanescent wave

$$u_{pw}^\sigma(t, x) = u_{pw}(t, x)\lambda_{\mathrm{att}}(x, \omega, k), \quad \lambda_{\mathrm{att}}(x, \omega, k) = \mathrm{e}^{-\frac{k\sigma_c(x-R_{\mathrm{pml}})}{\omega+i\gamma}}.$$

For $\gamma = \nu\sigma_c$, the attenuation factor is then given by $|\lambda_{\mathrm{att}}(x, \omega, k)| = \mathrm{e}^{-\frac{k\omega\sigma_c(x-R_{\mathrm{pml}})}{\omega^2+\nu^2\sigma_c^2}}$. In particular, for $\omega = k$,

$$|\lambda_{\mathrm{att}}(x, k, k)| \sim \mathrm{e}^{-\frac{k^2}{\nu^2\sigma_c}(x-R_{\mathrm{pml}})}, \text{ as } \sigma_c \to +\infty. \tag{51}$$

This indicates that the convergence can be assured only by increasing the PML width, proportionally to σ_c.

In the time domain, it is possible to prove in 1D that the best convergence rate is at most $O(\sigma_c^{-1/2})$, see [34] for more details. Let us illustrate this numerically. We consider a 1D wave equation on an interval $r \in (0, \infty)$ with the Dirichlet boundary condition $u(t, 0) = g(t) = \mathrm{e}^{-t^2}t^2$. We apply the PML change of variables (36) for $r > R_{\mathrm{pml}} = 0.2$, fix the PML width $L = 1$, and $\nu = 1$. We then plot the dependence of the PML error $e^{\sigma_c}(t, x) = |u(t, x) - u^\sigma(t, x)|$ at $t = 10$, $x = 0.1$ on σ_c, while keeping $\gamma = \nu^{-1}\sigma_c = \sigma_c$. Let us remark that the error is computed numerically using its expression in the Laplace domain and the convolution quadrature method [46].

The results are shown in Figure 5. Clearly, the PMLs based on (36) with $\sigma_c/\gamma = \text{const}$ do not converge as $\sigma_c \to +\infty$, and the only way the convergence can be assured is by taking $L \to +\infty$. Unfortunately, in this case the PMLs are hardly more efficient than the classical super-cell method: if one is interested in the solution inside the box $(-a, a) \times (-a, a)$, due to the finite velocity $v = 1$ of the wave propagation, for a fixed time $t > 0$, one can always compute the solution inside the larger box $(-a - L, a + L) \times (-a - L, a + L)$, with $L = t/2$ and e.g. homogeneous boundary conditions. Thus the improvement provided by the PMLs is only marginal.

In the section that follows we suggest two alternative strategies. The first one is based on the use of the infinite elements (Hardy-space methods) for the γ-shifted PML system. The second one is based on mapping of the exterior domain to a bounded domain, which is applied after the complex scaling. In both approaches no PML truncation is done, and thus at the continuous level the γ-shifted PMLs become exact.

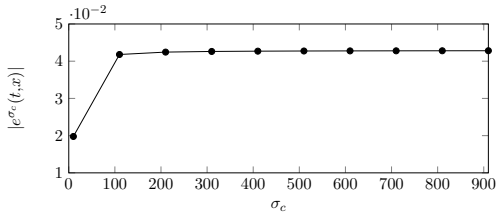

Figure 5: Illustration to the experiment of Section 4.4. Dependence of $|e^{\sigma_c}(t,x)|$ on σ_c.

5. Two different numerical methods

Both of the methods that we propose are Galerkin methods based on the following semi-discrete weak formulation of (44) to find $u^\sigma, v, w, \mathbf{p}^\sigma, \mathbf{q} \in C^1([0,T],\mathcal{V})^3 \times C^1([0,T],\boldsymbol{\mathcal{Q}})^2$ such that

$$\begin{aligned}
\langle \partial_t u^\sigma, u^\dagger\rangle &= \langle (-(\sigma+\tilde\sigma)u^\sigma + (\gamma(\sigma+\tilde\sigma)-\sigma\tilde\sigma)v + \gamma\sigma\tilde\sigma w, u^\dagger\rangle - \langle \mathbf{p}^\sigma, \nabla u^\dagger\rangle + \langle f, u^\dagger\rangle,\\
\langle \partial_t v, v^\dagger\rangle &= \langle u^\sigma - \gamma v, v^\dagger\rangle,\\
\langle \partial_t w, w^\dagger\rangle &= \langle v - \gamma w, w^\dagger\rangle,\\
\langle \mathbf{A}^{-1}\partial_t \mathbf{p}^\sigma, \mathbf{p}^\dagger\rangle &= \langle (\sigma-\tilde\sigma)\mathbf{A}^{-1}(\mathbf{p}^\sigma_\perp - \mathbf{q}_\perp), \mathbf{p}^\dagger_\perp\rangle - \langle (\sigma-\tilde\sigma)\mathbf{A}^{-1}(\mathbf{p}^\sigma_\parallel - \mathbf{q}_\parallel), \mathbf{p}^\dagger_\parallel\rangle + \langle \nabla u^\sigma, \mathbf{p}^\dagger\rangle,\\
\langle \partial_t \mathbf{q}, \mathbf{q}^\dagger\rangle &= \langle (\tilde\sigma+\gamma)\left(\mathbf{p}^\sigma_\parallel - \mathbf{q}_\parallel\right), \mathbf{q}^\dagger_\parallel\rangle + \langle (\sigma+\gamma)\left(\mathbf{p}^\sigma_\perp - \mathbf{q}_\perp\right), \mathbf{q}^\dagger_\perp\rangle,
\end{aligned} \tag{52}$$

for all $u^\dagger, v^\dagger, w^\dagger \in \mathcal{V}, \mathbf{p}^\dagger, \mathbf{q}^\dagger \in \boldsymbol{\mathcal{Q}}$ and some (discrete) spaces $\mathcal{V} \subset H^1(\Omega), \boldsymbol{\mathcal{Q}} \subset \left(L^2(\Omega)\right)^2$, where the radial and tangential components of vector unknowns are denoted by subscripts $\parallel, \perp$ (i.e., $\mathbf{f}_\parallel := \Pi_\parallel \mathbf{f}, \quad \mathbf{f}_\perp := \Pi_\perp \mathbf{f}$, with $\Pi_\parallel$ being the projection onto the space spanned by $\mathbf{x}$). The initial conditions are vanishing.

5.1. Method 1: infinite elements

As a first approach to construct the discrete spaces $\mathcal{V}, \boldsymbol{\mathcal{Q}}$ we use infinite elements. To be more specific, we use Hardy space infinite elements (HSIEs) [38, 29]. Note that so far HSIEs have been primarily used for time-harmonic problems, with the exception of [53], [58, 10.2.4], [49]. Since HSIEs are constructed by means of a rather technical apparatus working in the Laplace domain, we choose to work here with an equivalent, but more accessible presentation as in [48, 58]. That is we directly specify the infinite elements as discrete subspaces of $H^1(\Omega^\infty_{\text{pml}})$ and $\left(L^2(\Omega^\infty_{\text{pml}})\right)^2$. In Ω_{int} we use conforming finite element spaces $\mathcal{V}_{\text{int}} \subset H^1(\Omega_{\text{int}}), \boldsymbol{\mathcal{Q}}_{\text{int}} \subset \left(L^2(\Omega_{\text{int}})\right)^2$. In our particular implementation, we use Lagrange $\mathbb{P}_k$ finite elements for discretizing u^σ, and discontinuous Lagrange elements $(\mathbb{P}_{k-1}\text{-DG})^2$ for discretizing $\mathbf{p}^\sigma$. In $\Omega^\infty_{\text{pml}}$ we use tensor products of the the trace spaces of the interior spaces and (scalar) radial spaces, i.e.,

$$\begin{aligned}
\mathcal{V}_{\text{ext}} &:= \mathcal{V}_{\text{rad}} \otimes \mathcal{V}_\Sigma = \text{span}\{\mathbf{x} = r\hat{\mathbf{x}} \mapsto \tilde v(r)\hat v(R_{\text{pml}}\hat{\mathbf{x}}) \colon\ \tilde v \in \mathcal{V}_{\text{rad}},\ \hat v \in \mathcal{V}_\Sigma\},\\
\boldsymbol{\mathcal{Q}}_{\text{ext}} &:= \mathcal{Q}_{\text{rad}} \otimes \boldsymbol{\mathcal{Q}}_\Sigma = \text{span}\{\mathbf{x} = r\hat{\mathbf{x}} \mapsto \tilde q(r)\hat{\mathbf{q}}(R_{\text{pml}}\hat{\mathbf{x}}) \colon\ \tilde q \in \mathcal{Q}_{\text{rad}},\ \hat{\mathbf{q}} \in \boldsymbol{\mathcal{Q}}_\Sigma\},
\end{aligned}$$

where

$$\mathcal{V}_\Sigma := \{v|_\Sigma, v \in \mathcal{V}_{\text{int}}\}, \qquad\qquad \boldsymbol{\mathcal{Q}}_\Sigma := \{\mathbf{q}|_\Sigma, \mathbf{q} \in \boldsymbol{\mathcal{Q}}_{\text{int}}\}.$$

In the latter case, as the elements of $\boldsymbol{\mathcal{Q}}_{\text{int}}$ are piecewise-polynomials, the trace $\mathbf{q}|_\Sigma$ is well-defined on each mesh element adjacent to Σ. The spaces for discretizing the radial part are then defined as follows. To capture the combination of the exponential decay and the oscillatory behaviour of frequency-domain PML solutions, cf. Section 4.4, we use products of exponentially decaying functions and polynomials

$$\mathcal{V}_{\text{rad}}(\eta_0,\eta_1,N) := \mathcal{Q}_{\text{rad}}(\eta_0,\eta_1,N) := \text{span}\left\{\exp(-\eta_0 r)p(r),\ \exp(-\eta_1 r)p(r) : p \in \mathcal{P}^N\right\}, \tag{53}$$

with $N \in \mathbb{N}$, $\eta_0 \neq \eta_1 > 0$. In the above $\mathcal{P}^N$ denotes the space of polynomials of degree N, and thus the respective spaces are $2(N+1)$-dimensional. For a particular case $\eta_0 = \eta_1$, we define the $2(N+1)$-dimensional space (this definition is consistent with the definition of the two-pole Hardy spaces, cf. Appendix B)

$$\mathcal{V}_{\mathrm{rad}}(\eta_0, \eta_0, N) := \mathcal{Q}_{\mathrm{rad}}(\eta_0, \eta_0, N) := \mathrm{span}\left\{\exp(-\eta_0 r) p(r) : \; p \in \mathcal{P}^{2N+1}\right\}. \tag{54}$$

The space $\mathcal{V}_{\mathrm{rad}}(\eta_0, \eta_0, N) = \mathcal{Q}_{\mathrm{rad}}(\eta_0, \eta_0, N)$ corresponds to the classical Hardy infinite element space introduced in [38]. At the same time, the space $\mathcal{V}_{\mathrm{rad}}(\eta_0, \eta_1, N) = \mathcal{Q}_{\mathrm{rad}}(\eta_0, \eta_1, N)$ relates to the two-pole Hardy space, as introduced in [33] (specifically to the two-scale version from [32]).

The practical use of the above spaces relies on the choice of a 'good' basis (it should be well-conditioned, yield sparse discretization matrices, and allow for a 'sparse' coupling between the interior and the exterior, cf. [58, p.70]) and further evaluation of the matrix elements. For the classical method a convenient set of basis functions was constructed in [38] in the spacial Laplace domain. Afterwards in [48] the basis was translated into the physical space resulting in a subset of generalized Laguerre functions. The construction of such basis functions for the two-scale method is more subtle, and was done in the spacial Laplace domain in [33]. The numerical implementation of the above method relies on the knowledge of the mass and stiffness matrices ($\langle \tilde{v}_n, \tilde{v}_m \rangle_{L^2(\mathbb{R}^+)}$, $\langle r\tilde{v}_n, \tilde{v}_m \rangle_{L^2(\mathbb{R}^+)}$, $\langle \partial_r \tilde{v}_n, \partial_r \tilde{v}_m \rangle_{L^2(\mathbb{R}^+)}$, etc.), which can be computed semi-analytically. The corresponding expressions and computational procedures are stated for in Appendix B.

5.1.1. Numerical experiments

In all the experiments we use the Crank-Nicholson method for time discretization.

Stability. To illustrate numerically the stability of the system we discretize the same problem as in Section 2.3, this time adding the γ-shift and using infinite elements. In the interior we use the elements with the order $k = 4$ and vary mesh sizes h. The number of infinite elements in the exterior is then varied accordingly (as defined by $\mathcal{V}_\Sigma$, $\boldsymbol{\mathcal{Q}}_\Sigma$). Because the statement of Theorem 4.4 is not quantitative (i.e. there is no explicit expression of ν_0 given there), we choose ν satisfying (43). In particular, we take $\sigma_c = 20$ and $\gamma = 10$, which, together with $\beta = \frac{\lambda_{\max} - \lambda_{\min}}{\lambda_{\max} + \lambda_{\min}} = 4/5$, leads to (cf. (43)) $\nu = \frac{\sigma_c}{\gamma} = 2 < \nu_* = 3$.

The dependence of the energy of the solution on time is shown in Figure 6a. We observe a long-time stability both for coarse and fine discretizations. Figure 6b shows the discrete spectra of the corresponding time-harmonic problems. Contrary to the situation depicted in Figure 1b, even for finer discretizations the discrete resonances do not enter the positive complex half plane, as indicated by our theoretical arguments.

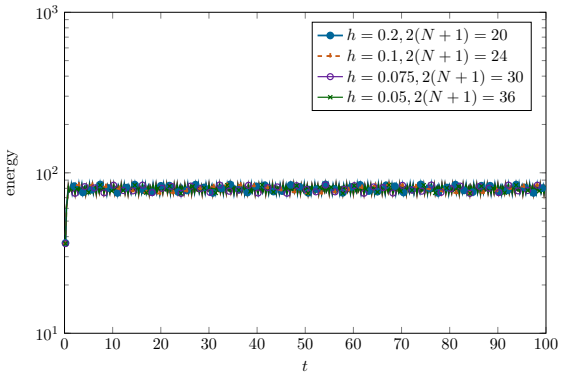

(a) Long-time stability of infinite element discretizations for different mesh sizes and number of infinite elements. The energy curves are hard to distinguish, since they lie exactly on top of each other.

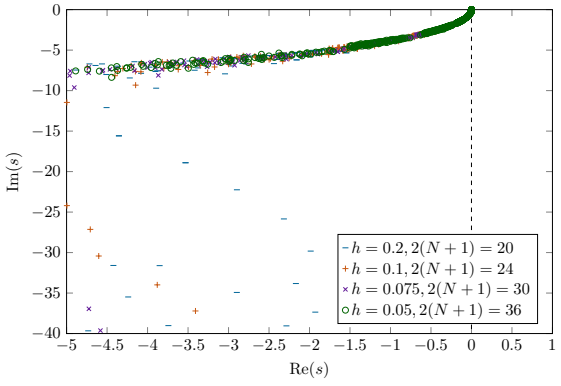

(b) Spectra of the time harmonic problems corresponding to Figure 6a.

Figure 6: Stability of the frequency shifted infinite element discretizations.

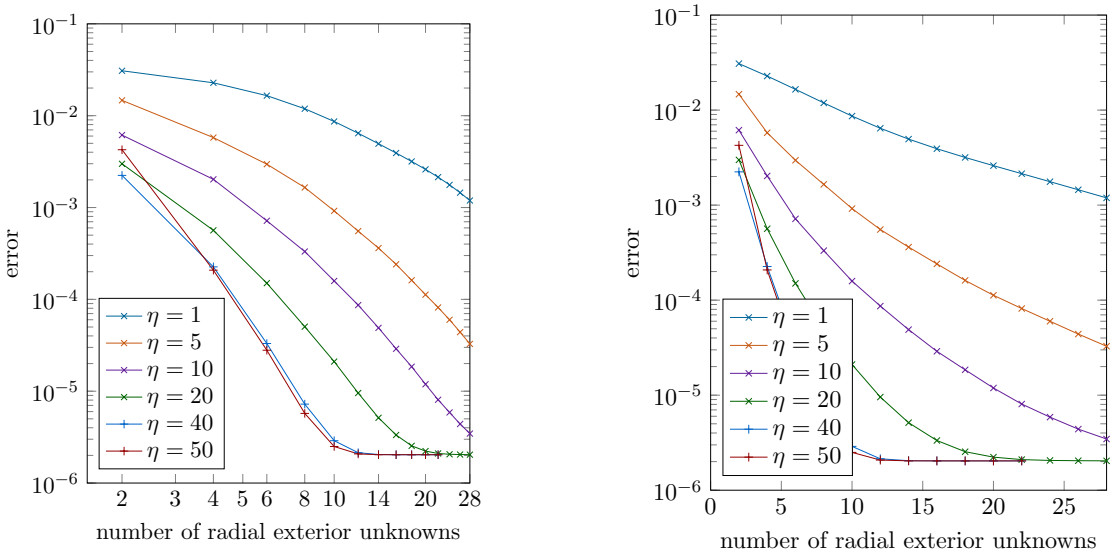

(a) Logarithmic plot of the errors

(b) Semi logarithmic plot of the errors

Figure 7: Convergence of two-scale complex scaled infinite elements w.r.t. the number of the elements in the basis of $\mathcal{V}_{\mathrm{rad}}$.

Convergence. The theory from [29, 48] predicts super-algebraic convergence of Hardy-space methods w.r.t. the number of the infinite elements for time-harmonic problems and a fixed frequency. The goal of this section is to verify numerically whether the same convergence rate can be achieved in our setting in the time-domain regime. We choose $\Omega_{\mathrm{int}} = B_1 \setminus \overline{B_{0.5}} := \{\mathbf{x} \in \mathbb{R}^2 : \|\mathbf{x}\| < 1\}$ and set $\mathbf{A} = \mathrm{diag}(1/8, 1)$. We use a piecewise-constant σ (i.e., satisfying Assumption 3.3), with $\sigma_c = 20$, $\gamma = 10$. As a source we choose

$$f(t, \mathbf{x}) = 2400 \sin(10t) \left(\exp\left(-160 \|\mathbf{x} - (0.7, 0)^\top\|^2\right) + \exp\left(-160 \|\mathbf{x} + (0.7, 0)^\top\|^2\right) \right),$$

As before, we merely simulate one quarter of the domain. The interior discretization is done by the finite elements of order $k = 6$ and a mesh-size of $h = 0.075$. For the infinite elements, in all our experiments, we set $\eta_0 = 1$, and $\eta_1 = \eta$, and vary η. We compare the numerical solution to the reference solution. The latter is computed by using homogeneous boundary conditions on a domain large enough such that the wave is not yet reflected back to the interior and finite elements of order $k = 8$.

Figure 7 displays convergence of the L^2-errors (in space and time in Ω_{int}) of the primal variable $u^\sigma(t, \mathbf{x})$ for end-time $T = 0.5$ for various choices of η. The error from the interior- and time-discretization is roughly $2 \cdot 10^{-6}$, thus the observed, converging dominating error is exclusively the error of the exterior discretization.

Like in the time-harmonic regime, we observe the super-algebraic convergence of the error with respect to the number of the infinite elements. Moreover, as we see, the two-scale Hardy finite element space drastically outperforms the one-pole method, though in both cases the super-algebraic convergence can be observed. This is most likely due to a poor quality of approximation of the high-frequency solutions by the one-pole method. Indeed, such solutions decay rapidly inside the complex-shifted layer, see the expression (51), and thus can be approximated better by $\mathrm{e}^{-\eta x}$, with sufficiently large η. Choosing optimal parameters for the performance of such infinite element methods, however, remains an open question.

5.2. Method 2: truncation-free PMLs

Let us now present an alternative method. We use the new change of variables, cf. (4):

$$\tilde{r}_{\sigma,\gamma} := \begin{cases} f_L(r) + \frac{1}{s+\gamma} \int_{R_{\mathrm{pml}}}^{f_L(r)} \sigma(r') dr', & r > R_{\mathrm{pml}}, \\ r, & r \le R_{\mathrm{pml}}. \end{cases} \tag{55}$$

with

$$f_L(r) = \frac{R_{\text{pml}} L}{R_{\text{pml}} + L - r}.$$

The change of variables defined by f_L is a bijective mapping from $[R_{\text{pml}}, R_{\text{pml}} + L)$ to $[R_{\text{pml}}, \infty)$ (and thus maps $\Omega^{\infty}_{\text{pml}}$ into a bounded layer Ω_{pml} of width L). It therefore yields a truncation-free version of the PML. Note that this approach follows the ideas for the frequency domain of [41, 59] and [30, Sect. 4.5.1], and is different to the one used in [16] where merely the imaginary part of the scaling is unbounded. To avoid singular integrals due to the change of variables defined above we use an approach similar to [59]. We apply the change of variables to the weak form (52) while the test functions $v^{\dagger}$ are replaced by $(R_{\text{pml}} + L - r)^3 v^{\dagger}$ (differing slightly from [59, 3.3.2] where also the trial function is scaled).

5.2.1. Numerical experiments

In all the experiments we set $L = 1$.

Stability. We conduct the same experiments as in Sections 2.3, 5.1.1, but using the approach described above. Similarly to the infinite element approach, we observe long-time stability in the time domain experiments in Figure 8a. This is again confirmed by the fact that, at least for the discretizations considered, the respective resonance problems have no spectrum in $\mathbb{C}^+$, as illustrated in Figure 8b.

Convergence. Contrary to the case of the infinite elements it is not straightforward to separate the interior from the exterior discretization error, due to the fact that the finite element meshes in the interior and exterior domains are not independent. Thus we use a uniform mesh size in the whole domain to study the convergence of the L^2-error (in time and space) of the primal variable $u^{\sigma}(t, x)$ in the interior domain (cf. Figure 9). The remaining parameters are identical to the ones in the convergence experiments in Section 5.1.1. For truncation-free PMLs we observe two kinds of errors (apart from the discretization error in Ω_{int}):

- the discretization error of the layer without the outmost elements which we expect to be $O(h^{k+1})$ (in the L^2-norm), and
- an additional error due to the fact that the outmost elements with homogeneous Dirichlet boundary conditions in the absorbing layer are mapped to an infinite domain, which causes the solutions to oscillate widely, and where the standard analysis does not apply.

In the experiments in Figure 9 we use an end time $T = 0.5$, and thus we observe the first kind of error and the convergence of order h^{k+1}. The plateau in Figure 9 occurring at errors of magnitude $2 \cdot 10^{-7}$ is the time-discretization error. In the section that follows we perform experiments on longer times.

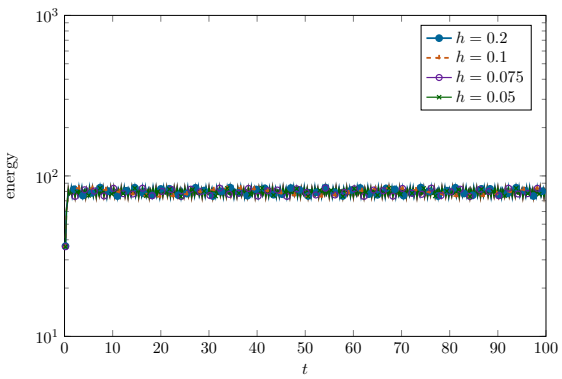

(a) Long-time stability of truncation-free PML discretizations for different mesh sizes. The energy curves are hard to distinguish, since they lie exactly on top of each other.

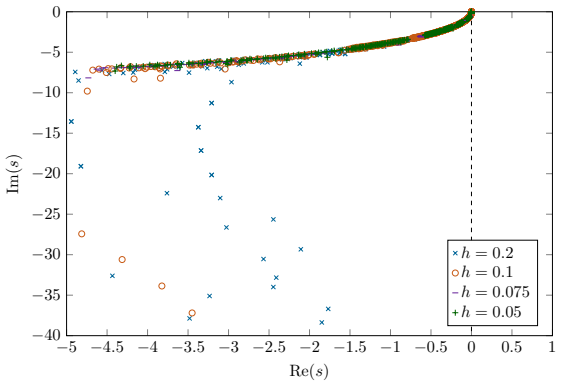

(b) Spectra of the time harmonic problems corresponding to Figure 8a.

Figure 8: Stability of the frequency shifted infinite PMLs.

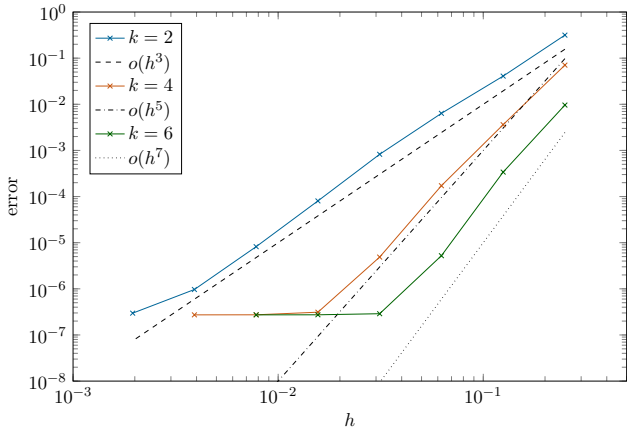

Figure 9: Convergence of the truncation-free PMLs.

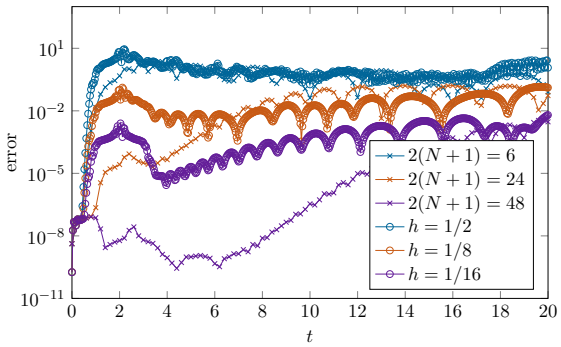

(a) The error of infinite PMLs and infinite elements for various discretizations with respect to time.

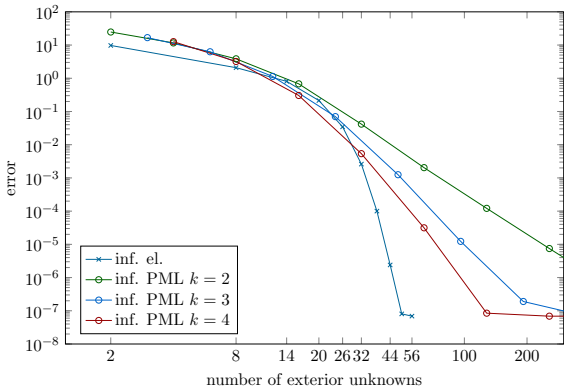

(b) Comparison of the error of the two methods with respect to exterior degrees of freedom.

Figure 10: Comparison of the error of truncation-free PMLs and infinite elements.

5.3. Comparison of the two methods

In this section we compare the methods presented in Sections 5.2 and 5.1 numerically. Since for larger end times T, due to the hardware limitations, we were not able to compute the reference solution with a very high accuracy, we will compare the performance of these methods for a model isotropic problem. In this setting, we consider the problem (3) with $\mathbf{A} = \mathrm{Id}$, vanishing source $f = 0$, and the initial conditions $u(t, r, \phi)|_{t=0} = 120 \exp(-50r)$, $\partial_t u(t, r, \phi)|_{t=0} = 0$, so that the solution does not depend on the variable ϕ. This allows to reduce the problem to a single spatial dimension. We next solve this new problem by applying two methods described above. We use the following parameters for the methods: $\sigma_c = 20$, $\gamma = 10$, $\eta_0 = 1$, $\eta_1 = 20$ and $L = 1$. We choose a very fine interior discretization, so that the interior error is dominated by the error from the exterior discretization (and until the wave reaches the absorbing layer it is dominated by the time stepping error; the time step is chosen as $\tau = 10^{-5}$ which gives an error of $\approx 10^{-7}$). In Figure 10a, we study the dependence of the L^2-spatial errors on time for both methods. The number of infinite elements and the exterior discretization of the truncation-free PMLs with order $k = 3$ is chosen so that the number of unknowns discretizing the exterior is equal in both methods.

We observe that the error starts growing when the wave hits the absorbing layer at $T = 1$. After an initial settling phase the errors grow. Nonetheless, on smaller time intervals the error of the infinite elements is by far smaller. At the end of the experiments the errors of the two methods are comparable.

Figure 10a shows the error of the two methods for various discretizations with respect to time. Figure 10b shows comparison of the two methods for the separated equation at the end time $T = 10$ with respect to the number of degrees of freedom in the exterior domain. For the chosen examples the infinite element method is more efficient than the truncation-free PML.

References

[1] S. Abarbanel, D. Gottlieb, and J. S. Hesthaven. Well-posed perfectly matched layers for advective acoustics. *J. Comput. Phys.*, 154(2):266–283, 1999.

[2] M. S. Agranovich. *Sobolev spaces, their generalizations and elliptic problems in smooth and Lipschitz domains. Translated from the Russian.* Springer Monogr. Math. Cham: Springer, 2015.

[3] J. Aguilar and J. M. Combes. A class of analytic perturbations for one-body Schrödinger Hamiltonians. *Comm. Math. Phys.*, 22:269–279, 1971.

[4] E. Balslev and J. M. Combes. Spectral properties of many-body Schrödinger operators with dilatation-analytic interactions. *Comm. Math. Phys.*, 22:280–294, 1971.

[5] L. Banjai, C. Lubich, and F.-J. Sayas. Stable numerical coupling of exterior and interior problems for the wave equation. *Numer. Math.*, 129(4):611–646, 2015.

[6] É. Bécache and M. Kachanovska. Stable perfectly matched layers for a class of anisotropic dispersive models. Part I: necessary and sufficient conditions of stability. *ESAIM: M2AN*, 51(6):2399–2434, 2017.

[7] E. Bécache and M. Kachanovska. Stable perfectly matched layers for a class of anisotropic dispersive models. Part I: Necessary and sufficient conditions of stability. Extended Version, 2017. `https://hal.science/hal-01356811`.

[8] E. Bécache and M. Kachanovska. Stability and convergence analysis of time-domain perfectly matched layers for the wave equation in waveguides. *SIAM J. Numer. Anal.*, 59(4):2004–2039, 2021.

[9] E. Bécache, S. Fauqueux, and P. Joly. Stability of perfectly matched layers, group velocities and anisotropic waves. *J. Comput. Phys.*, 188(2):399–433, 2003.

[10] É. Bécache, P. G. Petropoulos, and S. D. Gedney. On the long-time behavior of unsplit perfectly matched layers. *IEEE Trans. Antennas and Propagation*, 52(5):1335–1342, 2004.

[11] E. Bécache, D. Givoli, and T. Hagstrom. High-order Absorbing Boundary Conditions for anisotropic and convective wave equations. *J. Comput. Phys.*, 229(4):1099–1129, 2010.

[12] E. Bécache, P. Joly, and V. Vinoles. On the analysis of perfectly matched layers for a class of dispersive media and application to negative index metamaterials. *Math. Comp.*, 87(314):2775–2810, 2018.

[13] E. Bécache, M. Kachanovska, and M. Wess. Convergence analysis of time-domain PMLs for 2D electromagnetic wave propagation in dispersive waveguides. *ESAIM Math. Model. Numer. Anal.*, 57(4): 2451–2491, 2023.

[14] J.-P. Berenger. A perfectly matched layer for the absorption of electromagnetic waves. *J. Comput. Phys.*, 114(2):185–200, 1994.

[15] J.-P. Berenger. Three-dimensional perfectly matched layer for the absorption of electromagnetic waves. *J. Comput. Phys.*, 127(2):363–379, 1996.

[16] A. Bermúdez, L. Hervella-Nieto, A. Prieto, and R. Rodríguez. An exact bounded perfectly matched layer for time-harmonic scattering problems. *SIAM J. Sci. Comput.*, 30(1):312–338, 2007/08.

[17] D. Boffi, F. Brezzi, and M. Fortin. *Mixed finite element methods and applications*, volume 44 of *Springer Series in Computational Mathematics*. Springer, Heidelberg, 2013.

[18] A.-S. Bonnet-BenDhia, C. Chambeyron, and G. Legendre. On the use of perfectly matched layers in the presence of long or backward guided elastic waves. *Wave Motion*, 51(2):266–283, 2014.

[19] Z. Chen. Convergence of the time-domain perfectly matched layer method for acoustic scattering problems. *Int. J. Numer. Anal. Model.*, 6(1):124–146, 2009.

[20] W. C. Chew and W. H. Weedon. A 3d perfectly matched medium from modified Maxwell's equations with stretched coordinates. *Microwave Optical Tech. Letters*, 7:590–604, 1994.

[21] F. Collino and P. Monk. The perfectly matched layer in curvilinear coordinates. *SIAM J. Sci. Comput.*, 19(6):2061–2090, 1998.

[22] F. Collino and P. Monk. Optimizing the perfectly matched layer. *Comput. Methods Appl. Mech. Engrg.*, 164(1-2):157–171, 1998.

[23] E. Demaldent and S. Imperiale. Perfectly matched transmission problem with absorbing layers: application to anisotropic acoustics in convex polygonal domains. *Internat. J. Numer. Methods Engrg.*, 96 (11):689–711, 2013.

[24] J. Diaz and P. Joly. A time domain analysis of PML models in acoustics. *Comput. Methods Appl. Mech. Engrg.*, 195(29-32):3820–3853, 2006.

[25] DLMF. *NIST Digital Library of Mathematical Functions*. `https://dlmf.nist.gov/`, Release 1.1.12 of 2023-12-15. F. W. J. Olver, A. B. Olde Daalhuis, D. W. Lozier, B. I. Schneider, R. F. Boisvert, C. W. Clark, B. R. Miller, B. V. Saunders, H. S. Cohl, and M. A. McClain, eds.

[26] K. Duru and G. Kreiss. A well-posed and discretely stable perfectly matched layer for elastic wave equations in second order formulation. *Communications in Computational Physics*, 11(5):1643–1672, 2012.

[27] K. Duru and G. Kreiss. Numerical interaction of boundary waves with perfectly matched layers in two space dimensional elastic waveguides. *Wave Motion*, 51(3):445–465, 2014.

[28] K. Duru, A.-A. Gabriel, and G. Kreiss. On energy stable discontinuous Galerkin spectral element approximations of the perfectly matched layer for the wave equation. *Comput. Methods Appl. Mech. Engrg.*, 350:898–937, 2019.

[29] M. Halla. Convergence of Hardy space infinite elements for Helmholtz scattering and resonance problems. *SIAM J. Numer. Anal.*, 54(3):1385–1400, 2016.

[30] M. Halla. *Analysis of radial complex scaling methods for scalar resonance problems in open systems*. PhD thesis, Technische Universität Wien, 2019.

[31] M. Halla. Radial complex scaling for anisotropic scalar resonance problems. *SIAM J. Numer. Anal.*, 60 (5):2713–2730, 2022.

[32] M. Halla and L. Nannen. Two scale Hardy space infinite elements for scalar waveguide problems. *Advances in Computational Mathematics*, 44(3):611–643, 2018.

[33] M. Halla, T. Hohage, L. Nannen, and J. Schöberl. Hardy space infinite elements for time harmonic wave equations with phase and group velocities of different signs. *Numer. Math.*, 133(1):103–139, 2016.

[34] M. Halla, M. Kachanovska, and M. Wess. Radial perfectly matched layers and infinite elements for the anisotropic wave equation, 2024. `https://arxiv.org/abs/2401.13483`.

[35] L. Halpern and J. Rauch. Bérenger/Maxwell with discontinous absorptions: existence, perfection, and no loss. In *Séminaire Laurent Schwartz—Équations aux dérivées partielles et applications. Année 2012–2013*, Sémin. Équ. Dériv. Partielles, pages Exp. No. X, 20. École Polytech., Palaiseau, 2014.

[36] J. S. Hesthaven. On the analysis and construction of perfectly matched layers for the linearized Euler equations. *J. Comput. Phys.*, 142(1):129–147, 1998.

[37] P. D. Hislop and I. M. Sigal. *Introduction to spectral theory*, volume 113 of *Applied Mathematical Sciences*. Springer-Verlag, New York, 1996.

[38] T. Hohage and L. Nannen. Hardy space infinite elements for scattering and resonance problems. *SIAM Journal on Numerical Analysis*, 47(2):972–996, 2009.

[39] F. Q. Hu. On absorbing boundary conditions for linearized Euler equations by a perfectly matched layer. *J. Comput. Phys.*, 129(1):201–219, 1996.

[40] F. Q. Hu. A stable, perfectly matched layer for linearized Euler equations in unsplit physical variables. *J. Comput. Phys.*, 173(2):455–480, 2001.

[41] J. P. Hugonin and P. Lalanne. Perfectly matched layers as nonlinear coordinate transforms: a generalized formalization. *J. Opt. Soc. Amer. A*, 22(9):1844–1849, 2005.

[42] T. Kato. *Perturbation theory for linear operators*. Classics in Mathematics. Springer-Verlag, Berlin, 1995. Reprint of the 1980 edition.

[43] G. Kreiss and K. Duru. Discrete stability of perfectly matched layers for anisotropic wave equations in first and second order formulation. *BIT*, 53(3):641–663, 2013.

[44] M. Lassas and E. Somersalo. Analysis of the PML equations in general convex geometry. *Proc. Roy. Soc. Edinburgh Sect. A*, 131(5):1183–1207, 2001.

[45] J. H. Lee. Root-finding absorbing boundary condition for anisotropic scalar waves in infinite media. *Internat. J. Numer. Methods Engrg.*, 122(4):1031–1050, 2021.

[46] C. Lubich. Convolution quadrature and discretized operational calculus. I. *Numer. Math.*, 52(2):129–145, 1988.

[47] A. Modave, E. Delhez, and C. Geuzaine. Optimizing perfectly matched layers in discrete contexts. *Internat. J. Numer. Methods Engrg.*, 99(6):410–437, 2014.

[48] L. Nannen and M. Wess. Complex-scaled infinite elements for resonance problems in heterogeneous open systems. *Adv. Comput. Math.*, 48(2):Paper No. 8, 35, 2022.

[49] L. Nannen, K. Tichy, and M. Wess. Complex scaled infinite elements for wave equations in heterogeneous open systems. In *Proceedings of the 14th International Conference on Mathematical and Numerical Aspects of Wave Propagation*, pages 520–521, 2019.

[50] J. S. Pettigrew, A. J. Mulholland, and K. M. M. Tant. Towards a combined perfectly matching layer and infinite element formulation for unbounded elastic wave problems. *Mathematics and Mechanics of Solids*, 27(5):794–812, 2022.

[51] D. Rabinovich, S. Vigdergauz, D. Givoli, T. Hagstrom, and J. Bielak. Optimized first-order absorbing boundary conditions for anisotropic elastodynamics. *Comput. Methods Appl. Mech. Engrg.*, 350:719–749, 2019.

[52] J. A. Roden and S. D. Gedney. Convolution PML (CPML): An efficient FDTD implementation of the CFS–PML for arbitrary media. *Microwave and Optical Technology Letters*, 27(5):334–339, 2000.

[53] D. Ruprecht, A. Schädle, and F. Schmidt. Transparent boundary conditions based on the pole condition for time-dependent, two-dimensional problems. *Numer. Methods Partial Differential Equations*, 29(4): 1367–1390, 2013.

[54] S. Savadatti and M. N. Guddati. Absorbing boundary conditions for scalar waves in anisotropic media. Part 2: time-dependent modeling. *J. Comput. Phys.*, 229(18):6644–6662, 2010.

[55] S. Savadatti and M. N. Guddati. Accurate absorbing boundary conditions for anisotropic elastic media. Part 2: Untilted non-elliptic anisotropy. *J. Comput. Phys.*, 231(22):7608–7625, 2012.

[56] F.-J. Sayas. *Retarded potentials and time domain boundary integral equations*, volume 50 of *Springer Series in Computational Mathematics*. Springer, 2016.

[57] B. Simon. Resonances and complex scaling: A rigorous overview. *International Journal of Quantum Chemistry*, 14(4):529–542, 1978.

[58] M. Wess. *Frequency Dependent Complex Scaled Infinite Elements for Exterior Helmholtz Resonance Problems*. PhD thesis, TU Vienna, Wien, 2020.

[59] Z. Yang, L.-L. Wang, and Y. Gao. A truly exact perfect absorbing layer for time-harmonic acoustic wave scattering problems. *SIAM J. Sci. Comput.*, 43(2):A1027–A1061, 2021.

A. Auxiliary lemmas quantifying the behaviour of h_σ

We will assume everywhere in this section that σ satisfies Assumption 3.3, i.e., is piecewise-constant and equal to $\sigma_c > 0$ inside the perfectly matched layer. We additionally use the notation $\|\mathbf{x}\|_{\mathbf{B}} := \sqrt{\mathbf{x}^\top \mathbf{B}\mathbf{x}}$, for an arbitrary vector $\mathbf{x} \in \mathbb{R}^2$. Recall the definition (24), which we extend to $\mathbf{y} \in \Omega^\infty_{\text{pml}}$:

$$h_\sigma(s;\mathbf{x},\mathbf{y}) = (\mathbf{x}_\sigma - \mathbf{y}_\sigma)^\top \mathbf{B}(\mathbf{x}_\sigma - \mathbf{y}_\sigma), \quad \mathbf{x},\mathbf{y} \in \mathbb{R}^2.$$

In what follows, we will need more explicit expressions and bounds on h_σ in different regions of $\mathbb{R}^2 \times \mathbb{R}^2$. We will first state and prove these bounds for $\mathbf{x},\mathbf{y} \in \overline{\Omega^\infty_{\text{pml}}} \times \overline{\Omega^\infty_{\text{pml}}}$. The bounds for $\mathbf{x} \in \overline{\Omega^\infty_{\text{pml}}}$ and $\mathbf{y} \in \Omega_{\text{int}}$ can be obtained similarly, therefore we omit their derivation here. The interested reader can find them in Appendix A of the report [34]. We summarize all the bounds in Section A.2.

A.1. Bounds on $h_\sigma(s;\mathbf{x},\mathbf{y})$ for $(\mathbf{x},\mathbf{y}) \in \overline{\Omega^\infty_{\text{pml}}} \times \overline{\Omega^\infty_{\text{pml}}}$

A.1.1. Bounds for classical PMLs

As a preparation for the proofs of the following results we begin by rewriting

$$\mathbf{x}_\sigma - \mathbf{y}_\sigma = (\mathbf{x}-\mathbf{y})(1+s^{-1}\sigma_c) - s^{-1}\sigma_c(R_{\text{pml}}\hat{\mathbf{x}} - R_{\text{pml}}\hat{\mathbf{y}}) = \mathbf{p}(1+s^{-1}\sigma_c) - s^{-1}\sigma_c \mathbf{p}_{\text{pml}}, \tag{A.1}$$

with $\mathbf{p} = \mathbf{x}-\mathbf{y}$ and $\mathbf{p}_{\text{pml}} = (R_{\text{pml}}\hat{\mathbf{x}} - R_{\text{pml}}\hat{\mathbf{y}})$. We then have that

$$h_\sigma(s;\mathbf{x},\mathbf{y}) = \left(1+\frac{\sigma_c}{s}\right)^2 \mathbf{p}^\top \mathbf{B}\mathbf{p} - 2\frac{\sigma_c}{s}\left(1+\frac{\sigma_c}{s}\right)\mathbf{p}^\top \mathbf{B}\mathbf{p}_{\text{pml}} + \frac{\sigma_c^2}{s^2}\mathbf{p}_{\text{pml}}^\top \mathbf{B}\mathbf{p}_{\text{pml}}. \tag{A.2}$$

We start with the following bound.

Lemma A.1. *Let $\sigma_c > 0$. Then there exist $\gamma_{\mathbf{B}}$, $c_{\mathbf{B}} > 0$, which depend on $\mathbf{B}$, s.t. for all $s \in \mathbb{C}^+_\alpha$, with $\alpha = \gamma_{\mathbf{B}}\sigma_c$,*

$$\operatorname{Re} h_\sigma(s;\mathbf{x},\mathbf{y}) \geq c_{\mathbf{B}}\|\mathbf{x}-\mathbf{y}\|^2, \qquad \textit{for all } \mathbf{x},\mathbf{y} \in \overline{\Omega^\infty_{\text{pml}}}. \tag{A.3}$$

Proof of Lemma A.1. We make use of (A.2), (A.1). For all $s \in \mathbb{C}^+$ we have that $\operatorname{Re}(1+s^{-1}\sigma_c)^2 \geq \operatorname{Re}(1+s^{-2}\sigma_c^2)$, and therefore, in particular, for $s \in \mathbb{C}^+_\alpha$, it holds that

$$\operatorname{Re} h_\sigma(s;\mathbf{x},\mathbf{y}) \geq \left(1-\frac{\sigma_c^2}{\alpha^2}\right)\|\mathbf{p}\|_{\mathbf{B}}^2 - \frac{2\sigma_c}{\alpha}\left(1+\frac{\sigma_c}{\alpha}\right)\left|\mathbf{p}^\top \mathbf{B}\mathbf{p}_{\mathrm{pml}}\right| - \frac{\sigma_c^2}{\alpha^2}\|\mathbf{p}_{\mathrm{pml}}\|_{\mathbf{B}}^2.$$

We have that $\|\mathbf{p}\| \geq \|\mathbf{p}_{\mathrm{pml}}\|$.[4] Therefore,

$$\|\mathbf{p}\|_{\mathbf{B}} \geq \sqrt{\lambda_{\min}}\|\mathbf{p}\| \geq \sqrt{\lambda_{\min}}\|\mathbf{p}_{\mathrm{pml}}\| \geq \sqrt{\lambda_{\min}/\lambda_{\max}}\|\mathbf{p}_{\mathrm{pml}}\|_{\mathbf{B}}. \tag{A.4}$$

We conclude that for all $\alpha > \gamma_{\mathbf{B}}\sigma_c$, with $\gamma_{\mathbf{B}} > 0$ sufficiently large, all the sign-indefinite and negative terms are controlled by $\|\mathbf{p}\|_{\mathbf{B}}^2$. Hence the bound in the statement of the lemma. □

An upper bound on h_σ, stated below, is then obtained similarly, and thus we leave its proof to the reader.

Lemma A.2. *Let $\sigma_c > 0$. Then there exists a constant $C_{\mathbf{B}} > 0$, which depends on $\mathbf{B}$, s.t. for all $s \in \mathbb{C}^+$,*

$$|h_\sigma(s;\mathbf{x},\mathbf{y})| \leq C_{\mathbf{B}}\left(1+\frac{\sigma_c}{|s|}\right)^2\|\mathbf{x}-\mathbf{y}\|^2, \quad \textit{for all } \mathbf{x},\mathbf{y} \in \overline{\Omega^\infty_{\mathrm{pml}}}.$$

We also have another lower bound on h_σ which will be of use later.

Lemma A.3. *Let $\sigma_c > 0$. Then, there exist $\tilde{\gamma}_{\mathbf{B}}$, $\tilde{c}_{\mathbf{B}} > 0$, which depend on $\mathbf{B}$, s.t. for all $s \in \mathbb{C}^+_{\tilde{\alpha}}$, with $\tilde{\alpha} = \tilde{\gamma}_{\mathbf{B}}\sigma_c$,*

$$\operatorname{Re}(s\sqrt{h_\sigma(s;\mathbf{x},\mathbf{y})}) \geq \tilde{c}_{\mathbf{B}} \operatorname{Re} s\|\mathbf{x}-\mathbf{y}\|, \quad \textit{whenever } \mathbf{x},\mathbf{y} \in \overline{\Omega^\infty_{\mathrm{pml}}}. \tag{A.5}$$

Proof. We use the identity

$$\operatorname{Re}(s\sqrt{h_\sigma}) = \operatorname{Re} s \operatorname{Re}\sqrt{h_\sigma} - \operatorname{Im} s \operatorname{Im}\sqrt{h_\sigma}.$$

Recall the explicit expression for the complex root:

$$\sqrt{z} = \sqrt{\frac{|z|+\operatorname{Re} z}{2}} + i \operatorname{sign}\operatorname{Im} z\sqrt{\frac{|z|-\operatorname{Re} z}{2}}. \tag{A.6}$$

A lower bound for $\operatorname{Re}\sqrt{h_\sigma} > \sqrt{\operatorname{Re} h_\sigma}$ can be obtained from Lemma A.1. This yields

$$\operatorname{Re}(s\sqrt{h_\sigma(s;\mathbf{x},\mathbf{y})}) = \operatorname{Re} s \operatorname{Re}\sqrt{h_\sigma(s;\mathbf{x},\mathbf{y})} - \operatorname{Im} s \operatorname{Im}\sqrt{h_\sigma(s;\mathbf{x},\mathbf{y})} \geq c_{\mathbf{B}}^{1/2} \operatorname{Re} s\|\mathbf{x}-\mathbf{y}\| - |\operatorname{Im} s \operatorname{Im}\sqrt{h_\sigma(s;\mathbf{x},\mathbf{y})}|. \tag{A.7}$$

To bound $\operatorname{Im}\sqrt{h_\sigma}$, we use that, for $z \in \mathbb{C}\setminus\mathbb{R}_0^-$, cf. (A.6),

$$\left|\operatorname{Im}\sqrt{z}\right| = \sqrt{\frac{|z|-\operatorname{Re} z}{2}}.$$

We next use the inequality $\sqrt{a^2+b^2}-a \leq \frac{b^2}{a}$, valid for $a > 0$, with $a = \operatorname{Re} h_\sigma$ and $b = \operatorname{Im} h_\sigma$. This inequality implies that $\left|\operatorname{Im}\sqrt{h_\sigma}\right| \leq \frac{|\operatorname{Im} h_\sigma|}{\sqrt{\operatorname{Re} h_\sigma}}$. With Lemma A.1, for $s \in \mathbb{C}^+_\alpha$, it holds that

$$\left|\operatorname{Im}\sqrt{h_\sigma}\right| \leq \frac{|\operatorname{Im} h_\sigma|}{c_{\mathbf{B}}^{1/2}\|\mathbf{p}\|}. \tag{A.8}$$

[4] Indeed, denoting by $b := \hat{\mathbf{x}}^\top\hat{\mathbf{y}}$, we remark that the minimum of the linear in $b \in [-1,1]$ function

$$\|\mathbf{p}\|^2 - \|\mathbf{p}_{\mathrm{pml}}\|^2 = \|\mathbf{x}\|^2 + \|\mathbf{y}\|^2 - 2\|\mathbf{x}\|\|\mathbf{y}\|b - 2R_{\mathrm{pml}}^2(1-b)$$

is achieved at $b = 1$ ($\|\mathbf{x}\|, \|\mathbf{y}\| > R_{\mathrm{pml}}$), and equal to $|\|\mathbf{x}\| - \|\mathbf{y}\||^2 \geq 0$.

Finally, it remains to bound $|\operatorname{Im} h_\sigma|$. From the expression (A.2), it follows that

$$\begin{aligned}\operatorname{Im} h_\sigma(s;\mathbf{x},\mathbf{y}) &= \left(2\sigma_c \operatorname{Im}\frac{1}{s} + \sigma_c^2 \operatorname{Im}\frac{1}{s^2}\right)\|\mathbf{p}\|_{\mathbf{B}}^2 - \left(2\sigma_c \operatorname{Im}\frac{1}{s} + 2\sigma_c^2 \operatorname{Im}\frac{1}{s^2}\right)\mathbf{p}^\top \mathbf{B}\mathbf{p}_{\mathrm{pml}} + \sigma_c^2 \operatorname{Im}\frac{1}{s^2}\|\mathbf{p}_{\mathrm{pml}}\|_{\mathbf{B}}^2 \\ &= -2\sigma_c \frac{\operatorname{Im} s}{|s|^2}(\|\mathbf{p}\|_{\mathbf{B}}^2 - \mathbf{p}^\top \mathbf{B}\mathbf{p}_{\mathrm{pml}}) - 2\sigma_c^2 \frac{\operatorname{Re} s \operatorname{Im} s}{|s|^4}\|\mathbf{p}-\mathbf{p}_{\mathrm{pml}}\|_{\mathbf{B}}^2. \end{aligned} \tag{A.9}$$

With the inequality (A.4) $\|\mathbf{p}\|_{\mathbf{B}} \geq \sqrt{\lambda_{\min}/\lambda_{\max}}\|\mathbf{p}_{\mathrm{pml}}\|_{\mathbf{B}}$, and using $\frac{|\operatorname{Im} s|}{|s|} < 1$, $\frac{\operatorname{Re} s}{|s|} < 1$, the above yields, with some constant $\tilde{C}_{\mathbf{B}} > 0$,

$$|\operatorname{Im} h_\sigma(s;\mathbf{x},\mathbf{y})| \leq \tilde{C}_{\mathbf{B}} \frac{\sigma_c}{|s|}\left(1+\frac{\sigma_c}{|s|}\right)\|\mathbf{p}\|. \tag{A.10}$$

Inserting the above inequality into (A.8), and next inserting (A.8) into (A.7), we obtain,

$$\begin{aligned}\operatorname{Re}(s\sqrt{h_\sigma(s;\mathbf{x},\mathbf{y})}) &\geq c_{\mathbf{B}} \operatorname{Re} s\|\mathbf{x}-\mathbf{y}\| - \frac{\tilde{C}_{\mathbf{B}}\sigma_c|\operatorname{Im} s|}{c_{\mathbf{B}}^{1/2}|s|}\left(1+\frac{\sigma_c}{|s|}\right)\|\mathbf{x}-\mathbf{y}\| \\ &\geq c_{\mathbf{B}} \operatorname{Re} s\left(1 - \frac{\tilde{C}_{\mathbf{B}}}{c_{\mathbf{B}}^{3/2}}\frac{\sigma_c}{\operatorname{Re} s}\left(1+\frac{\sigma_c}{\operatorname{Re} s}\right)\right)\|\mathbf{x}-\mathbf{y}\|.\end{aligned}$$

Choosing $\operatorname{Re} s > \tilde{\gamma}_{\mathbf{B}}\sigma_c$ with sufficiently large $\tilde{\gamma}_{\mathbf{B}}$ depending on $\mathbf{B}$ only yields the desired estimate. □

A.1.2. Bounds on complex-shifted PMLs

For the complex-shifted PMLs, the counterpart of (A.2) reads

$$h_\sigma(s+\gamma;\mathbf{x},\mathbf{y}) = \left(1+\frac{\sigma_c}{s+\gamma}\right)^2 \mathbf{p}^\top \mathbf{B}\mathbf{p} - 2\frac{\sigma_c}{s+\gamma}\left(1+\frac{\sigma_c}{s+\gamma}\right)\mathbf{p}^\top \mathbf{B}\mathbf{p}_{\mathrm{pml}} + \frac{\sigma_c^2}{(s+\gamma)^2}\mathbf{p}_{\mathrm{pml}}^\top \mathbf{B}\mathbf{p}_{\mathrm{pml}}. \tag{A.11}$$

We start with the following auxiliary result.

Lemma A.4. *There exist constants $\nu_0 > 0$ and $c_{\mathbf{B}} > 0$ depending on $\mathbf{B}$, s.t. for all $\sigma_c < \nu_0\gamma$ the inequality*

$$\operatorname{Re} h_\sigma(s+\gamma;\mathbf{x},\mathbf{y}) > c_{\mathbf{B}}\|\mathbf{x}-\mathbf{y}\|^2 \tag{A.12}$$

holds true for all $s \in \mathbb{C}^+$ and $\mathbf{x},\mathbf{y} \in \overline{\Omega_{\mathrm{pml}}^\infty}$.

Proof. By Lemma A.1, one has $\operatorname{Re} h_\sigma(s;\mathbf{x},\mathbf{y}) > c_{\mathbf{B}}\|\mathbf{x}-\mathbf{y}\|^2$, whenever $\operatorname{Re} s > \gamma_{\mathbf{B}}\sigma_c$. In other words, $\operatorname{Re} h_\sigma(s+\gamma;\mathbf{x},\mathbf{y}) > c_{\mathbf{B}}\|\mathbf{x}-\mathbf{y}\|^2$ whenever $\operatorname{Re} s + \gamma > \gamma_{\mathbf{B}}\sigma_c$. If $\gamma > \gamma_{\mathbf{B}}\sigma_c$ (i.e. $\nu_0 = \gamma_{\mathbf{B}}^{-1}$), the estimate $\operatorname{Re} h_\sigma(s+\gamma;\mathbf{x},\mathbf{y}) > c_{\mathbf{B}}\|\mathbf{x}-\mathbf{y}\|^2$ holds for all $s \in \mathbb{C}^+$. □

With the above lemma, we can prove the following proposition.

Proposition A.5. *There exist constants ν_0, $C_\pm$, $c_\pm > 0$ depending on $\mathbf{B}$ only, s.t. for all $\sigma_c, \gamma > 0$: $\sigma_c < \nu_0\gamma$, for any $s \in \mathbb{C}^+$, any $\mathbf{x},\mathbf{y} \in \overline{\Omega_{\mathrm{pml}}^\infty}$, the following bounds hold true:*

$$|s\sqrt{h_\sigma(s+\gamma;\mathbf{x},\mathbf{y})}| \geq C_-|s|\|\mathbf{x}-\mathbf{y}\|, \tag{A.13}$$

$$|s\sqrt{h_\sigma(s+\gamma;\mathbf{x},\mathbf{y})}| \leq C_+|s|\|\mathbf{x}-\mathbf{y}\|, \tag{A.14}$$

$$\operatorname{Re}(s\sqrt{h_\sigma(s+\gamma;\mathbf{x},\mathbf{y})}) \geq (c_+ \operatorname{Re} s - c_-\sigma_c)\|\mathbf{x}-\mathbf{y}\|. \tag{A.15}$$

If, additionally, $\|\mathbf{x}-\mathbf{y}\| > \rho_* = 2R_{\mathrm{pml}}\sqrt{\lambda_{\max}/\lambda_{\min}}$, then

$$\operatorname{Re}\left(s\sqrt{h_\sigma(s+\gamma;\mathbf{x},\mathbf{y})}\right) \geq c_+ \operatorname{Re} s\|\mathbf{x}-\mathbf{y}\|. \tag{A.16}$$

The value of ρ_* in the above is not optimal, but we do not pursue the goal of optimizing it.

Proof. The bound (A.13) follows from Lemma A.4. The upper bound (A.14) can be obtained by straightforward computations from (A.11), thus we leave the proof to the reader. Let us now prove the bound (A.15). We have that

$$\operatorname{Re}(s\sqrt{h_\sigma(s+\gamma;\mathbf{x},\mathbf{y})}) = \operatorname{Re} s \operatorname{Re}\sqrt{h_\sigma(s+\gamma;\mathbf{x},\mathbf{y})} - \operatorname{Im} s \operatorname{Im}\sqrt{h_\sigma(s+\gamma;\mathbf{x},\mathbf{y})}. \tag{A.17}$$

By Lemma A.4, and using the expression (A.6), we have that

$$\operatorname{Re}\sqrt{h_\sigma(s+\gamma;\mathbf{x},\mathbf{y})} > c_{\mathbf{B}}^{1/2}\|\mathbf{x}-\mathbf{y}\|. \tag{A.18}$$

Therefore, it remains to bound $\left|\operatorname{Im} s \operatorname{Im}\sqrt{h_\sigma(s+\gamma;\mathbf{x},\mathbf{y})}\right|$. We proceed like in the proof of Lemma A.8; in particular, we have, with (A.10) that

$$|\operatorname{Im} h_\sigma(s+\gamma;\mathbf{x},\mathbf{y})| \leq \tilde{C}_{\mathbf{B}}\frac{\sigma_c}{|s+\gamma|}\left(1+\frac{\sigma_c}{|s+\gamma|}\right)\|\mathbf{x}-\mathbf{y}\|.$$

Inserting the two above bounds into (A.17) yields

$$\operatorname{Re}(s\sqrt{h_\sigma(s+\gamma;\mathbf{x},\mathbf{y})}) \geq c_{\mathbf{B}}^{1/2}\operatorname{Re} s\|\mathbf{x}-\mathbf{y}\| - \tilde{C}_{\mathbf{B}}\frac{\sigma_c|\operatorname{Im} s|}{|s+\gamma|}\left(1+\frac{\sigma_c}{|s+\gamma|}\right)\|\mathbf{x}-\mathbf{y}\|.$$

With $|\operatorname{Im} s| < |s+\gamma|$ and using that $\gamma > \nu_0^{-1}\sigma_c$, we obtain the desired estimate (A.15).

Let us finally prove (A.16). We use again (A.17) and (A.18). The goal is to prove that for $\|\mathbf{x}-\mathbf{y}\| > \rho_*$, $\operatorname{Im} s \operatorname{Im}\sqrt{h_\sigma(s+\gamma;\mathbf{x},\mathbf{y})} < 0$. For this we consider the following expression, cf. (A.9):

$$\operatorname{Im} h_\sigma(s+\gamma;\mathbf{x},\mathbf{y}) = -\frac{2\sigma_c \operatorname{Im} s}{|s+\gamma|^2}\underbrace{(\|\mathbf{p}\|_{\mathbf{B}}^2 - \mathbf{p}^\top\mathbf{B}\mathbf{p}_{\mathrm{pml}})}_{S} - \frac{2\sigma_c^2 \operatorname{Im} s(\operatorname{Re} s+\gamma)}{|s+\gamma|^4}\|\mathbf{p}-\mathbf{p}_{\mathrm{pml}}\|_{\mathbf{B}}^2. \tag{A.19}$$

Next consider the term

$$S = \|\mathbf{p}\|_{\mathbf{B}}^2 - \mathbf{p}^\top\mathbf{B}\mathbf{p}_{\mathrm{pml}} \geq \|\mathbf{p}\|_{\mathbf{B}}^2 - \|\mathbf{p}\|_{\mathbf{B}}\|\mathbf{p}_{\mathrm{pml}}\|_{\mathbf{B}}.$$

We have $\|\mathbf{p}_{\mathrm{pml}}\| = R_{\mathrm{pml}}\|\hat{\mathbf{x}}-\hat{\mathbf{y}}\| \leq 2R_{\mathrm{pml}}$, and thus $\|\mathbf{p}_{\mathrm{pml}}\|_{\mathbf{B}} < 2\lambda_{\max}^{1/2}R_{\mathrm{pml}}$. On the other hand, $\|\mathbf{p}\| \geq \lambda_{\min}^{1/2}\|\mathbf{p}\|_{\mathbf{B}}$. Therefore, for $\|\mathbf{p}\|_{\mathbf{B}} > 2\lambda_{\max}^{1/2}/\lambda_{\min}^{1/2}R_{\mathrm{pml}}$, we have that $\|\mathbf{p}\|_{\mathbf{B}} > \|\mathbf{p}_{\mathrm{pml}}\|_{\mathbf{B}}$, and the quantity S is positive. Thus, under the condition $\|\mathbf{x}-\mathbf{y}\| > \rho_*$, $\operatorname{Im} s \operatorname{Im} h_\sigma(s+\gamma;\mathbf{x},\mathbf{y}) \leq 0$ and since $\operatorname{Im}\sqrt{h_\sigma}\operatorname{Im} h_\sigma \geq 0$ (cf. (A.6)), we have that $\operatorname{Im} s \operatorname{Im}\sqrt{h_\sigma(s+\gamma;\mathbf{x},\mathbf{y})} \leq 0$. We then have that (A.17), with the use of (A.18) rewrites as (A.16):

$$\operatorname{Re}(s\sqrt{h_\sigma(s+\gamma;\mathbf{x},\mathbf{y})}) \geq c_{\mathbf{B}}^{1/2}\operatorname{Re} s\|\mathbf{x}-\mathbf{y}\|.$$

□

A.2. Summary of the results

Below we summarize all the bounds we obtained before. They are evident for $\mathbf{x},\mathbf{y} \in \Omega_{\mathrm{int}}$, and follow from previous section for $\mathbf{x},\mathbf{y} \in \overline{\Omega_{\mathrm{pml}}^{\infty}}$, and from the computations summarized in the report [34] otherwise.

Lemma A.6. *Let $\sigma_c > 0$. Then there exist $\gamma_{\mathbf{B}}$, $c_{\mathbf{B}} > 0$, which depend on $\mathbf{B}$, s.t. for all $s \in \mathbb{C}_\alpha^+$, with $\alpha = \gamma_{\mathbf{B}}\sigma_c$,*

$$\operatorname{Re} h_\sigma(s;\mathbf{x},\mathbf{y}) \geq c_{\mathbf{B}}\|\mathbf{x}-\mathbf{y}\|^2, \qquad \textit{for all } \mathbf{x},\mathbf{y} \in \mathbb{R}^2. \tag{A.20}$$

Lemma A.7. *Let $\sigma_c > 0$. Then there exists a constant $C_{\mathbf{B}} > 0$, which depends on $\mathbf{B}$, s.t. for all $s \in \mathbb{C}^+$,*

$$|h_\sigma(s;\mathbf{x},\mathbf{y})| \le C_{\mathbf{B}} \left(1 + \frac{\sigma_c}{|s|}\right)^2 \|\mathbf{x}-\mathbf{y}\|^2, \quad \text{for all } \mathbf{x},\mathbf{y} \in \mathbb{R}^2.$$

Lemma A.8. *Let $\sigma_c > 0$. Then, there exist $\tilde{\gamma}_{\mathbf{B}}$, $\tilde{c}_{\mathbf{B}} > 0$, which depend on $\mathbf{B}$, s.t. for all $s \in \mathbb{C}^+_{\tilde{\alpha}}$, with $\tilde{\alpha} = \tilde{\gamma}_{\mathbf{B}}\sigma_c$,*

$$\operatorname{Re}(s\sqrt{h_\sigma(s;\mathbf{x},\mathbf{y})}) \ge \tilde{c}_{\mathbf{B}} \operatorname{Re} s \|\mathbf{x}-\mathbf{y}\|, \ \text{ for all } \mathbf{x},\mathbf{y} \in \mathbb{R}^2. \tag{A.21}$$

For the complex-scaled PMLs, the corresponding bounds are stated below.

Proposition A.9. *There exist constants ν, $C_\pm$, $c_\pm, C_{\mathbf{B}} > 0$ depending on $\mathbf{B}$ only, s.t. for all $\sigma_c, \gamma > 0$: $\sigma_c < \nu\gamma$, the following bounds hold true.*
1. For $(\mathbf{x},\mathbf{y}) \in \mathbb{R}^2 \times \mathbb{R}^2$,

$$C_+|s|\|\mathbf{x}-\mathbf{y}\| \ge |s\sqrt{h_\sigma(s+\gamma;\mathbf{x},\mathbf{y})}| \ge C_-|s|\|\mathbf{x}-\mathbf{y}\|. \tag{A.22}$$

2. For all $(\mathbf{x},\mathbf{y}) \in \overline{\Omega^\infty_{\mathrm{pml}}} \times \mathbb{R}^2$, s.t. $\|\mathbf{x}-\mathbf{y}\| > \rho = C_{\mathbf{B}} R_{\mathrm{pml}}$, it holds that

$$\operatorname{Re}\left(s\sqrt{h_\sigma(s+\gamma;\mathbf{x},\mathbf{y})}\right) \ge c_+ \operatorname{Re} s \|\mathbf{x}-\mathbf{y}\|. \tag{A.23}$$

3. For $(\mathbf{x},\mathbf{y}) \in \overline{\Omega^\infty_{\mathrm{pml}}} \times \mathbb{R}^2$,

$$\operatorname{Re}(s\sqrt{h_\sigma(s+\gamma;\mathbf{x},\mathbf{y})}) \ge c_+ \operatorname{Re} s \|\mathbf{x}-\mathbf{y}\| - c_-\sigma_c\|\mathbf{x}-\mathbf{y}\|. \tag{A.24}$$

Proof. The bounds (A.22) for $\mathbf{x},\mathbf{y} \in \Omega_{\mathrm{int}}$ are obvious. For $\mathbf{x},\mathbf{y} \in \Omega^\infty_{\mathrm{pml}}$ they stem from Proposition A.5. The remaining bounds follow for $\mathbf{x},\mathbf{y} \in \overline{\Omega^\infty_{\mathrm{pml}}}$ from Proposition A.5. For the case $\mathbf{x} \in \overline{\Omega^\infty_{\mathrm{pml}}}$, $\mathbf{y} \in \Omega_{\mathrm{int}}$, these bounds can be found in [34]. □

B. Implementation

B.1. Infinite elements

For this section we assume that Assumption 3.3 holds and additionally that $R_{\mathrm{pml}} = 1$, i.e., we have

$$\tilde{\sigma}(r) = \frac{(r-1)\sigma_c}{r}, \quad \Sigma = \mathbb{S}^1.$$

We describe the discretization in the exterior domain $\Omega^\infty_{\mathrm{pml}}$, since the discretization in Ω_{int} is standard. As discussed in Section 5.1, the implementation of the complex scaled infinite elements requires rewriting the bilinear forms in the weak formulation (52) in polar coordinates. Let us define the coordinate transformation

$$\Psi : (1,\infty) \times \Sigma \to \Omega^\infty_{\mathrm{pml}}, \quad (r,\hat{\mathbf{x}}) \mapsto r\hat{\mathbf{x}}, \quad \hat{\mathbf{x}} = (\cos\theta, \sin\theta), \quad \theta \in [0,\, 2\pi).$$

Let us additionally introduce the notation $v_{\mathrm{rad}} := v \circ \Psi$. We denote by $\nabla_\Sigma v_{\mathrm{rad}}$ the tangential gradient of v_{rad} on the surface Σ (i.e. $\partial_\theta v_{\mathrm{rad}} \hat{\mathbf{x}}_\perp$). As seen from (52), we need to express only the following two types of the integrals in polar coordinates, for real-valued integrands:

$$\langle v, v^\dagger \rangle = \int_{(1,\infty)\times\Sigma} r v_{\mathrm{rad}}\, v^\dagger_{\mathrm{rad}} dr d\hat{\mathbf{x}}, \qquad \langle \nabla v, \mathbf{q}^\dagger \rangle = \int_{(1,\infty)\times\Sigma} r\partial_r v_{\mathrm{rad}} \hat{\mathbf{x}} \cdot \mathbf{q}^\dagger_{\mathrm{rad}} + \nabla_\Sigma v_{\mathrm{rad}} \cdot \Pi_\perp \mathbf{q}^\dagger_{\mathrm{rad}} dr d\hat{\mathbf{x}}.$$

Plugging in basis functions (Section cf. 5.1) of the form $v_{\mathrm{rad}}(r,\hat{\mathbf{x}}) = \tilde{v}(r)\hat{v}(\hat{\mathbf{x}})$, $v^{\dagger}_{\mathrm{rad}}(r,\hat{\mathbf{x}}) = \tilde{v}^{\dagger}(r)\hat{v}^{\dagger}(\hat{\mathbf{x}})$, $\mathbf{q}^{\dagger}_{\mathrm{rad}}(r,\hat{\mathbf{x}}) = \tilde{q}^{\dagger}(r)\hat{\mathbf{q}}^{\dagger}(\hat{\mathbf{x}})$ leads to

$$\begin{aligned}\langle v, v^{\dagger}\rangle &= \int_{(1,\infty)} r\tilde{v}(r)\tilde{v}^{\dagger}(r)dr \int_{\Sigma} \hat{v}(\hat{\mathbf{x}})\hat{v}^{\dagger}(\hat{\mathbf{x}})d\hat{\mathbf{x}},\\ \langle \nabla v, \mathbf{q}^{\dagger}\rangle &= \int_{(1,\infty)} r\partial_r\tilde{v}(r)\tilde{q}^{\dagger}(r)dr \int_{\Sigma} \hat{v}(\hat{\mathbf{x}})\hat{\mathbf{x}}\cdot\hat{\mathbf{q}}^{\dagger}(\hat{\mathbf{x}})d\hat{\mathbf{x}} + \int_{(1,\infty)} \tilde{v}(r)\tilde{q}^{\dagger}(r)dr \int_{\Sigma} \nabla_{\Sigma}\hat{v}(\hat{\mathbf{x}})\cdot\Pi_{\perp}\hat{\mathbf{q}}^{\dagger}(\hat{\mathbf{x}})d\hat{\mathbf{x}}.\end{aligned} \tag{B.1}$$

The surface integrals can be evaluated by applying numerical integration on the surface mesh on Σ and lead to sparse, well-conditioned matrices if the underlying volume finite element spaces are chosen properly. It remains to choose a basis for the radial component of the space given in (53). We proceed to explain how this is done in the case of standard complex-scaled infinite elements and state the resulting radial discretization matrices. Subsequently we extend this approach to the case of two-scale infinite elements.

B.1.1. Hardy space infinite elements

Let us consider the following space, which is a special case of (54):

$$\mathcal{V}^M_{\mathrm{rad}} = \mathcal{Q}^M_{\mathrm{rad}} = \mathrm{span}\left\{\exp(-r)p(r) : p \in \mathcal{P}^M\right\}. \tag{B.2}$$

One basis in this space is given by, cf. [58, Section 6.3.2] and [48, Section 4.2],

$$\{r \mapsto \varphi_n(r) = \exp(1-r)L_{n,-1}(2r-2), n = 0,\dots,M\},$$

where the functions $L_{n,-1}$ are generalized Laguerre polynomials, defined by

$$L_{n,-1}(x) = \begin{cases} 1, & n = 0,\\ \sum_{k=1}^{n} \frac{k}{n}\binom{n}{k}\frac{(-x)^k}{k!} = \frac{x\mathrm{e}^x}{n}\left(\frac{d}{dx}\right)^n\left(x^{n-1}\mathrm{e}^{-x}\right), & n \geq 1.\end{cases} \tag{B.3}$$

The above defines a basis in the space (B.2), because the degree of the polynomial $L_{n,-1}$ is equal exactly to n. This choice of the basis ensures that the radial discretization matrices (B.1) are sparse, see [58, Section 6.3]. Moreover, their entries can be computed in a closed form using the orthogonality of Laguerre polynomials $L_{n,-1}$ with respect to the weight $\mathrm{e}^{-x}x^{-1}$. Alternatively the matrices can be computed using numerical quadrature, i.e., weighted Gauss rules with respect to the weight $\exp(-2x)$.

Since later on we will use a two-scale version of the infinite elements, for which such computations are far from obvious, we choose an alternative approach. It[5] is based on passing to the Laplace domain *with respect to the radial variable* $r-1$, and next working with discretization matrices in the Laplace domain only. This technique then can then be generalized to define the basis and compute the entries of the discretization matrices for the two-scale method. As it is simpler to understand the main ideas for the classical Hardy space infinite elements, we choose this, more pedagogical, way of presenting the method.

Given a function $r \mapsto \varphi(r)$, with $r \in [1,\infty)$, let us introduce its (shifted) Laplace transform (where the index r indicates that we work with the radial variable, rather than with time):

$$(\mathcal{L}_r\varphi)(p) := \Phi(p) := \int_0^{\infty} \mathrm{e}^{-p\xi}\varphi(\xi+1)d\xi.$$

Remark that by capital letters we will denote $\mathcal{L}_r$-transformed quantities. With the above definition, we can prove the following result.

Lemma B.1. *Let* $\mathrm{Re}\, p > -1$. *Then the Laplace transforms of* φ_n *are given by the expressions*

$$(\mathcal{L}_r\varphi_0)(p) = \Phi_0(p) = \frac{1}{p+1}, \qquad (\mathcal{L}_r\varphi_n)(p) = \Phi_n(p) = -\frac{2}{(p+1)^2}\left(\frac{p-1}{p+1}\right)^{n-1}, \quad n \geq 1. \tag{B.4}$$

[5]Historically, this is how Hardy space infinite elements were introduced and analyzed in the first place in [38]

Also, for their derivatives it holds that

$$(\mathcal{L}_r\varphi_0')(p) = -\frac{1}{p+1}, \qquad (\mathcal{L}_r\varphi_n')(p) = -\frac{2p}{(p+1)^2}\left(\frac{p-1}{p+1}\right)^{n-1}, \quad n \geq 1. \tag{B.5}$$

Finally,

$$(\mathcal{L}_r(r\varphi_n))(p) = D_p\Phi_n(p), \quad D_p = 1 - \partial_p. \tag{B.6}$$

Proof. Proof of (B.4). For $n = 0$ the result follows by a direct computation. For $n \geq 1$, we rewrite

$$\Phi_n(p) = \int_0^\infty \mathrm{e}^{-px}\mathrm{e}^{-x}L_{n,-1}(2x)dx. \tag{B.7}$$

Replacing $L_{n,-1}$ by its expression (B.3) and using the identity

$$\int_0^\infty \mathrm{e}^{-px}x^k\mathrm{e}^{-x}dx = k!(p+1)^{-k-1}, \quad k \in \mathbb{N},$$

yields the following expression:

$$\Phi_n(p) = \sum_{k=1}^n \frac{k}{n}\binom{n}{k}\frac{(-2)^k}{(p+1)^{k+1}} = \frac{1}{p+1}\left(\frac{x}{n}\frac{d}{dx}\sum_{k=0}^n\binom{n}{k}x^k\right)\Big|_{x=-\frac{2}{p+1}} = \frac{1}{p+1}\,x(1+x)^{n-1}\big|_{x=-\frac{2}{p+1}},$$

from which the desired expression follows immediately.
Proof of (B.5). The expressions for the Laplace transforms of the derivatives are immediate, if we recall additionally that $\varphi_0(1) = 1$ and $\varphi_n(1) = 0$ for all $n \geq 1$ (cf. (B.3)).
Proof of (B.6). The identity follows by a direct computation:

$$\mathcal{L}_r(r\varphi_n) = \int_0^\infty \mathrm{e}^{-p\xi}(\xi+1)\varphi_n(\xi+1)d\xi = (1 - \frac{d}{dp})\int_0^\infty \mathrm{e}^{-p\xi}\varphi_n(\xi+1)d\xi.$$

□

In order to relate (B.1) evaluated at radial basis functions φ_n to their Laplace domain expressions, we use the following lemma, see also [38, Lemma A.1]. It follows from the Plancherel identity, by continuing u, v to causal functions and by making use of the fact that they are real-valued.

Lemma B.2. *Let $u, v \in L^2((1,\infty);\mathbb{R})$. Then $\int_1^\infty u(r)v(r)dr = \frac{1}{2\pi i}\int_{i\mathbb{R}} U(p)V(-p)dp$.*

The above lemma states that evaluating the entries of the mass matrix reduces to computing the integrals in the right-hand side of

$$\int_{(1,\infty)} \varphi_n(r)\varphi_m(r)dr = \frac{1}{2\pi i}\int_{i\mathbb{R}} \Phi_n(p)\Phi_m(-p)dp. \tag{B.8}$$

The main idea is then to rewrite the matrix in the right-hand side by using an alternative basis, in which its representation will be sparse. Even better, this representation will provide us a factorization of the matrix in the right-hand side with the help of tri-diagonal matrices. We introduce

$$\mathcal{S}_M^\Phi := \mathrm{span}\{\Phi_n,\, n = 0, 1, \ldots, M\}.$$

Moreover,we define new basis functions Ψ_n and related basis functions $\boldsymbol{\beta}_n$ (the latter ones constitute a basis used in the Hardy space methods):

$$\Psi_n(p) := -\frac{2}{p+1}\left(\frac{p-1}{p+1}\right)^n, n \geq 0, \quad \Psi_{-1}(p) := 0, \quad \boldsymbol{\beta}_n := \begin{pmatrix}\delta_{n,-1}\\ \Psi_n\end{pmatrix}, \quad n \in \mathbb{N}\cup\{-1\}, \tag{B.9}$$

with $\delta_{n,-1} = 1$ if $n = -1$ and 0 otherwise. We will denote by $\mathcal{S}_M^\Psi := \mathrm{span}\{\Psi_n,\, n = 0, \ldots, M\}$ and by $\mathcal{S}_M^{\boldsymbol{\beta}} := \mathrm{span}\{\boldsymbol{\beta}_n,\, n = -1, \ldots, M-1\}$.

Remark B.3. The basis functions Ψ_n are introduced so that, as we will see later (Lemma B.7), the matrix defined by the right-hand side of (B.8) becomes diagonal in this basis.This allows to avoid evaluation of the integrals over infinite lines. The basis $\boldsymbol{\beta}_n$ is introduced to make a connection to the Hardy-space methods.

The main goal is then to rewrite the 'radial' matrices arising in (B.1) using Lemma B.2 and the new basis $\mathcal{S}_M^\Psi$ (resp. $\mathcal{S}_M^{\boldsymbol{\beta}}$). We start by expressing Φ_n via $\boldsymbol{\beta}_n$.

Lemma B.4. *Let the operators $\mathcal{T}_\pm : \mathcal{S}_M^{\boldsymbol{\beta}} \mapsto \mathcal{S}_M^\Phi$ be given by, for $\boldsymbol{\beta} = (\beta, B)^\top$,*

$$(\mathcal{T}_-\boldsymbol{\beta})(p) := \frac{\beta + B(p)}{p+1}, \qquad (\mathcal{T}_+\boldsymbol{\beta})(p) := \frac{-\beta + pB(p)}{p+1}.$$

Then, for all $0 \le n \le M$,

$$\mathcal{L}_r\varphi_n = \mathcal{T}_-\boldsymbol{\beta}_{n-1}, \quad \mathcal{L}_r\varphi_n' = \mathcal{T}_+\boldsymbol{\beta}_{n-1}. \tag{B.10}$$

Proof. First of all, remark that, Range$(\mathcal{T}_\pm) \subseteq \mathcal{S}_M^\Phi$. This is straightforward from (B.9) and equalities of Lemma B.1. Both identities in (B.10) then follow by an explicit computation, using Lemma B.1. □

With the above we also have the following.

Lemma B.5. $\mathcal{T}_\pm(\mathcal{S}_M^{\boldsymbol{\beta}}) \subseteq \mathcal{S}_M^\Psi$.

The above follows from $\mathcal{S}_M^\Phi \subseteq \mathcal{S}_M^\Psi$. We however express $\mathcal{T}_\pm\boldsymbol{\beta}_n$ in a basis of $\mathcal{S}_M^\Psi$ directly, since we will need the corresponding expressions later.

Proof. Let us prove the result for $\mathcal{T}_-$. It is straightforward to see that $\mathcal{T}_-\boldsymbol{\beta}_{-1} = -\frac{1}{2}\Psi_0$. For $n \neq -1$, we have that $(\mathcal{T}_-\boldsymbol{\beta}_n)(p) = \frac{\Psi_n(p)}{p+1}$, and we rewrite

$$\frac{\Psi_n(p)}{p+1} = -\frac{2}{(p+1)^2}\left(\frac{p-1}{p+1}\right)^n, \text{ and } \frac{1}{p+1} = -\frac{1}{2}\left(\frac{p-1}{p+1} - 1\right). \tag{B.11}$$

Thus, for $n \ge 0$, the result follows from the expression:

$$(\mathcal{T}_-\boldsymbol{\beta}_n)(p) = -\frac{1}{2}(\Psi_{n+1}(p) - \Psi_n(p)). \tag{B.12}$$

As for $\mathcal{T}_+$, we have that $\mathcal{T}_+\boldsymbol{\beta}_{-1} = \frac{1}{2}\Psi_0$ and $(\mathcal{T}_+\boldsymbol{\beta}_n)(p) = \Psi_n(p) - \frac{\Psi_n(p)}{p+1} = \frac{1}{2}(\Psi_n(p) + \Psi_{n+1}(p))$, $n > -1$. □

These relations, together with Lemma B.2, allow us to express the matrices occurring in (B.1) with the help of the bilinear form

$$q(U,V) := \frac{1}{2\pi i}\int_{i\mathbb{R}} U(p)V(-p)dp, \tag{B.13}$$

defined for U, V being the Laplace transforms of one of the functions φ_n or their derivatives. We then have the following result, whose proof is based on Lemmas B.4 and B.2, and thus is left to the reader.

Lemma B.6. *For all $n, m \ge 0$ (where q is defined in* (B.13) *and D_p in* (B.6)*), it holds that*

$$\int_{(1,\infty)} \varphi_n\varphi_m = q(\mathcal{T}_-(\boldsymbol{\beta}_{n-1}), \mathcal{T}_-(\boldsymbol{\beta}_{m-1})), \qquad \int_{(1,\infty)} r\varphi_n(r)\varphi_m(r)dr = q(D_p\mathcal{T}_-(\boldsymbol{\beta}_{n-1}), \mathcal{T}_-(\boldsymbol{\beta}_{m-1})),$$
$$\int_{(1,\infty)} r\varphi_n'(r)\varphi_m(r)dr = q(D_p\mathcal{T}_+(\boldsymbol{\beta}_{n-1}), \mathcal{T}_-(\boldsymbol{\beta}_{m-1})). \tag{B.14}$$

Therefore, instead of directly computing the matrices in the left-hand side of (B.14), we can factorize them with the help of the expressions in the right-hand side of (B.14), by computing the matrix representations of the operators $\mathcal{T}_\pm : \mathcal{S}^{\boldsymbol{\beta}}_M \to \mathcal{S}^\Psi_M$, $D_p : \mathcal{S}^\Phi_M \to \mathcal{S}^\Phi_{M+1}$[6], and of the bilinear form $q : \mathcal{S}^\Psi_M \times \mathcal{S}^\Psi_M \mapsto \mathbb{C}$. Importantly, in this new basis q becomes a diagonal matrix. To state the result that follows, let us introduce the q-orthogonal projection operator $P^\Psi_M : \mathcal{S}^\Psi_{M+1} \to \mathcal{S}^\Psi_M$, defined by, for $U \in \mathcal{S}^\Psi_{M+1}$,

$$q(P^\Psi_M U, V) = q(U, V), \qquad \text{for all } V \in \mathcal{S}^\Psi_M.$$

We then have the following result.

Lemma B.7. *The matrix representations $\mathbb{T}_\pm$ of $\mathcal{T}_\pm : \mathcal{S}^{\boldsymbol{\beta}}_M \to \mathcal{S}^\Psi_M$, $\mathbb{Q}$ of $q : \mathcal{S}^\Psi_M \times \mathcal{S}^\Psi_M \to \mathbb{R}$, $\tilde{\mathbb{D}}_p$ of $P^\Psi_M D_p : \mathcal{S}^\Psi_M \mapsto \mathcal{S}^\Psi_M$ are given by:*

$$\mathbb{T}_\pm = \frac{1}{2}\begin{pmatrix} \pm 1 & 1 & & & \\ & \pm 1 & 1 & & \\ & & \ddots & \ddots & \\ & & & \pm 1 & 1 \\ & & & & \pm 1 \end{pmatrix}, \quad \tilde{\mathbb{D}}_p = \mathrm{Id} - \frac{1}{2}\begin{pmatrix} -1 & 1 & & & \\ 1 & -3 & 2 & & \\ & 2 & -5 & \ddots & \\ & & \ddots & \ddots & M \\ & & & M & -2M-1 \end{pmatrix}, \quad \mathbb{Q} = 2\,\mathrm{Id}\,.$$

Proof. Expressions of $\mathbb{T}_\pm$. See Lemma B.5.

Expression of $\mathbb{Q}$. By a direct computation it follows that

$$\mathbb{Q}_{nm} = \frac{1}{2\pi i}\int_{i\mathbb{R}} \Psi_n(p)\Psi_m(-p)dp = \frac{1}{2\pi i}\int_{i\mathbb{R}} \frac{4}{(p+1)(-p+1)}\frac{(p-1)^n(-p-1)^m}{(p+1)^n(-p+1)^m}dp = -\frac{2}{\pi i}\int_{i\mathbb{R}} \frac{(p-1)^{n-m-1}}{(p+1)^{n-m+1}}dp.$$

Let us assume without loss of generality that $n \geq m$. For $n \geq m+1$, we can use the Cauchy residue theorem to show that the corresponding integral vanishes, i.e. $\mathbb{Q}_{nm} = 0$. For $n = m$, we have that

$$\mathbb{Q}_{mm} = 4\,\mathrm{Res}_{p=1}\frac{1}{(p+1)(p-1)} = 2.$$

Expression of $\tilde{\mathbb{D}}_p$. Let us first of all compute

$$\frac{d}{dp}\Psi_n(p) = \frac{2(n+1)(p-1)^n}{(p+1)^{n+2}} - \frac{2n(p-1)^{n-1}}{(p+1)^{n+1}}.$$

With (B.11), we express $(p+1)^{-1} = -\frac{1}{2}\left(\frac{p-1}{p+1} - 1\right)$. This yields

$$\begin{aligned}\frac{d}{dp}\Psi_n(p) &= -\frac{(n+1)}{(p+1)}\left(\left(\frac{p-1}{p+1}\right)^{n+1} - \left(\frac{p-1}{p+1}\right)^n\right) + \frac{n}{p+1}\left(\left(\frac{p-1}{p+1}\right)^n - \left(\frac{p-1}{p+1}\right)^{n-1}\right) \\ &= \frac{1}{2}\left((n+1)\Psi_{n+1} - (2n+1)\Psi_n + n\Psi_{n-1}\right).\end{aligned}$$

Finally, as $\mathbb{Q}_{nm} = 2\delta_{nm}$, we conclude with the stated form of the matrix expression of $P^\Psi_M D_p$. □

Using the result of the above lemma and (B.14), we conclude that the entries of the discrete matrices in (B.1) can be written as follows:

$$\begin{aligned}&\int_{(1,\infty)} \varphi_n\varphi_m = \left(\mathbb{T}_-^\top \mathbb{Q}\mathbb{T}_-\right)_{n,m}, \qquad \int_{(1,\infty)} r\varphi_n(r)\varphi_m(r)dr = \left(\mathbb{T}_-^\top \widetilde{\mathbb{D}}_p^\top \mathbb{Q}\mathbb{T}_-\right)_{n,m}, \\ &\int_{(1,\infty)} r\varphi_n'(r)\varphi_m(r)dr = \left(\mathbb{T}_+^\top \widetilde{\mathbb{D}}_p^\top \mathbb{Q}\mathbb{T}_-\right)_{n,m}.\end{aligned} \tag{B.15}$$

[6]Remark that the multiplication operator $u(r) \mapsto ru(r)$ sends $\mathcal{V}^M_{\mathrm{rad}}$ into $\mathcal{V}^{M+1}_{\mathrm{rad}}$. We can thus show that the shifted derivative D_p maps $\mathcal{S}^\Psi_M \to \mathcal{S}^\Psi_{M+1}$.

B.1.2. Two scale Hardy space infinite elements

Let us consider the two-scale space (53). In this case, up to our knowledge, no convenient closed form for the spacial basis functions as for the classical Hardy space infinite elements is known. In the following, we assume that $\eta_0 = 1$, set $\eta_1 = \eta$, and define the basis in the Laplace domain first (following [32, 33]). The corresponding spacial basis functions can then be found by computing the inverse Laplace transform. This is in general not necessary: as we are not interested in the solution outside of Ω_{int}, the explicit representation of these functions is not needed. We define the two-scale Hardy basis of (B.9) by

$$\Psi_n^\eta(p) := -\frac{1+\eta}{p+\eta}\left(\frac{p-1}{p+1}\right)^{\lfloor (n+1)/2\rfloor}\left(\frac{p-\eta}{p+\eta}\right)^{\lfloor n/2\rfloor}, \quad n \geq 0, \quad \Psi_{-1}^\eta(p) := 0, \tag{B.16}$$

$$\boldsymbol{\beta}_n^\eta(p) := \begin{pmatrix}\delta_{n,-1}\\ \Psi_n^\eta(p)\end{pmatrix}, \quad n \in \mathbb{N}\cup\{-1\}. \tag{B.17}$$

The set of $\{\Psi_n^\eta, n \in \mathbb{N}_0\}$ can be shown to form a Riesz basis in an appropriate Hardy space, see [33]. We will comment more on a particular form of the above basis functions below, see Remark B.10 after Lemma B.9. We then define the basis functions φ_n^η by making use of an analogue of Lemma B.4. In particular, first of all we define their shifted Laplace transform $\mathcal{L}_r\varphi_n^\eta = \Phi_n^\eta$ by a counterpart of (B.10):

$$\mathcal{L}_r\varphi_n^\eta := \mathcal{T}_-^\eta \boldsymbol{\beta}_{n-1}^\eta, \quad n \geq 0.$$

with the operator $\mathcal{T}_-^\eta$ defined as follows. Provided the spaces

$$\mathcal{S}_M^{\boldsymbol{\beta}^\eta} := \operatorname{span}\{\boldsymbol{\beta}_n^\eta, n = -1, \dots, M-1\}, \quad \mathcal{S}_M^{\Psi^\eta} := \operatorname{span}\{\Psi_n^\eta, n = 0, \dots, M\}, \quad \mathcal{S}_M^{\Phi^\eta} := \operatorname{span}\{\Phi_n^\eta, n = 0, \dots, M\},$$

the operator $\mathcal{T}_-^\eta : \mathcal{S}_M^{\boldsymbol{\beta}^\eta} \to \mathcal{S}_M^{\Phi^\eta}$ is defined via

$$(\mathcal{T}_-^\eta\boldsymbol{\beta})(p) := \frac{\beta + B(p)}{p+1}, \quad \boldsymbol{\beta} = (\beta, B)^\top.$$

With the definition of the operator $\mathcal{T}_-^\eta$, it is straightforward to verify that φ_n^η are linearly independent. Moreover, our first result shows that we have indeed constructed the basis of $\mathcal{V}_{\text{rad}}(1, \eta, N)$.

Lemma B.8. *It holds that* $\operatorname{span}\{\mathcal{L}_r^{-1}\Phi_n^\eta,\, n = 0, \dots, 2N+1\} = \mathcal{V}_{\text{rad}}(1, \eta, N)$.

Proof. Because Φ_n^η are linearly independent, it suffices to show that $\operatorname{span}\{\mathcal{L}_r^{-1}\Phi_n^\eta,\, n = 0, \dots, 2N+1\} \subset \mathcal{V}_{\text{rad}}(1, \eta, N)$. We will show how the result is proven for the simplest cases (for $N = 0$ and $N = 1$), and the result for $N \geq 2$ will follow by the same reasoning. Let us first study the case $N = 0$. Indeed, in this case $\mathcal{V}_{\text{rad}}(1, \eta, 0) = \operatorname{span}\{\mathrm{e}^{-p}, \mathrm{e}^{-\eta p}\}$. On the other hand,

$$\Phi_0^\eta(p) = \frac{1}{p+1}, \quad \Phi_1^\eta(p) = -\frac{1+\eta}{(p+\eta)(p+1)}, \text{ therefore, } \phi_0^\eta(r) = \mathrm{e}^{-(r-1)}, \quad \phi_1^\eta(r) = -\frac{1+\eta}{1-\eta}\left(\mathrm{e}^{-\eta(r-1)} - \mathrm{e}^{-(r-1)}\right).$$

Thus the result of the lemma holds for $\mathcal{V}_{\text{rad}}(1, \eta, 0)$. Let us now consider the case $N = 1$. We rewrite

$$\Phi_2^\eta(p) = \frac{p-1}{p+1}\Phi_1^\eta(p) = \Phi_1^\eta(p) - \frac{2}{p+1}\Phi_1^\eta(p), \qquad \Phi_3^\eta(p) = \frac{p-\eta}{p+\eta}\Phi_2^\eta(p) = \Phi_2^\eta(p) - \frac{2\eta}{p+\eta}\Phi_2^\eta(p). \tag{B.18}$$

Evidently, $\phi_1^\eta \in \mathcal{V}_{\text{rad}}(1, \eta, 1)$. Therefore, let us now consider $u(r) = \mathcal{L}_r^{-1}\frac{1}{p+1}\Phi_1^\eta(p)$. Applying the shifted inverse Laplace transform, we remark that u solves

$$\left(\frac{d}{dr} + 1\right)u(r+1) = \Phi_1^\eta(r+1), \quad u(1) = 0, \implies u(r+1) = \int_0^r \mathrm{e}^{-(r-r')}\Phi_1^\eta(r'+1)dr'.$$

Now remark that $\phi_1^\eta(r) = \mathrm{e}^{-r}p_0^{(1)}(r) + \mathrm{e}^{-\eta r}p_0^{(2)}(r)$, where $p_0^{(j)} \in \mathcal{P}_0$, and $j = 1, 2$ (i.e., constants). It then can be verified by plugging in this explicit form of Φ_1^η in the above expression that $u(r) = \mathrm{e}^{-r}p_1^{(1)}(r) + \mathrm{e}^{-\eta r}\tilde{p}_0^{(2)}(r)$,

where $p_1^{(1)} \in \mathcal{P}_1$, and $\tilde{p}_0^{(2)} \in \mathcal{P}_0$. Crucially, the polynomial degree in the multiplier of $\mathrm{e}^{-\eta r}$ did not increase after this integration. The above computation shows that indeed, $\varphi_2^\eta \in \mathcal{V}_{\mathrm{rad}}(1,\eta,1)$, and, moreover, writes

$$\varphi_2^\eta(r) = \mathrm{e}^{-r} p_1(r) + \mathrm{e}^{-\eta r} p_0(r), \text{with } p_1 \in \mathcal{P}_1, \quad p_0 \in \mathcal{P}_0.$$

In a similar manner, cf. (B.18), we can show that $\phi_3^\eta \in \mathcal{V}_{\mathrm{rad}}(1,\eta,1)$. Because

$$\Phi_{2N+2}^\eta(p) = \frac{p-1}{p+1}\Phi_{2N+1}^\eta(p), \quad \Phi_{2N+3}^\eta(p) = \frac{p-\eta}{p+\eta}\Phi_{2N+2}^\eta(p), \tag{B.19}$$

cf. the relation (B.18), the desired result can be proven for $N > 1$ by using similar ideas. □

To formulate a counterpart of Lemma B.5, let us introduce an auxiliary basis, very similar to Ψ_n^η, namely

$$\tilde{\Psi}_n^\eta(p) := -\frac{1+\eta}{p+1}\left(\frac{p-\eta}{p+\eta}\right)^{\lfloor (n+1)/2 \rfloor}\left(\frac{p-1}{p+1}\right)^{\lfloor n/2 \rfloor}, \quad n \geq 0. \tag{B.20}$$

We define $\tilde{\mathcal{S}}_M^{\Psi^\eta} := \mathrm{span}\{\tilde{\Psi}_n^\eta,\, n = 0, \ldots, M\}$. We then have the following result, which clarifies relations between different spaces.

Lemma B.9. *$\tilde{\mathcal{S}}_M^{\Psi^\eta} = \mathcal{S}_M^{\Phi^\eta}$, for all $M \geq 0$. Therefore $\mathcal{T}_-^\eta(\mathcal{S}_M^{\boldsymbol{\beta}^\eta}) = \tilde{\mathcal{S}}_M^{\Psi^\eta}$.*

Proof. Remark that $\Phi_0^\eta(p) = \frac{1}{p+1} = -\frac{1}{1+\eta}\tilde{\Psi}_0^\eta(p)$. For $n \geq 1$, with odd $n = 2k+1$, we have

$$\begin{aligned}\Phi_n^\eta(p) = \frac{1}{p+1}\Psi_{2k}^\eta(p) &= -\frac{(1+\eta)}{(p+\eta)(p+1)}\left(\frac{p-1}{p+1}\right)^k\left(\frac{p-\eta}{p+\eta}\right)^k \\ &= -\frac{(1+\eta)}{2\eta(p+1)}\left(1 - \frac{p-\eta}{p+\eta}\right)\left(\frac{p-1}{p+1}\right)^k\left(\frac{p-\eta}{p+\eta}\right)^k = \frac{1}{2\eta}\left(\tilde{\Psi}_{2k}^\eta(p) - \tilde{\Psi}_{2k+1}^\eta(p)\right).\end{aligned}$$

In a similar manner, for even $n = 2(k+1)$, we have that

$$\begin{aligned}\Phi_n^\eta(p) = \frac{1}{p+1}\Psi_{2k+1}^\eta(p) &= -\frac{(1+\eta)}{(p+\eta)(p+1)}\left(\frac{p-1}{p+1}\right)^{k+1}\left(\frac{p-\eta}{p+\eta}\right)^k \\ &= \frac{(p-1)}{(p+\eta)(p+1)}\frac{-(1+\eta)}{p+1}\left(\frac{p-1}{p+1}\right)^k\left(\frac{p-\eta}{p+\eta}\right)^k.\end{aligned}$$

Next, let us develop

$$\frac{p-1}{(p+\eta)(p+1)} = \frac{\eta-1}{2\eta(\eta+1)} + \frac{p-\eta}{2\eta(p+\eta)} - \frac{(p-1)(p-\eta)}{(1+\eta)(p+1)(p+\eta)}.$$

With the above, we obtain

$$\Phi_{2k+2}^\eta = \frac{1}{2\eta}\left(\frac{\eta-1}{\eta+1}\tilde{\Psi}_{2k}^\eta + \tilde{\Psi}_{2k+1}^\eta - \frac{2\eta}{1+\eta}\tilde{\Psi}_{2k+2}^\eta\right).$$

□

Remark B.10. The above lemma partially justifies the particular definition of functions $\Psi_n^\eta(p)$ (B.16) and $\tilde{\Psi}_n^\eta(p)$ (B.20). Remark that $\tilde{\Psi}_n^\eta$ are defined like Ψ_n^η with η and 1 being interchanged. The functions $\tilde{\Psi}_n^\eta$ are introduced in order to ensure $\tilde{\mathcal{S}}_M^{\Psi^\eta} = \mathcal{S}_M^{\Phi^\eta}$, which does not hold true for $\tilde{\mathcal{S}}_M^{\Psi^\eta}$ replaced by $\mathcal{S}_M^{\Psi^\eta}$.

To formulate the next result, let us introduce the operator $\mathcal{T}_+^\eta : \mathcal{S}_M^{\boldsymbol{\beta}^\eta} \to \tilde{\mathcal{S}}_M^{\Psi^\eta}$, defined by

$$(\mathcal{T}_+^\eta \boldsymbol{\beta})(p) := \frac{-\beta + pB(p)}{p+1}, \quad \boldsymbol{\beta} = (\beta, B)^\top.$$

It is straightforward to verify that it holds that

$$\mathcal{L}_r \left(\varphi_n^\eta\right)' = \mathcal{T}_+^\eta(\boldsymbol{\beta}_{n-1}), \quad n \geq 0.$$

I.e., the same relations for the integrals as in Lemma B.6 hold and the discrete matrices for the corresponding operators and the bilinear form q can be obtained by similar computations as above as given in the following lemmas. Since the computations are very tedious and technical we omit them at this point.

Lemma B.11. *Let $M+1 = 2N$. Then the operators $\mathcal{T}_\pm^\eta : \mathcal{S}_M^{\boldsymbol{\beta}^\eta} \to \tilde{\mathcal{S}}_M^{\Psi^\eta}$ can be represented by the matrices*

$$\mathbb{T}_-^\eta = -\frac{1}{2\eta}\,\mathrm{Id} + \frac{1}{2\eta}\mathcal{T}^\eta, \qquad \mathbb{T}_+^\eta = \frac{1}{2}\,\mathrm{Id} + \frac{1}{2}\mathcal{T}^\eta,$$

with

$$\mathcal{T}^\eta := \begin{pmatrix} T & T^U & & \\ & \ddots & \ddots & \\ & & T & T^U \\ & & & T \end{pmatrix}, \qquad T := \begin{pmatrix} \frac{1-\eta}{1+\eta} & 1 \\ 0 & 0 \end{pmatrix}, \qquad T^U := \begin{pmatrix} \frac{\eta-1}{\eta+1} & 0 \\ 1 & 0 \end{pmatrix},$$

Moreover, the matrix representation of the bilinear form $q : \tilde{\mathcal{S}}_M^{\Psi^\eta} \times \tilde{\mathcal{S}}_M^{\Psi^\eta} \to \mathbb{R}$ is given by

$$\mathbb{Q}^\eta = \frac{(1+\eta)^2}{2} \begin{pmatrix} Q & & \\ & \ddots & \\ & & Q \end{pmatrix}, \qquad Q = \begin{pmatrix} 1 & \frac{1-\eta}{1+\eta} \\ \frac{1-\eta}{1+\eta} & 1 \end{pmatrix}.$$

Similar to the classical space we use a projection $P_M^{\tilde{\Psi}^\eta} : \mathcal{S}_{M+2}^{\tilde{\Psi}^\eta} \to \mathcal{S}_M^{\tilde{\Psi}^\eta}$ which is given by truncating the expansion with respect to the basis functions $\tilde{\Psi}_n^\eta$ to $n \leq M$. Then the corresponding square matrix of the differential operator is given by the following lemma.

Lemma B.12. *The matrix of the differential operator $P_N^{\tilde{\Psi}} D_p : \tilde{\mathcal{S}}_N^{\Psi^\eta} \to \tilde{\mathcal{S}}_N^{\Psi^\eta}$ (cf. (B.6)) is given by*

$$\widetilde{\mathbb{D}}^\eta = \mathrm{Id} - \frac{1}{2} \begin{pmatrix} D_0 & D_1^U & & & \\ D_1^L & D_1 & D_2^U & & \\ & \ddots & \ddots & \ddots & \\ & & D_{N-2}^L & D_{N-2} & D_{N-1}^U \\ & & & D_{N-1}^L & D_{N-1} \end{pmatrix},$$

with

$$D_l = \begin{pmatrix} -\frac{1}{1+\eta} & \frac{1}{2\eta} \\ \frac{1}{2\eta} & -\frac{1+4\eta+\eta^2}{2\eta(1+\eta)} \end{pmatrix} + l \begin{pmatrix} \frac{1+6\eta+\eta^2}{2\eta(1+\eta)} & \frac{1+\eta}{2\eta} \\ \frac{1+\eta}{2\eta} & -\frac{1+6\eta+\eta^2}{2\eta(1+\eta)} \end{pmatrix},$$

$$D_l^U = l \begin{pmatrix} \frac{\eta-1}{2\eta(1+\eta)} & 0 \\ \frac{1+\eta}{2\eta} & \frac{1-\eta}{2(1+\eta)} \end{pmatrix}, \qquad D_l^L = l \begin{pmatrix} \frac{1-\eta}{2(1+\eta)} & \frac{1+\eta}{2\eta} \\ 0 & \frac{\eta-1}{2\eta(1+\eta)} \end{pmatrix}.$$